IN - 14318   211 P.

COMPUTER-AIDED MODELING AND ANALYSIS OF POWER PROCESSING SYSTEMS (CAMAPPS) - PHASE I

Final Report

MAR. 1 5 1986

V161O1O9

Prepared by

S. Kim, J. Lee, B.H. Cho and F.C. Lee
Department of Electrical Engineering
Virginia Polytechnic Institute
and State University
Blacksburg, Virginia 24061

for

CONTENTS

CHAPTER 5. SHUNT REGULATOR MODELING

CHAPTER 6. BATTERY-DISCHARGER MODELING

CHAPTER 7. SYSTEM LEVEL MODELING

CHAPTER 1

INTRODUCTION AND SUMMARY

1.1 INTRODUCTION

The ever increasing demand on spacecraft power systems for improved efficiency and reliability, smaller size and lighter weight, coupled with continuous growth in dimension and complexity of the spacecraft's payloads, has focused attention on a major deficiency - the ability to design, test, and trouble-shoot large-scale power systems.

During the past several decades, numerous efforts have been made to develop new and more powerful techniques for modeling and analysis of spacecraft power components (equipments) and subsystems. However, when the components and subsystems are interconnected to form a complex system, it is quite difficult to predict the total system response even though the behavior of individual components may be well understood and documented. This is due to many undesired interactions that exist among highly nonlinear components. The need of a comprehensive power system modeling tool is, therefore, most critical since the elaborate design verification through integrated systems hardware testing is prohibitively expensive or often impossible. This is particularly true in the future space station system since, due to the large dimension and complexity, the complete system can only be assembled in space. Therefore, a comprehen-

sive computer model that can actually predict a system's local and global behaviors is most critical for the success of future missions.

1.2 OBJECTIVES

The study objectives in Phase 1, 'Large-Signal Modeling and Analysis of Spacecraft Power System' are described as follows:

1. Incorporation of all component models generated under the previous NAVY contracts into CAMAPPS.

    The large-signal models developed under the previous NAVY contracts consist of:

    *   Solar array models - an analytical model and an empirical data model for the solar array dc models.

    *   Shunt regulator model - a particular shunt circuit model for dc, small-signal and large-signal analysis.

    *   Switching converter model - A buck converter with constant frequency and single-loop control.

    *   Payload models - reactive load and empirical data model.

2. Generation of large-signal componet models and the macro component model library.

Large-signal component models need to be generated to facilitate analysis and simulation of comprehensive spacecraft power systems. The component models are in the form of macro-models which can be easily configured into a particular spacecraft power system. The macro-model library to be generated shall include:

- Solar array

- Solar array switching unit and control

- Shunt regulators

- Battery chargers/dischargers

- DC-DC converters

- Payload

3. Analysis and simulation of a spacecraft power processing system

Large-signal behaviors of solar array power systems will be analayzed. A spacecraft power system will be configured and simulated using various type of component

modules to demonstrate the utility of the proposed CAMAPPS.

4. Transfer of software program of CAMAPPS to NASA

5. To identify future development effort on CAMAPPS and possible integrated system configuration for CAMAPPS executive, data base management and user interface.

1.3 SUMMARY OF THE WORK

The proposed works for Phase 1 are accomplished and summarized in the following:

Task 1. **Component model library for switching converters - Chapter 3**

Since there exist many different types of power stage topologies and control methods, the large-signal behaviors of a regulator depend largely on the type of power circuit topology and control. Thus, for maximum flexibility, it is best to develop models for each functional block as independent modules. A regulator can then be configured by collecting appropriate pre-defined modules for each functional block. Also, any of these block modules can be freely replaced with alternatives, it provides maximum flexibility in building a variety of regulators. The macro modules developed for each functional block are in the following.

4

Converter topologies

- Buck

- Boost

- Buck/boost (Flyback)

- Forward

Control methods

- Single-loop and multi-loop feedback with the following duty-cycle controls

  - Constant frequency

  - Constant T_{on}

  - Constant T_{off}

- Current-injected and SCM control with

  - Constant frequency

  - Constant T_{off} control

Task 2. Other component model generation

In order to complete the component model generation for a comprehensive spacecraft power system, the following macro-modules are developed. The capability of each module is demonstrated using a simplified Direct Energy Transfer (DET) system.

- Solar array switching unit and control - Chapter 4

- Shunt regulators - Chapter 5

- Battery discharger - Chapter 6

Task 3. Analysis and simulation of spacecraft power processing system - Chapter 7

Large-signal behaviors of solar array power systems are analyzed. Stability of the solar array system operating points with a nonlinear load is analyzed. The state-plane analysis illustrates trajectories of the system operating point under various operating condition. Stability and transient responses of the system operating near the solar array's maximum power point are also analyzed. The solar array system's mode of operation are described using the Direct Energy Transfer spacecraft power system. The DET system is simulated for various system operating conditions.

Task 4. Transfer of software program of CAMAPPS to NASA/GSFC

- Software program

    The software program developed under Phase 1 effort is ready to be transferred on tape to NASA

- User's handbook

    The user's handbook is included in this report and consists of the following documentation

    — Macro-model generation

    — Macro-model description

    — User's input requirement

    — Macro-model output

    — Sample modeling and simulation

    — Program listings

CHAPTER 2

MODELING APPROACH OF LARGE-SCALE SPACECRAFT POWER SYSTEM

2.1 INTRODUCTION

Considering the size and complexity of today's spacecraft power processing systems, the digital computer is perhaps the only viable tool for system modeling and simulation. Two general classes of power system modeling programs appear in the literatures. These are :

* Generalized circuit and system analysis models.

* Dedicated models of specific systems.

The generalized circuit analysis models, as a class, are represented by programs such as SPICE, SCEPTRE, SYSCAP, ICAP, ASTAP and a number of others. All are similar in that they offer a set of typical device modules which are assembled into a network of interconnecting nodes. This class of computer programs shares a common drawback, such that with an increasing number of components, the memory requirements increase dramatically. By use of dynamic memory management it may be possible to analyze a large-scale system, but only at the cost of a geometric increase in computation time. The labor involved in model-building is rather extensive and the resulting model, in general, lacks flexibility for future

8

modifications. Furthermore, the analysis capability of these canned programs is limited and usually not effective for design aid or trouble-shooting.

Dedicated models of specific power systems have been used successfully but only on a limited basis. Typically this class of model is capable only of dc analysis. Execution speed and cost of such programs tend to be much less than that for generalized circuit and system routines [1].

One way to develop a model with such attributes is to modularize various components of the power system. Therefore, a comprehensive power system model must be capable of performing various analyses: dc, small-signal and large-signal transient. The model should have the following attributes :

- flexibility for future modification of component models and system configuration,

- accuracy to provide sufficient details about the behavior of individual components for design and troubleshooting,

- verifiable whenever equipment or subsystem experimental testing is possible,

- efficiency to minimize computer core memory and computation time.

9

2.2 MODELING APPROACH OF LARGE-SCALE SYSTEMS

As discussed in Chapter 1, defining a complete spacecraft power system entirely in terms of circuit elements is not feasible. A practical approach is to consider that a large-scale system can be defined by the interconnection of many smaller subsystems. The system dynamics, therefore, stem from the individual subsystems and their interconnection laws that identify the signal flows among them. Due to the complexity of the individual components and their interconnection scheme it is usually very difficult to predict the system's overall behavior. A desirable analysis or synthesis procedure for a large-scale system is the separation of these two levels (component and system). One thus prefers an analysis or synthesis procedure to be based, on one hand, on "local" subsystems and, on the other hand, on the "global" interconnection laws.

In order to utilize the modular concept, each component should be modeled as an unterminated two-port network because the terminal characteristics of both source and load are unknown until the complete system is configured. Thus, the information flow can be obtained in both directions. The interconnection law should not only describe accurately the signal flows between the subsystems but also be standardized. There exist several kinds of two-port representations such as impedance, admittance, chain, and hybrid matrices. The impedance or admittance matrices cannot be used as a standard

interconnection law because their inputs and outputs are in alternate forms. The chain matrix is not as flexible as the hybrid matrix because it only characterizes a system in uni-direction.

Figure 2.1 illustrates the interconnection law for unter-minated modules. Each component, in general, receives two inputs, v_1 and i_2, from the preceding and following modules, and provides two outputs, i_1 and v_2, to the adjacent modules. The terminal characteristics of each component are described by the matrix equation called "hybrid g-parameters" in Eq.(2.1).

$$
\begin{bmatrix} i_1 \\ v_2 \end{bmatrix} = \begin{bmatrix} g_{11} & g_{12} \\ g_{21} & g_{22} \end{bmatrix} \cdot \begin{bmatrix} v_1 \\ i_2 \end{bmatrix}
\tag{2.1}
$$

For modeling a two-port, one can always define the output and input variables as shown in Fig.2.1. For example, a single stage LC low-pass filter can be modeled with state equations as shown in Fig.2.2. Since these unterminated two-port com-ponents have the same interconnection law, they can be interconnected arbitrarily to form a system.

Having identified the two-port component coupling ap-proach, efforts have been made to find a software system which can be adapted to multi-port component modeling and system integration. The program EASY5 developed by Boeing Computer Service has been selected as the host software sys-tem.

11
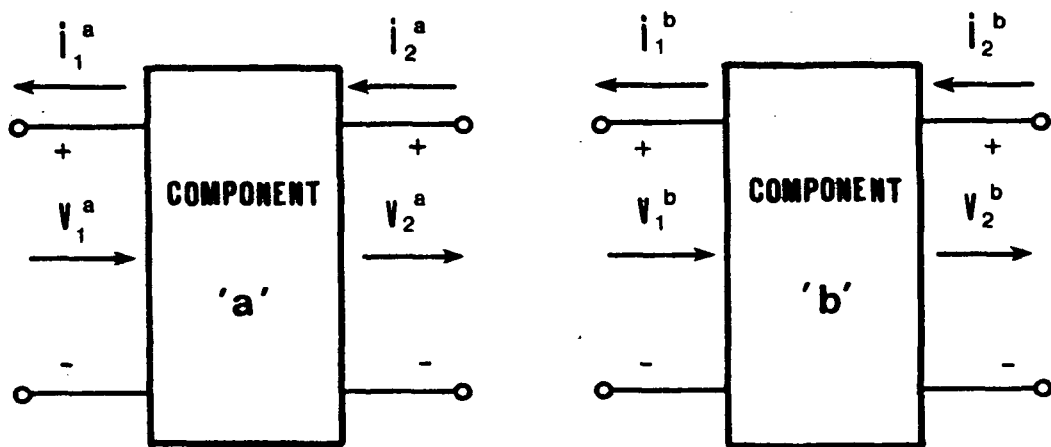
Figure 2.1   Two-port subsystem coupling using the hybrid G-matrix
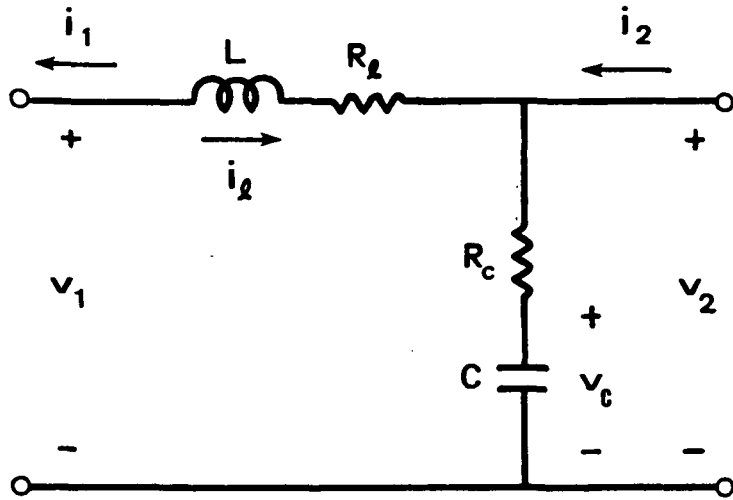
$$
\begin{bmatrix} \dot{i}_\ell \\ \dot{v}_c \end{bmatrix} = \begin{bmatrix} \dfrac{-(R_\ell + R_c)}{L} & \dfrac{-1}{L} \\ \dfrac{1}{C} & 0 \end{bmatrix} \begin{bmatrix} i_\ell \\ v_c \end{bmatrix} + \begin{bmatrix} \dfrac{1}{L} & \dfrac{-R_c}{L} \\ 0 & \dfrac{1}{C} \end{bmatrix} \begin{bmatrix} v_1 \\ i_2 \end{bmatrix}
$$

$$
\begin{bmatrix} i_1 \\ v_2 \end{bmatrix} = \begin{bmatrix} -1 & 0 \\ R_c & 0 \end{bmatrix} \begin{bmatrix} i_\ell \\ v_c \end{bmatrix} + \begin{bmatrix} 0 & 0 \\ 0 & R_c \end{bmatrix} \begin{bmatrix} v_1 \\ i_2 \end{bmatrix}
$$

Figure 2.2   Example of an unterminated two-port modeling
with state equations

2.3 EASY5 SYSTEM MODEL GENERATION AND ANALYSIS

For a large-scale spacecraft power system, the large-signal performance evaluation is invariably limited to tactics closely identified with time-domain simulation techniques. The actual operating point trajectories or transient responses due to the large-signal disturbances can be simulated by a digital computer. In this way, the existence of unstable solutions can be observed along with peak values and actual waveforms. Thus, the model development of each nonlinear component of a spacecraft power system involves two separate models, the large-signal time-domain simulation model and the small-signal linearized model.

For time-domain simulation, the EASY5 numerical integration routine calculates current values of the states and output variables for each component from the input values. It then passes along the output values according to the interconnection law. There are seven different types of numerical integration routines available in EASY5. Each offers different numerical stability and computational efficiency dependent on the type of nonlinearity of a system. To examine the approximate large-signal behavior of a system analytically, rather than by time-domain simulation, one may simplify the system focusing on a particular component of interest. For instance, the large-signal behavior of the solar array system's operating point can be analyzed by sim-

plifying the system to a second order nonlinear system as illustrated in Chapter 7 .

The EASY5 software [2] provides a modular approach to dynamic system model building and analysis. It was chosen particularly for its effective means of assembling complex component modules into a system. Predefined component modules can be stored in the EASY5 component library. The component modules can have several input and output ports and, in each port, information can flow into and out of the port. All detailed connections of signal paths between component blocks are programmed with minimal user intervention.

Once all the necessary components are modeled, they are stored in the EASY5 macro component library. As shown in Fig.2.3, the EASY5 consists of two programs, Model Generation Program and Analysis Program, and a library of predefined Standard Components. Predefined Standard Component models include many of the common effects found in dynamic systems such as standard analog and discrete controllers (proportional, integral, differential, etc.) transfer functions, nonlinearities (relay, saturation, hysteresis and switches), linear state equation model, etc.

Model generation: The EASY5 Model Generation Program uses a block diagram approach for constructing various system models. All interconnections between the component models are accomplished by the Model Generation Program according to the user specified Model Description Data. This is ac-
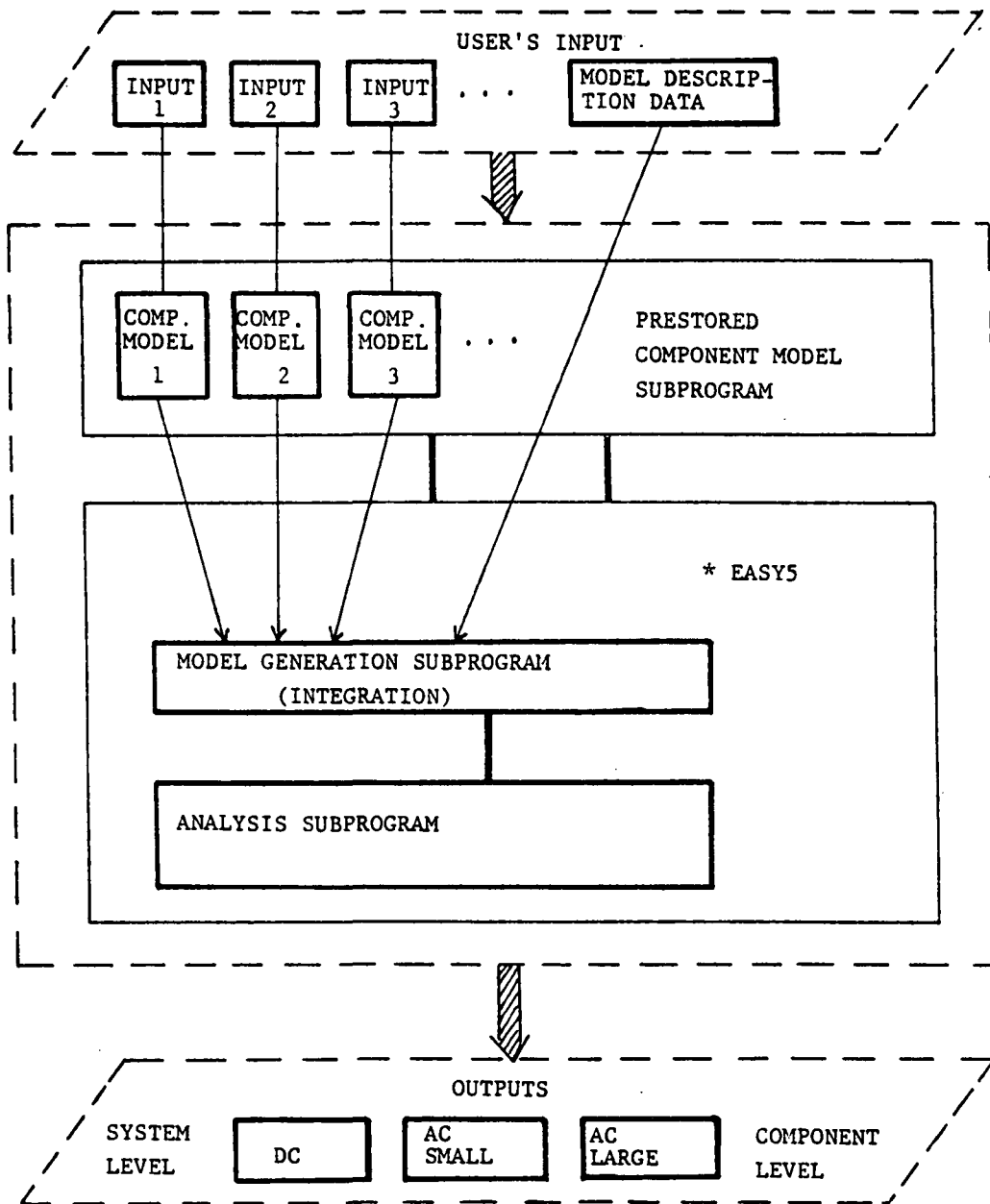
Figure 2.3 System modeling and analysis with the program EASY5

complished by matching the input and output port quantities of each interconnection. The program also produces a complete list of input data that is required by each component to complete the model description. The scalar and vector parameters and tabular data required for the analysis are included in this list.

Analysis:. Once a system model has been constructed, the Analysis Program performs various dynamics analyses according to the user provided Analysis Data. The Analysis Data includes parameter values, initial conditions of states, various analysis controls and commands. Among the various analysis controls in EASY5, it is important to note that the INTEGRAL control allows one to perform the analysis at various levels such as system, subsystem, or component. The analysis in the component or subsystem level is done by 'freezing' the states of the subsystem of little interest. This control feature is particularly useful when one is interested in investigating behaviors of a component or a subsystem in the presence of the entire system. A list of the analysis techniques available through the Analysis Program are given as follows.

- Time history generation - nonlinear simulation
- Linear model generation with eigenvalue and eigenvector calculations

- Frequency response analysis
- Root locus calculation
- Steady-state analysis
- Stability margin calculations
- Optimal controller synthesis

CHAPTER 3

SWITCHING REGULATOR MODELING

3.1 INTRODUCTION

Because of high efficiency, small size and light weight, switching regulators are widely used in spacecraft power systems. Switching regulators can be characterized, as shown in Fig.3.1, by the three basic functional blocks: power stage, analog feedback controller, and digital signal processor.

The power stage consists of energy storage elements and switches. Transfer of the input power to the load is controlled by the duty ratio of the switch (transistor). The analog feedback controller usually contains an error amplifier and a compensation network. For a single-loop control it senses the output (load voltage), and for a multiple-loop control it senses the output and states (i.e., load voltage, inductor current, capacitor voltage). The digital signal processor includes a ramp generator, a comparator, and latches. It takes the control voltage from the analog feedback and converts it to the pulse-width-modulated (PWM) signal which controls the switches in the power stage.
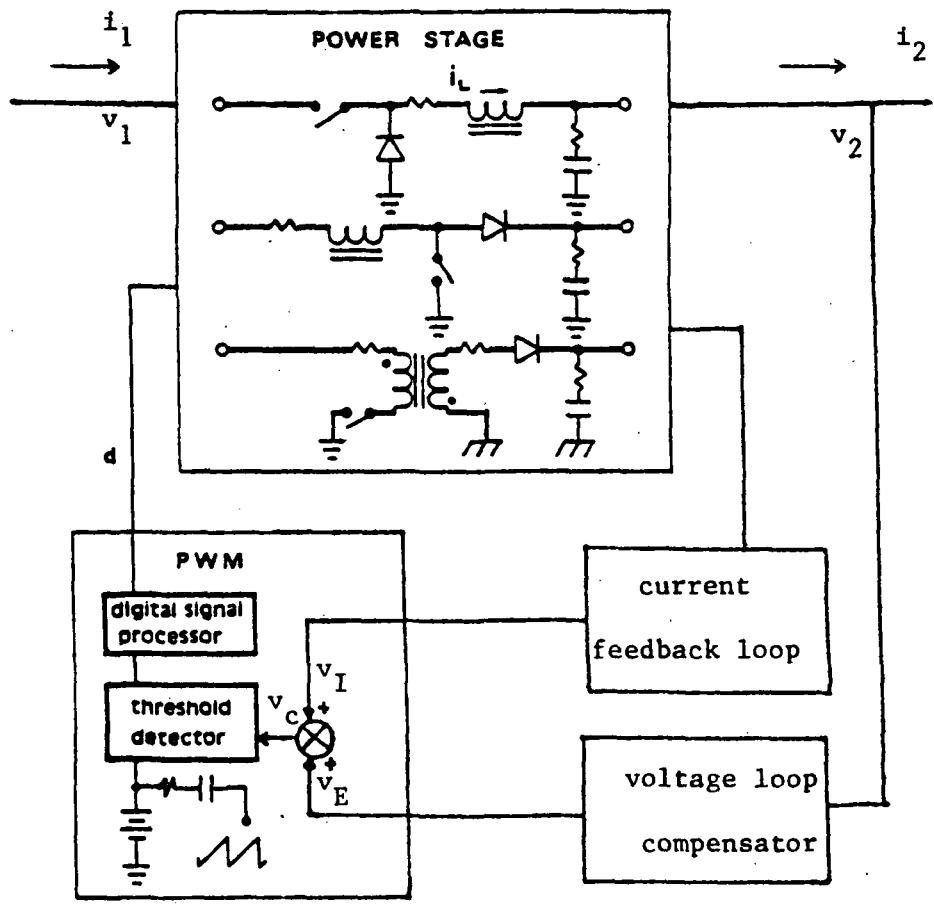
Figure 3.1 Switching regulator model

Since there exist many different types of power stage topologies and control methods, the large-signal behaviors of a regulator depend largely on the type of power circuit topology and control. Thus, for maximum flexibility, it is best to develop models for each functional block as independent modules. A regulator can then be configured by collecting appropriate pre-defined modules for each functional block. Also, any of these block modules can be freely replaced with alternatives, providing maximum flexibility in building a variety of regulators.

## 3.2 POWER STAGE MODELING

Generally, three different circuit topologies exist in the course of a complete switching cycle. A converter is characterized by three sets of state equations during a switching cycle as follows:

$$\dot{x} = A_1 x + B_1 u$$

$$y = C_1 x + E_1 u \ , \quad \text{for interval } T_{ON} \qquad (3.1)$$

$$\dot{x} = A_2 x + B_2 u \ ,$$

$$y = C_2 x + E_2 u \ , \quad \text{for interval } T_{F1} \qquad (3.2)$$

$$\dot{x} = A_3 x + B_3 u \ ,$$

$$y = C_3 x + E_3 u \ , \quad \text{for interval } T_{F2} \qquad (3.3)$$

Here x is the state vector, u the input vector and T_s the switching period. A_i and B_i (i=1,2,3) are square matrices which describe the three circuit topologies and the effects of the input vector, u. These three matrix equations can be combined into one by using the three switching functions shown in Fig.3.2. With use of these switching functions, a single state equation suffices to describe the converter, as in Eq.(3.4).
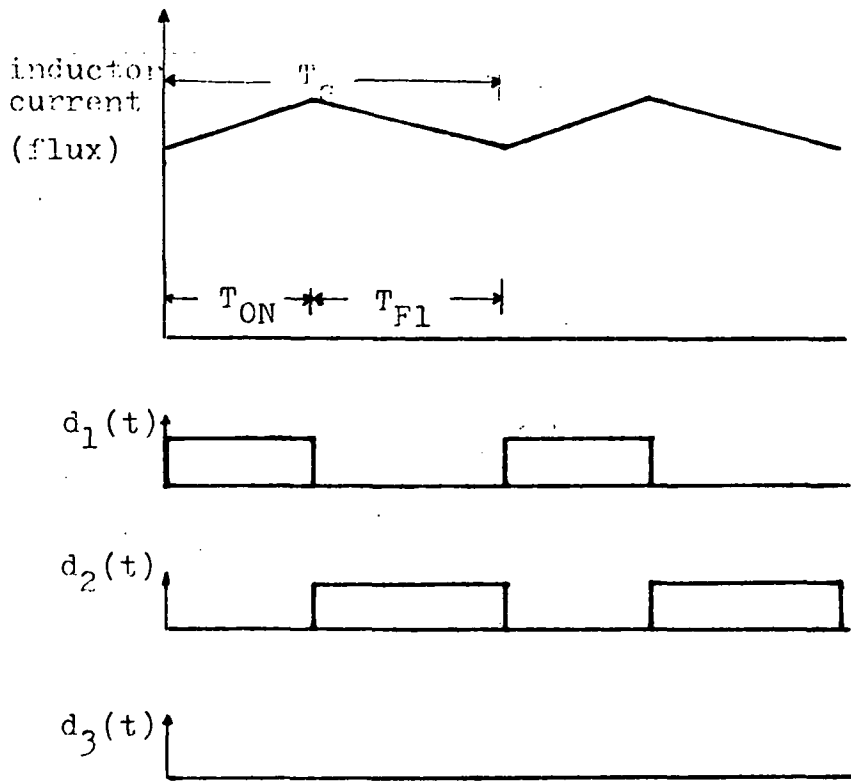
(a) continuous conduction mode
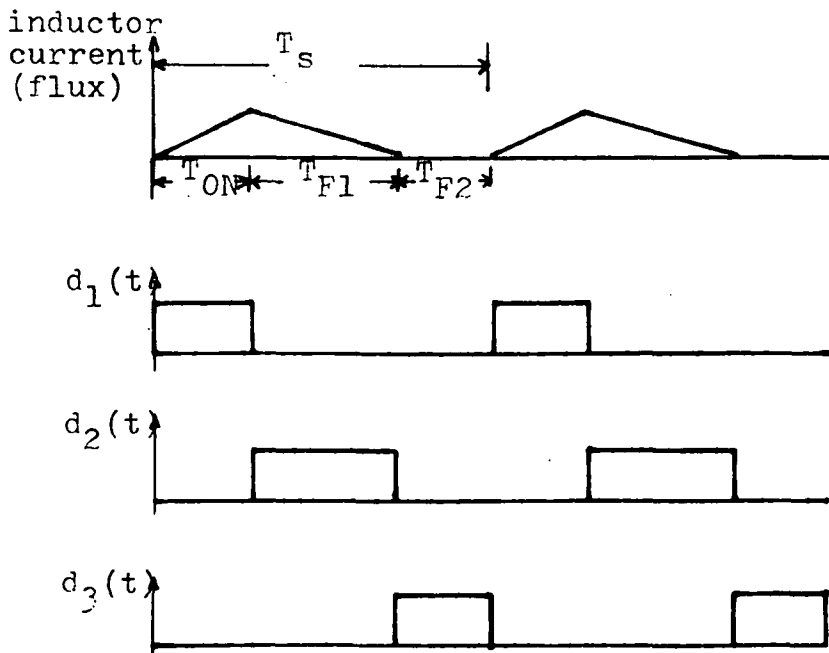
(b) discontinuous-conduction mode

Figure 3.2 Switching functions

23

$$\dot{x} = \sum_{i=1}^{3} [A_i x + B_i u] d_i(t) \ ,$$

$$y = \sum_{i=1}^{3} [C_i x + E_i u] d_i(t) \ , \quad i = 1,2,3 \quad (3.4)$$

where d_i's are either zero or one depending on the specific time interval involved.

Equation (3.4) is not only discrete but also nonlinear because $d_i(t)$ is a function of the state vector, x, and the input vector, u. The power stage model shown in Eq.(3.4) is directly implemented with the appropriate switching function for the time-domain model. The intervals defined above include the possible inductor-current discontinuous-conduction mode (DCM), as illustrated in Fig.3.2(b). For the continuous-conduction mode (CCM), there are only two switching intervals, T_{ON} and T_{F1}, as shown in Fig.3.2(a). In the time-domain model, these two different modes of operation (DCM or CCM) are naturally determined depending on circuit parameter values and input and output requirements.

3.2.1 EASY5 MODEL FOR CONVERTER POWER STAGES

As described in the previous section, power stage, in general, has three sets of equations. These three sets of matrices coefficients are stored in the power stage module and appropriate sets of matrices are selected according to the status of d(t) which is determined by the digital signal processor module. As illustrated in Fig.3.3, when d(t) is equal to one, (interval T_{ON}), the first matrix set, A_1, B_1, C_1, and D_1, is used to calculate state equations, the second matrix set is used when d(t) is zero, (interval T_{F1}), and the third matrix set when both inductor current and d(t) are equal to zero (interval T_{F2}).

The state variables are $x = [i_L \ v_C]$ where i_L is the energy-storage inductor current and v_C is the output-filter capacitor voltage. For the buck/boost (flyback) converter, $x = [\phi \ v_C]$ where ϕ is the flux in the two-winding energy-storage inductor. Input vectors are $u = [v_1 \ i_2]$, where v_1 is the input voltage and i_2 is the load current.

All switches (transistors and diodes) are regarded as ideal switches, and the winding resistance (R_1) of the inductor and ESR (R_C) of the capacitor are included in the power stage model.
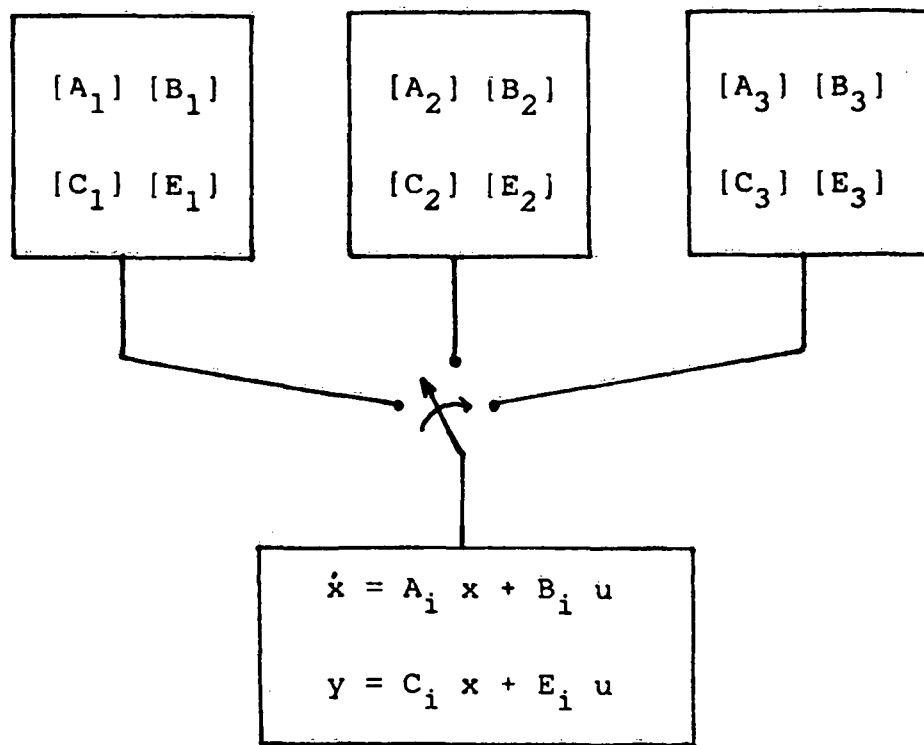
Figure 3.3   Power stage model

For the buck power stage denoted as [BC], the three, linear equivalent-circuit models can be generated according to the time intervals T_{ON}, T_{F1}, and T_{F2}, which are illustrated in Figs.3.4. The power stage is then described by the piecewise linear equations for each subinterval as following:

For

$$x = \begin{bmatrix} i_L \\ v_C \end{bmatrix} \qquad u = \begin{bmatrix} v_1 \\ i_2 \end{bmatrix} \qquad y = \begin{bmatrix} v_2 \\ i_1 \end{bmatrix},$$

during the interval T_{ON},

$$A_1 = \begin{bmatrix} -\dfrac{R_1+R_C}{L} & -\dfrac{1}{L} \\ \dfrac{1}{C} & 0 \end{bmatrix} \qquad B_1 = \begin{bmatrix} \dfrac{1}{L} & \dfrac{R_C}{L} \\ 0 & -\dfrac{1}{C} \end{bmatrix}$$

$$C_1 = \begin{bmatrix} R_C & 1 \\ 1 & 0 \end{bmatrix} \qquad E_1 = \begin{bmatrix} 0 & -R_C \\ 0 & 0 \end{bmatrix}$$

for the interval T_{F1},

$$A_2 = \begin{bmatrix} -\dfrac{R_1+R_C}{L} & -\dfrac{1}{L} \\ \dfrac{1}{C} & 0 \end{bmatrix} \qquad B_2 = \begin{bmatrix} 0 & \dfrac{R_C}{L} \\ 0 & -\dfrac{1}{C} \end{bmatrix}$$

$$C_2 = \begin{bmatrix} R_C & 1 \\ 0 & 0 \end{bmatrix} \qquad E_2 = \begin{bmatrix} 0 & -R_C \\ 0 & 0 \end{bmatrix}$$
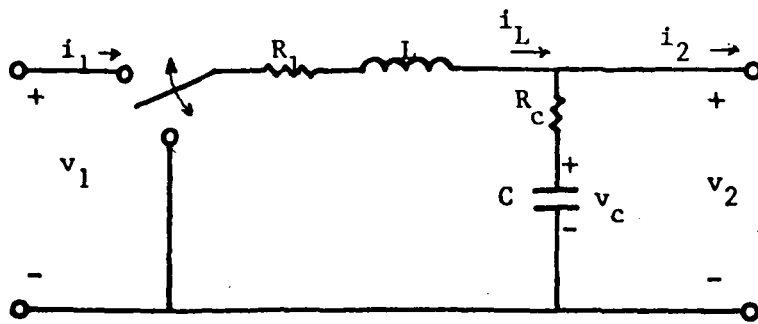
27

Figure 3.4(a)   Buck converter power stage
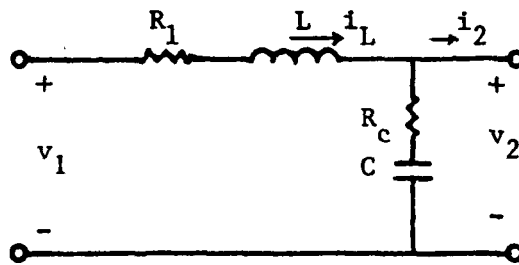
interval T_{ON}
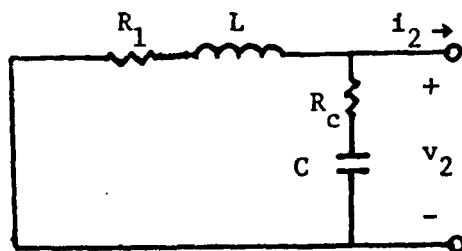
interval T_{F1}

interval T_{F2}

Figure 3.4(b)   Three switched equivalent circuits

28

for the interval T_{F2},

$$A_3 \cong \begin{bmatrix} 0 & 0 \\ 0 & 0 \end{bmatrix} \qquad B_3 = \begin{bmatrix} 0 & 0 \\ 0 & -\dfrac{1}{C} \end{bmatrix}$$

$$C_3 \cong \begin{bmatrix} 0 & 1 \\ 0 & 0 \end{bmatrix} \qquad E_3 = \begin{bmatrix} 0 & -R_c \\ 0 & 0 \end{bmatrix}$$

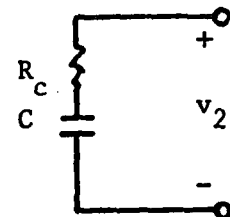For the following converter topologies, EASY5 macro modules are also generated. Detailed macro-model descriptions are given in the User's Handbook.

- [BT] ----- boost-converter power stage

- [FB] ----- buck/boost (flyback) converter power stage

- [FW] ----- forward-converter power stage

29

3.3 ANALOG FEEDBACK CONTROLLER

The commonly used analog feedback controller is basically linear for normal modes of operation. The controller can be modeled by either transfer functions or state equations.

The transfer-function model provides more design insight so both analysis and synthesis of the controller can be done quite easily. Pole-zero compensations of the closed-loop system can be directly implemented using the Bode plot technique. However, the second-order effects of the feedback, such as the steady-state switching ripple component, is lost.

Modeling with state equations can describe the circuit in more detail and can easily include the nonlinearities such as op-amp saturation and protection circuits. However, the circuit topology must be pre-determined and, generally, the model requires more memory space. Also, the model does not provide direct information about the location of poles and zeros to facilitate design of the feedback compensator.

The choice of model depends on the objective. For design and frequency-domain analysis the transfer-function model suits better; for more accurate time-domain analysis and simulation, the state-equation model is preferable.

A typical multiple-loop controller for switching regulators senses the state (inductor current) and output (output

voltage). The sum of the outputs from the current-feedback loop and the output-voltage loop forms the control voltage or error voltage, which is input to the digital signal processor.

3.3.1 EASY5 MODEL FOR ANALOG FEEDBACK CONTROLLER

The EASY5 model for the analog feedback controller is characterized generally by the voltage-feedback module and current-feedback module. When a single-loop feedback control is used, the current feedback module is omitted.

3.3.1.1 VOLTAGE-FEEDBACK COMPENSATOR

The following two commonly used compensators are modeled with transfer functions.

- [MP] --- two-pole one-zero compensation

$$v_E = \frac{\omega_m(1 + s/\omega_z)}{s(1 + s/\omega_p)} [K v_o - E_R] \qquad (3.5)$$

v_o : switching regulator output voltage

K : voltage dividing factor

E_R : reference voltage of op.amp.

v_E : compensator output voltage

One possible circuit implementation of the above transfer function is shown Fig.3.5(a) and its gain characteristic is shown in Fig.3.5(b). The transfer function of the compensator circuit shown in Fig.3.5(a) is

$$F(s) = \frac{\hat{v}_E}{\hat{v}_o} = \frac{1 + sC_2(R_1 + R_2)}{sR_1C_1(1 + sC_2R_3)} \tag{3.6}$$

By comparing Eqs.(3.5) and (3.6) one can determine the circuit parameter values for resistors and capacitors in Eq.(3.6) from its design parameter values, $\omega_m, \omega_z,$ and ω_p or vice versa. For EASY5 modeling, the transfer function in Eq.(3.5) is internally converted to state equations.
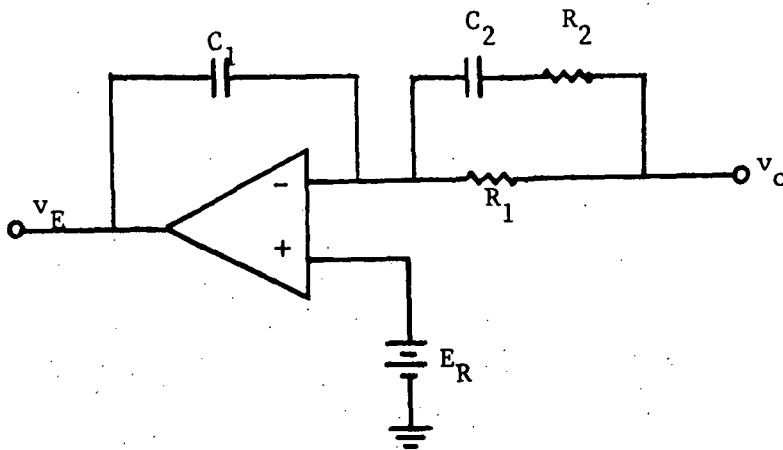
(a) circuit implementation
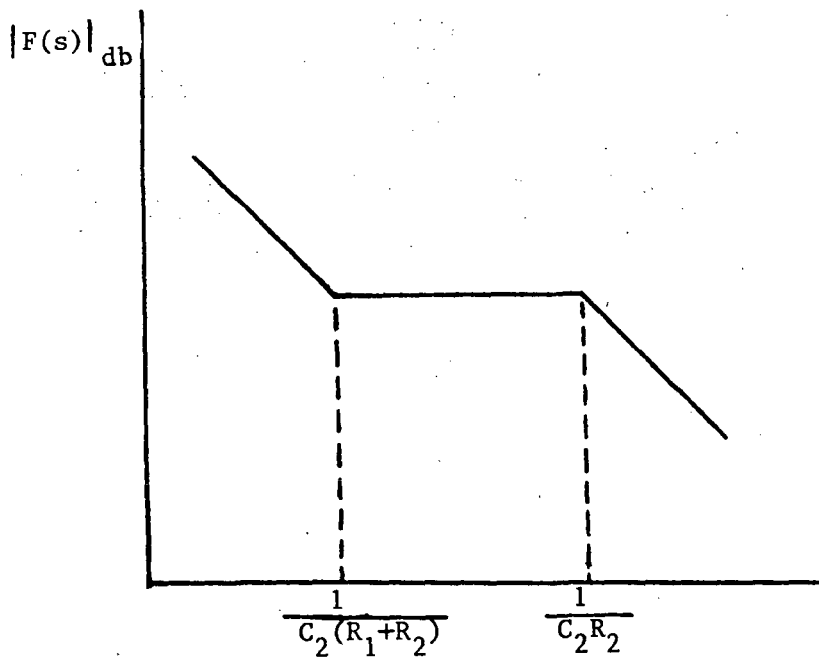
(b) gain characteristic

Figure 3.5 Two-pole one-zero compensator

33

• [PZ] --- Two-pole two-zero compensation

$$v_E = \frac{\omega_m (1 + s/\omega_{z1})(1 + s/\omega_{z2})}{s(1 + s/\omega_p)} [K v_o - E_R] \qquad (3.8)$$

Figure 3.6 shows one possible circuit implementation of the two-pole two-zero compensator and its gain characteristic. The transfer function of the circuit is

$$F(s) = \frac{(1 + sC_1 R_3)[1 + sC_2(R_1 + R_2)]}{sR_1 C_1 (1 + sC_2 R_2)} \qquad (3.9)$$

Internal to EASY5, the transfer functions are converted into state equations.

(a)   circuit implementation

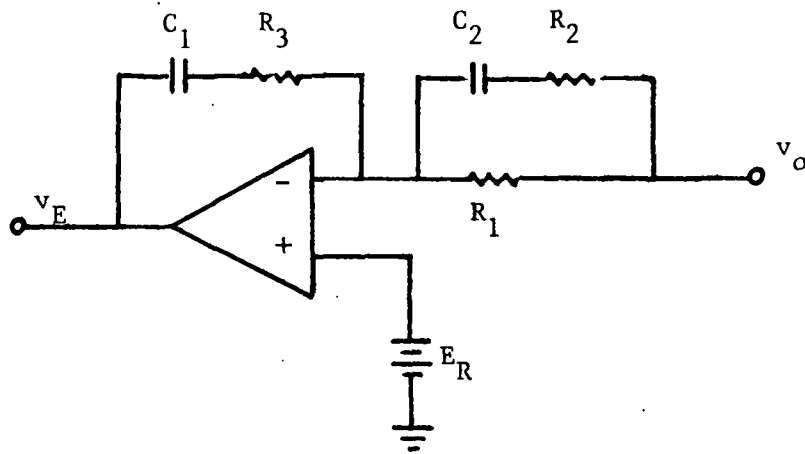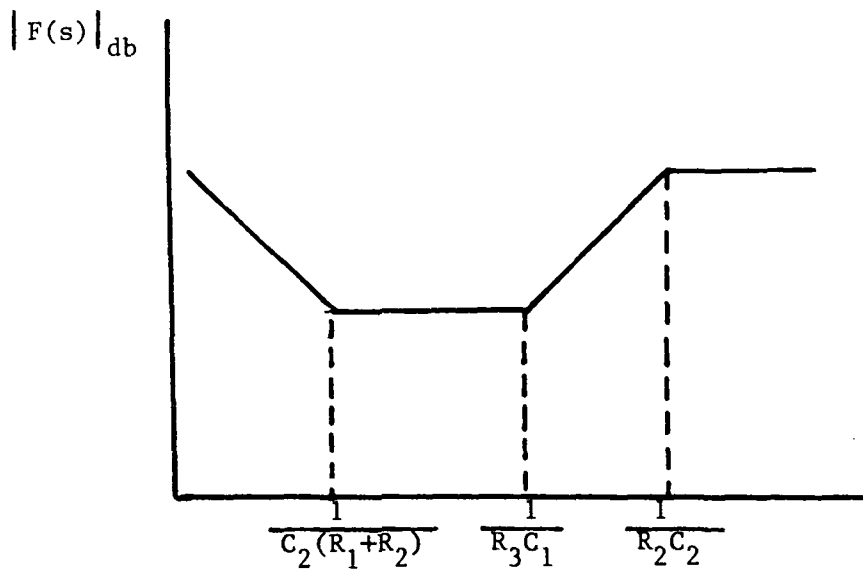(b) gain characteristic

Figure 3.6   Two-pole two-zero compensator

35

3.3.1.2 CURRENT-FEEDBACK MODULE

Two current feedback schemes are modeled; one is referred to as standardized control module (SCM), the other is current-injected control (CIC).

- [SM] --- Standardized control module(S.C.M)[11]

In SCM, as shown in Fig.3.7(a), voltage v_L across the energy-storage inductor is sensed through a transformer and is integrated, so that the integrated voltage (v_I) has the same shape as the ac component of the inductor current. That is, the transfer function from the inductor current to the output voltage of the current-feedback loop (v_I) is a simple gain. These relations are shown in the following:

$$v_{ac} = n \ L \ di_L/dt \qquad\qquad (3.11)$$

Taking the Laplace transform of equation (3.11)

$$v_{ac}(s) = n \ L \ s \ i_L(s) \qquad\qquad (3.12)$$

Since

$$v_I(s) = - \ v_{ac}(s)/(s \ C_1 R_4) \qquad (3.13)$$

from equations (3.12) and (3.13)

$$v_I(s)/i_L(s) = - \ n \ L/(C_1 R_4) \qquad\qquad (3.14)$$
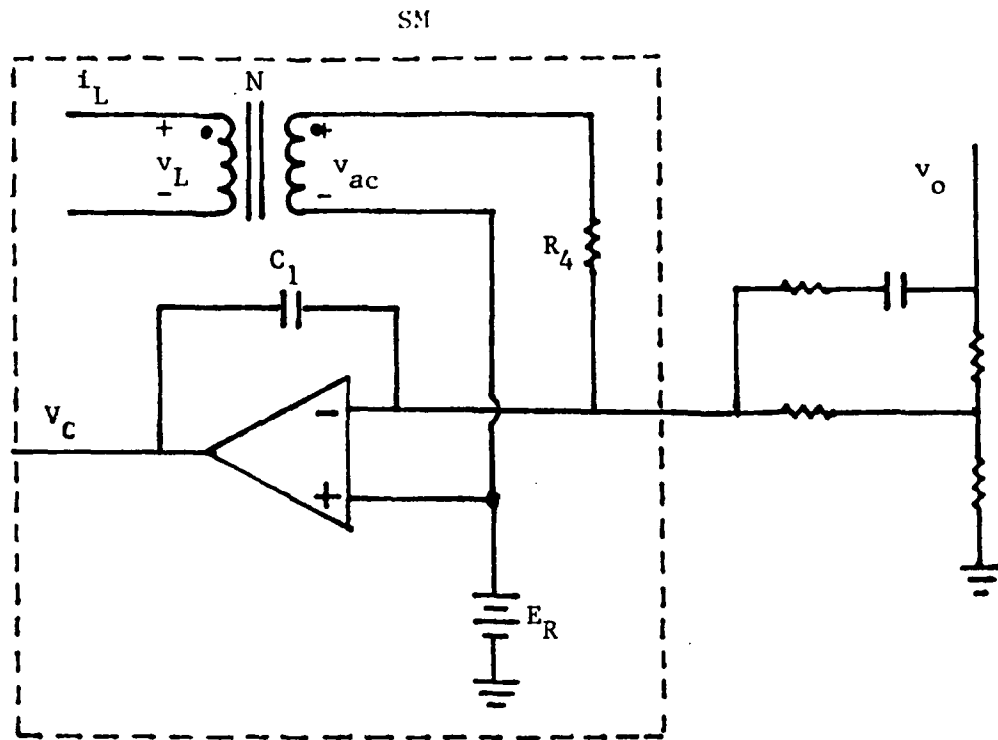
(a) SCM
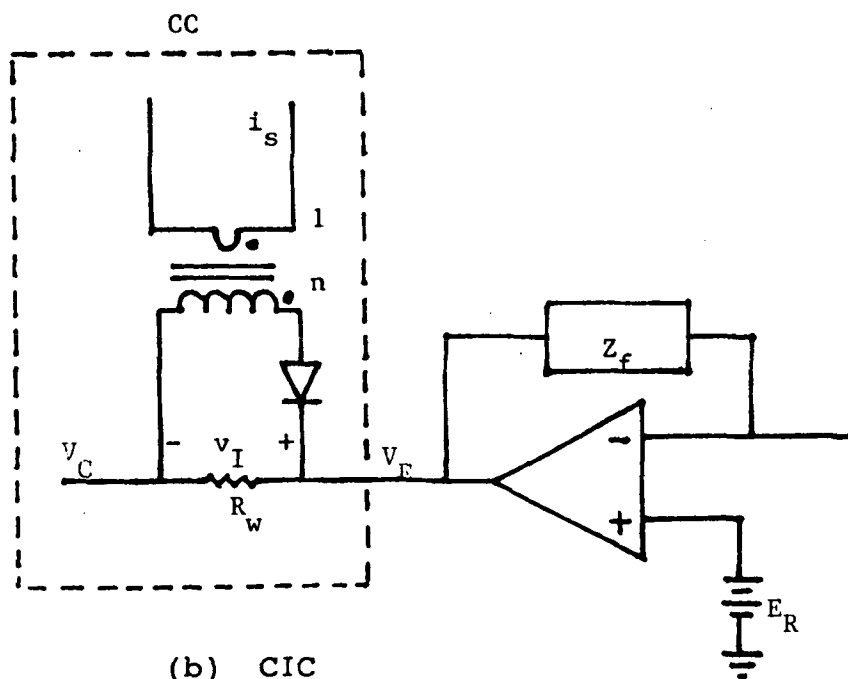
(b) CIC

Figure 3.7 Current-feedback module

37

As illustrated in Fig.3.7(a), the op-amp and capacitor C1 are common to both the current loop and the voltage loop. Thus, the control voltage (v_C) represents the total error voltage derived from both the current loop and the voltage loop.

- [CC] --- Current-injected control module(C.I.C)

In CIC, as shown in Fig.3.7(b), the switch current is sensed through a current transformer. The voltage drop across the current-sensing resistor (R_w) is proportional to the switch current as described in following equations.

$$i_i = i_s/n$$

$$
\begin{aligned}
v_I &= i_i R_w \\
&= \frac{R_w i_s}{n}
\end{aligned}
\qquad (3.15)
$$

Thus, the control voltage after summing the output voltages of both the current-loop and the voltage-loop becomes

$$v_C = - v_E - v_I \qquad (3.16)$$

3.4 DIGITAL SIGNAL PROCESSOR

The digital signal processor(DSP) converts the control signal v_C from the analog feedback controller into discrete-time pulses to control the ON-OFF of the power switch. The DSP includes the threshold detector (comparator), the ramp function and the latch circuit.

The threshold detector compares the control signal, v_C, and the reference signal (either dc or a ramp) to generate the trigger signal for the switch command. For the multiple loop control, the control signal, v_C, is the sum of the outputs from all feedback loops. In this case, the v_C waveform already includes a ramp function (proportional to the inductor current or the switch current). The external ramp function is optional, it is needed to stabilize the system operating at a constant frequency and a duty ratio greater than fifty percent. Figure 3.8 illustrates the PWM model for a constant-frequency control. For each different duty-ratio-control law, such as constant frequency, constant T_{ON} and constant T_{OFF}, the PWM model is different. These different modules are stored in the component module library, as in the case of power stage models.
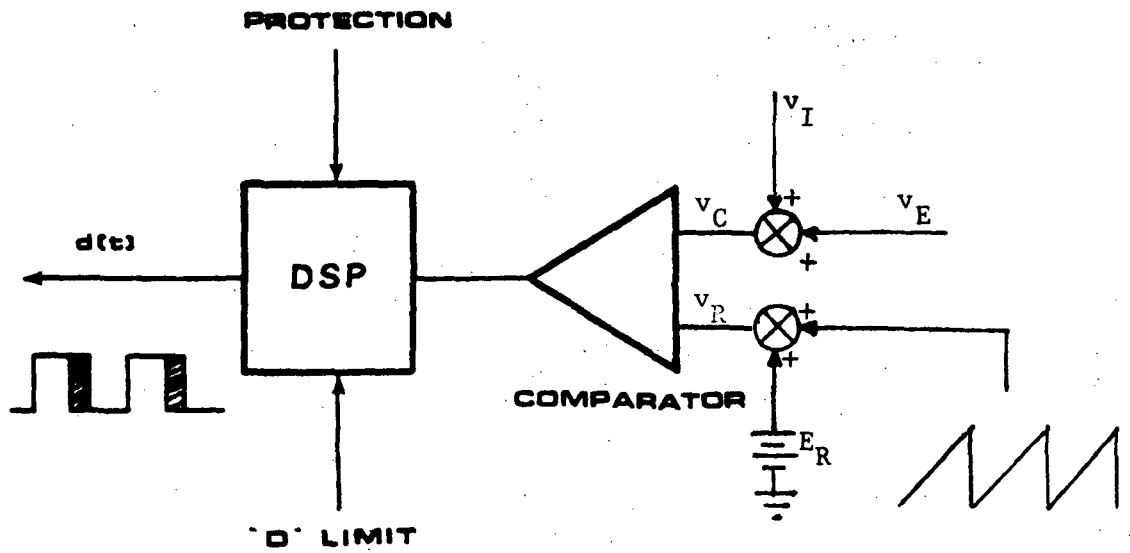
Figure 3.8 Pulse-width-modulator (PWM)

3.4.1 EASY5 MODEL FOR DIGITAL SIGNAL PROCESSOR

The digital signal processor is modeled according to its control law such as constant-frequency control--[WM], constant on-time control--[NN], and constant off-time control--[FF].

The protection functions are also included in the model, such as the peak-current limiter for power components and the converter shut-down in the event of sensed abnormalities such as over-voltage, under-voltage, or over-current beyond a predetermined and tolerable level. Nonlinearities, such as op-amp saturation and duty-cycle limiter, are also included in this module.

● [WM] ---- constant-frequency control

For a single-loop control model, as shown Fig.3.9(a), an external ramp is used to implement the duty-cycle signal and the frequency of the external ramp function is identical to the switching frequency. For two-loop control, as shown in Figs.3.9(b) and (c), the inductor-current or switch-current information determines the point at which the control voltage (v_C) intersects the reference voltage (v_R). The reference voltage (v_R) is simply a fixed threshold voltage (v_{TH}) when an external ramp is not used. If an external ramp is used to solve the instability problem, which occurred when the

41

(a) single-loop control

(b) SCM

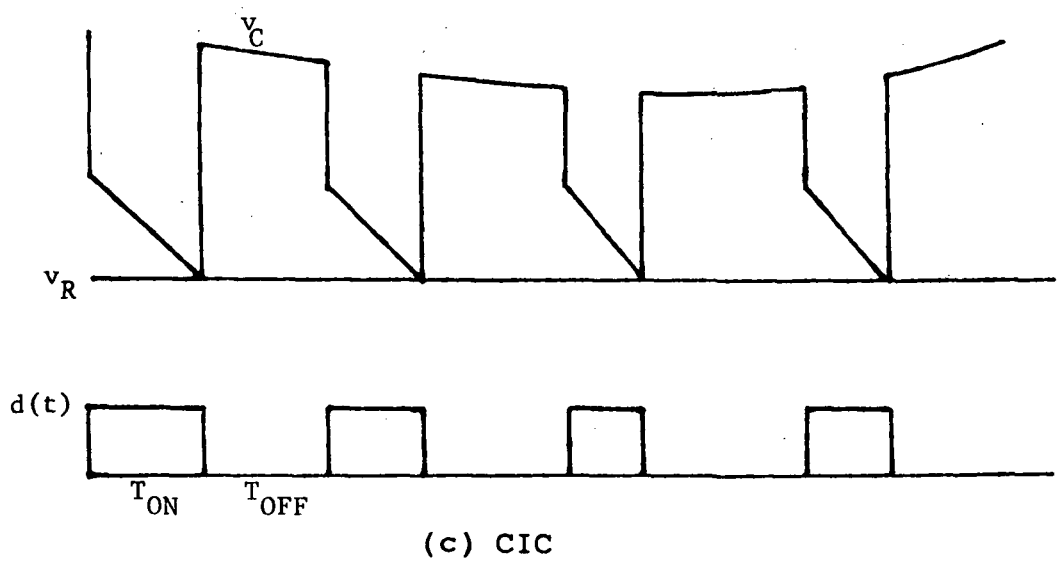(c) CIC
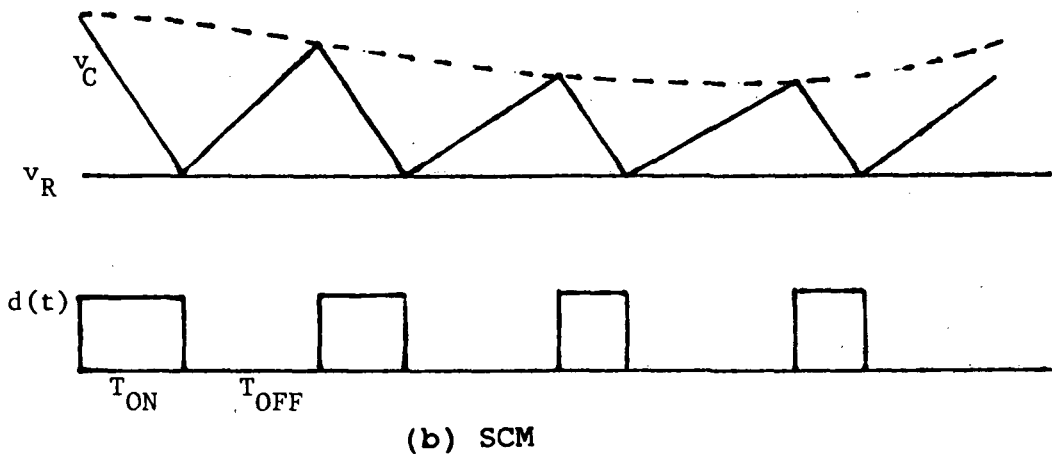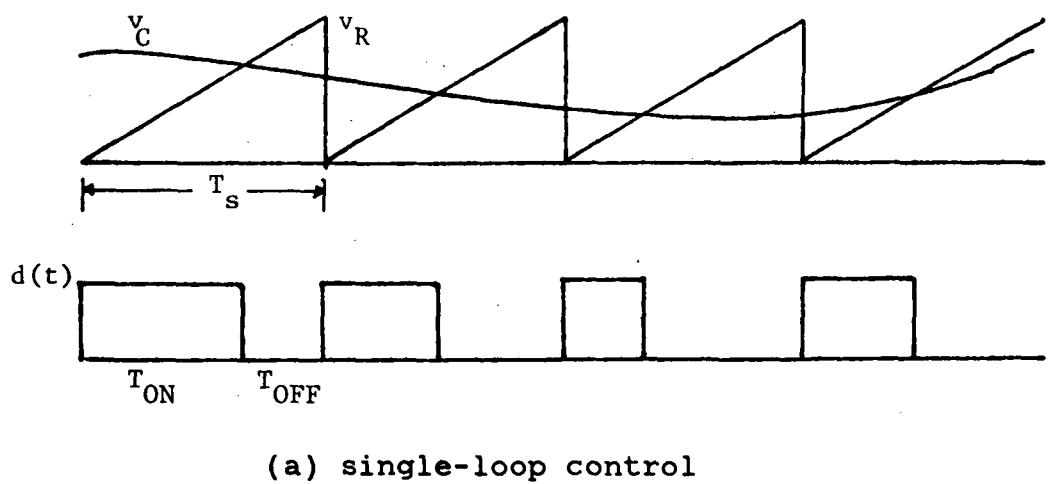
Figure 3.9 Constant-frequency control

42

duty ratio exceeds fifty percent[11], the reference voltage becomes the sum of the threshold voltage and ramp voltage.

The FORTRAN implementation of this module is shown in the flow diagram, Fig.3.10. It consists of four basic elements: the ramp-function generator, selection of the control method, comparator and protection. To generate the ramp function, a normalized time (T_N) is defined by using the EASY5 internal variable TIME.

$$T_N = (TIME + T_s)/ T_s$$

where T_s is the switching period. By subtracting integer N which is generated by the library function IDINT(T_N) from T_N, the normalized ramp function(T_N - N) is produced. Then the ramp function (V_{ramp}) is generated by multiplying the desired amplitude. These waveforms are shown in Fig.3.11.

Since this module can handle the single-loop control and multi-loop control (with or without external ramp function), one of these options is selected and the appropriate reference voltage(v_R) and control voltage(v_C) are assigned. The reference voltage and the control voltage are compared to determine the status of the switch according to the switching logic illustrated in Fig.3.9. Whenever one switching period ends, the switch is reset to the ON position and the process is repeated for the next cycle. Duty-cycle limiter and overcurrent-protection logic are included in this module.

43

$$T_N = (TIME + T_s)/T_s$$
$$N = NP$$
$$N = IDINT(T_N)$$
$$v_R = v_p(T_N - N)$$

single loop? or two loop

single loop

two loop

$$v_R = v_R + v_{th}$$
$$v_c = \quad - v_E$$

external ramp ?

no

yes

$$v_R = v_{th}$$
$$v_c = \quad - v_E - v_I$$

$$v_R = v_R + v_{th}$$
$$v_c = \quad - v_E - v_I$$

A

$$(T_N - N) < D_{max}$$

no

yes

SW = OFF

SW : ON ?

no

yes

$$v_R \geq v_o$$

no

yes

SW = OFF

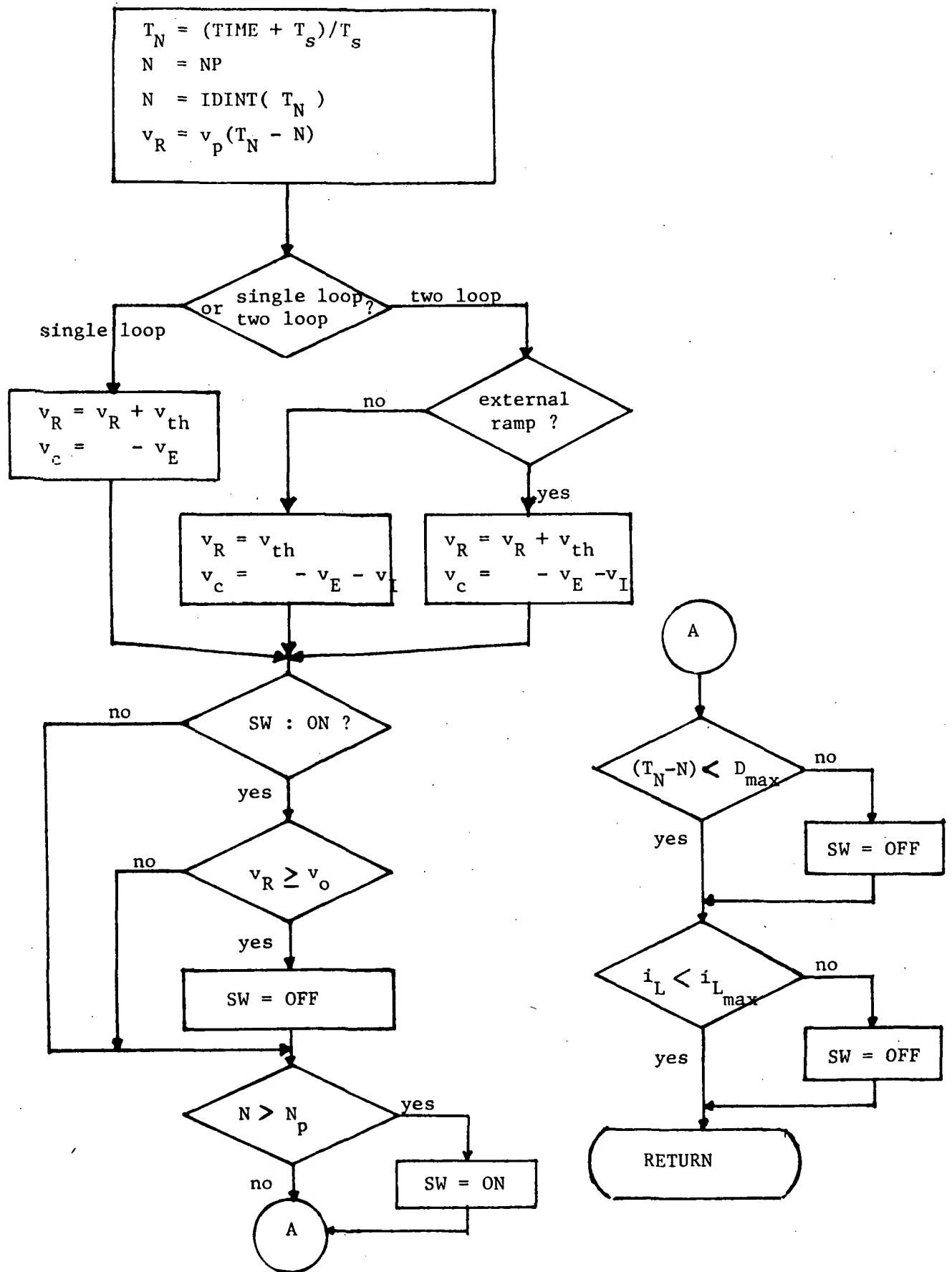$$i_L < i_{L_{max}}$$

no

yes

SW = OFF

$$N > N_p$$

yes

no

SW = ON

A

RETURN

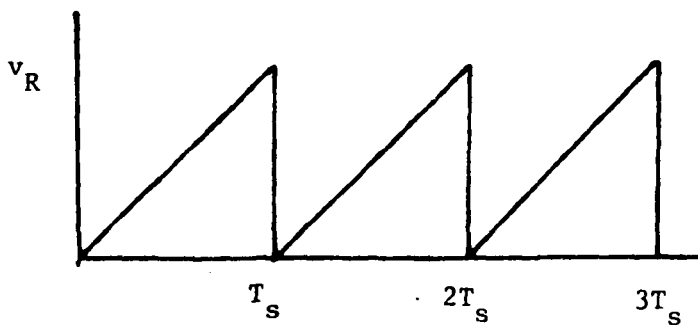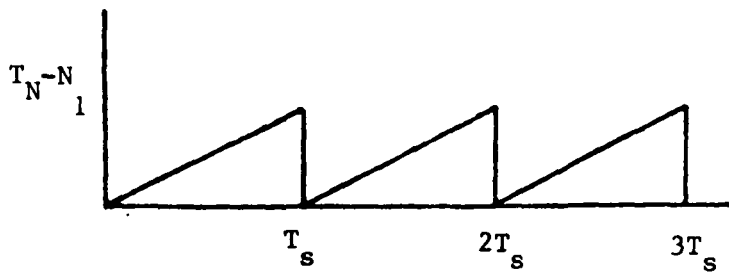Figure 3.10   Flow-chart for constant-frequency control

44
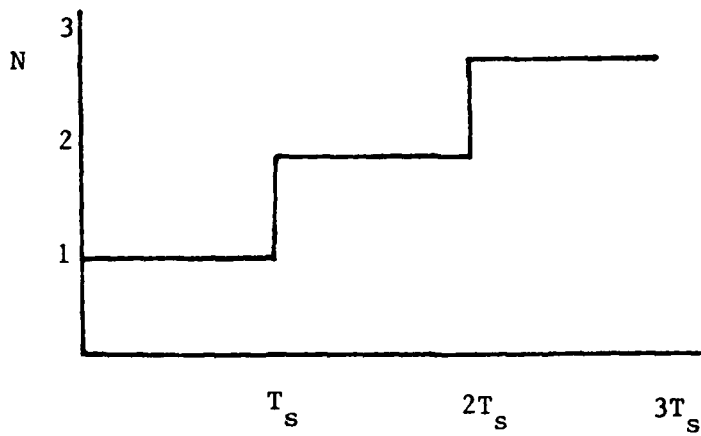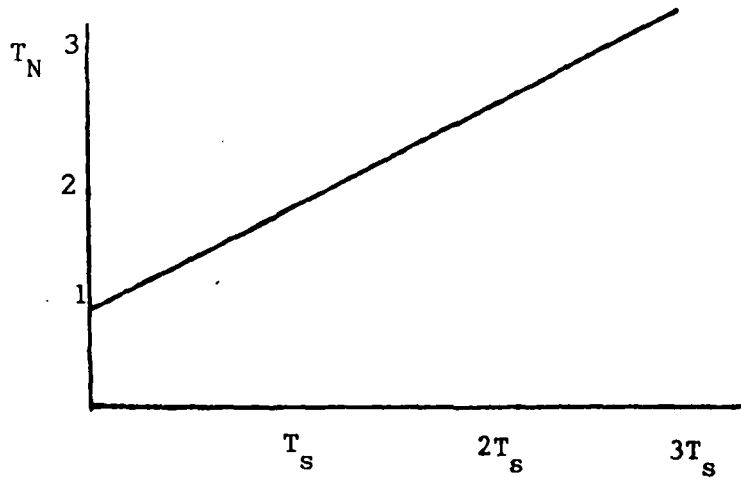
Figure 3.11   Ramp function generation

45

If any aforementioned abnormalities are sensed, the shut-down command will turn off the switch. The switch status (ON or OFF) determined in these processes, d(t), is transferred to the power stage to execute the corresponding state equations.

- [FF] ---- constant-OFF-time control

In the constant-OFF-time control, regulation is achieved by controlling ON-time interval T_{ON}. When the two-loop control is implemented, as shown in Fig.3.12(b), the intersection of the descending control voltage (v_C) with the threshold level marks the end of the ON-time interval. For the single-loop control, however, additional elements are required because the control voltage has only the output voltage information. One possible implementation is illustrated in Fig.3.12(a). An external ramp function is initiated at the end of the constant-off-time interval. The intersection of the control voltage with the ramp function determines the end of the ON-time interval.

In the EASY5 model, as shown in Fig.3.13, the control voltage, v_C, and the reference voltage, v_R, are determined according to the choice of the control technique, single-loop or two-loop control. If the switch is ON, those two voltages, v_C and v_R, are compared to determine the instant of turn off (T_C). Once the switch is turned OFF, it will remain for a pre-determined OFF-time interval (T_{OFF}). At the end
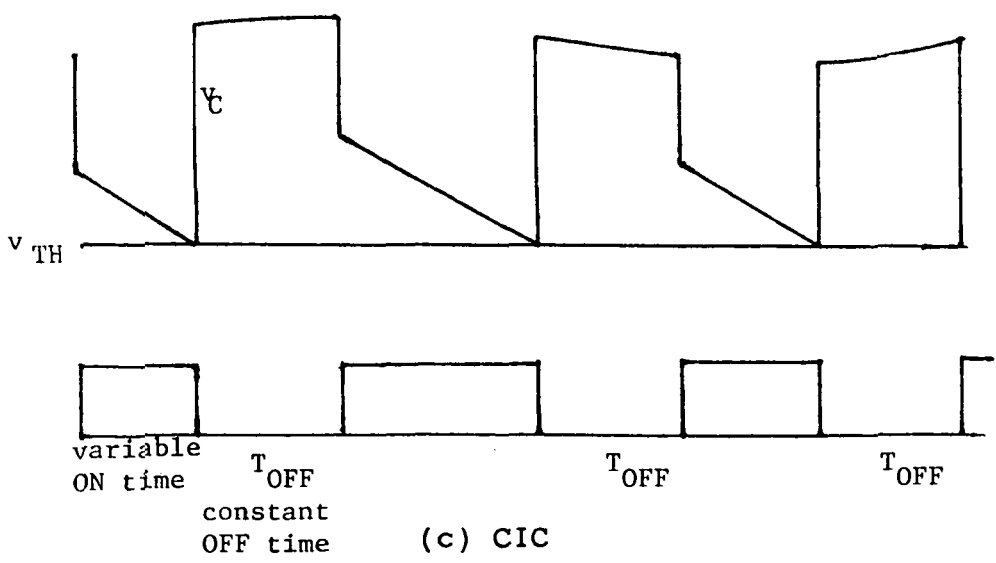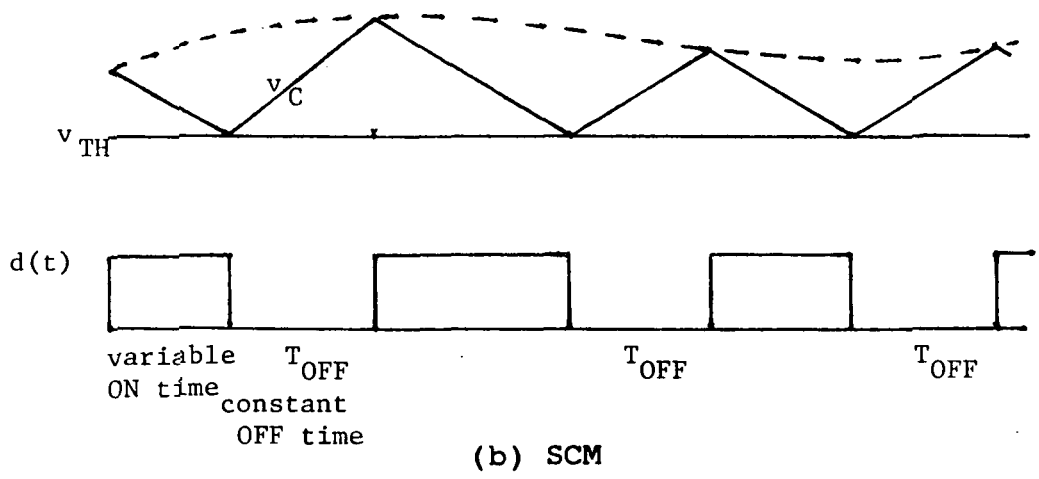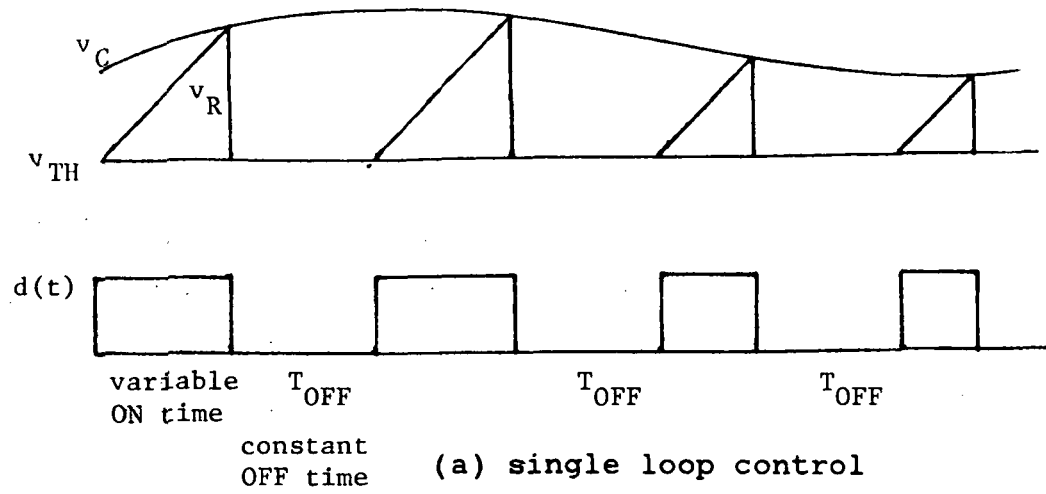
Figure 3.12　Constant OFF-time control

47

FF --- CONSTANT OFF TIME CONTROL
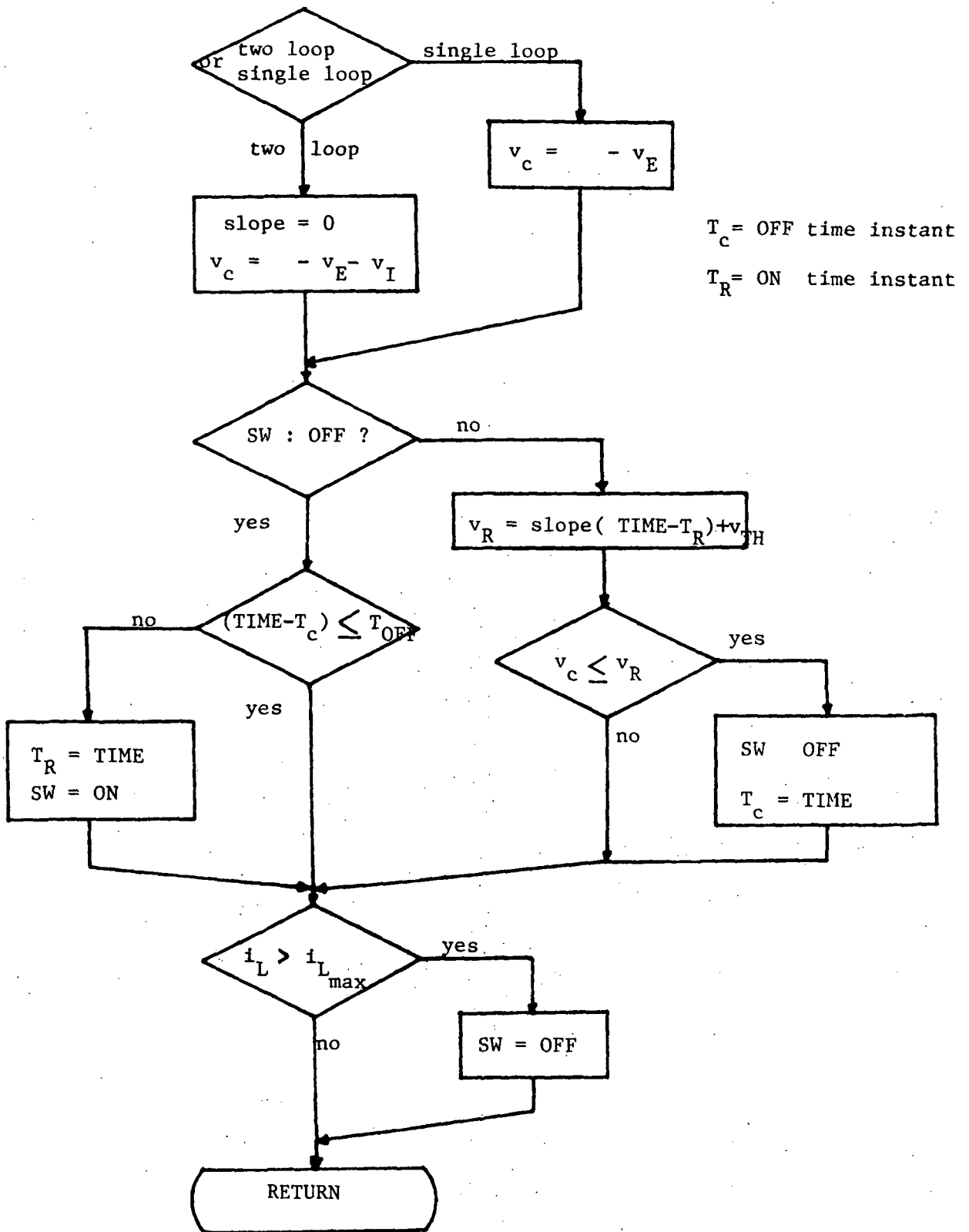
Figure 3.13 Flow-chart for constant OFF-time control

48

of the T_{OFF}, the switch is turned ON and the on-time instant (T_R) is reset.

- [NN] ---- constant-ON-time control

In constant-ON-time control, the output regulation is achieved by controlling the OFF-time interval. For two-loop control, as shown Fig.3.14(b), the intersection of the ascending control voltage with the threshold level marks the end of OFF-time interval T_{OFF}. For single-loop control, as shown in Fig.3.14(a), the intersection between the control voltage and descending ramp signal decides the turn-on instance. Figure 3.15 shows the flow chart of constant ON-time control module. In this module, control logic is basically the reverse of the constant-OFF-time control. Comparison between v_C and v_R occurs during OFF-time interval, and after a predetermined ON-time interval, the switch is turned off and the OFF-time instant (T_R) is reset.
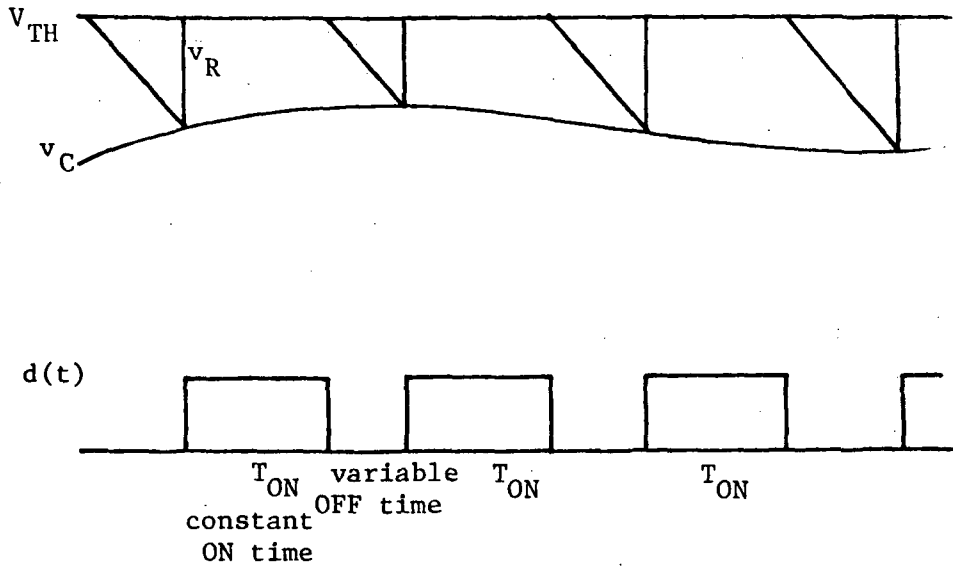
(a) single loop control
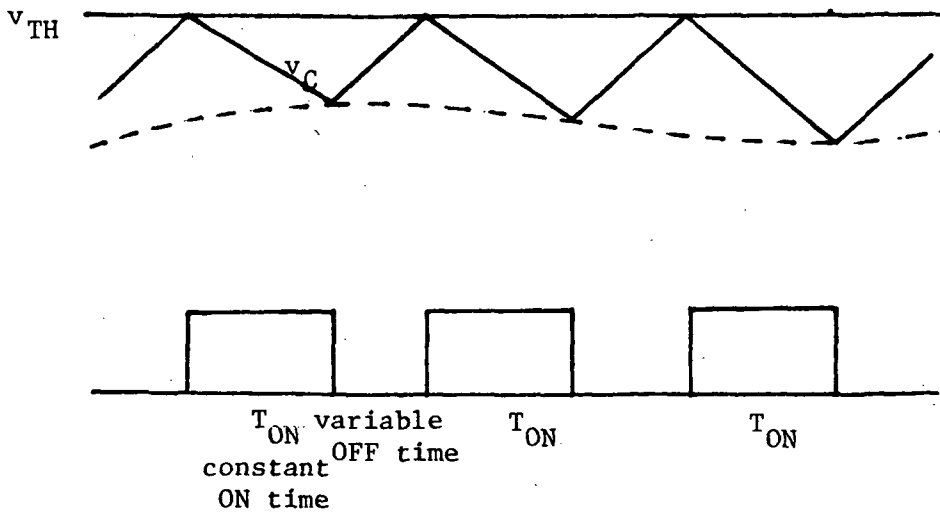
(b) SCM

Figure 3.14   Constant ON-time control
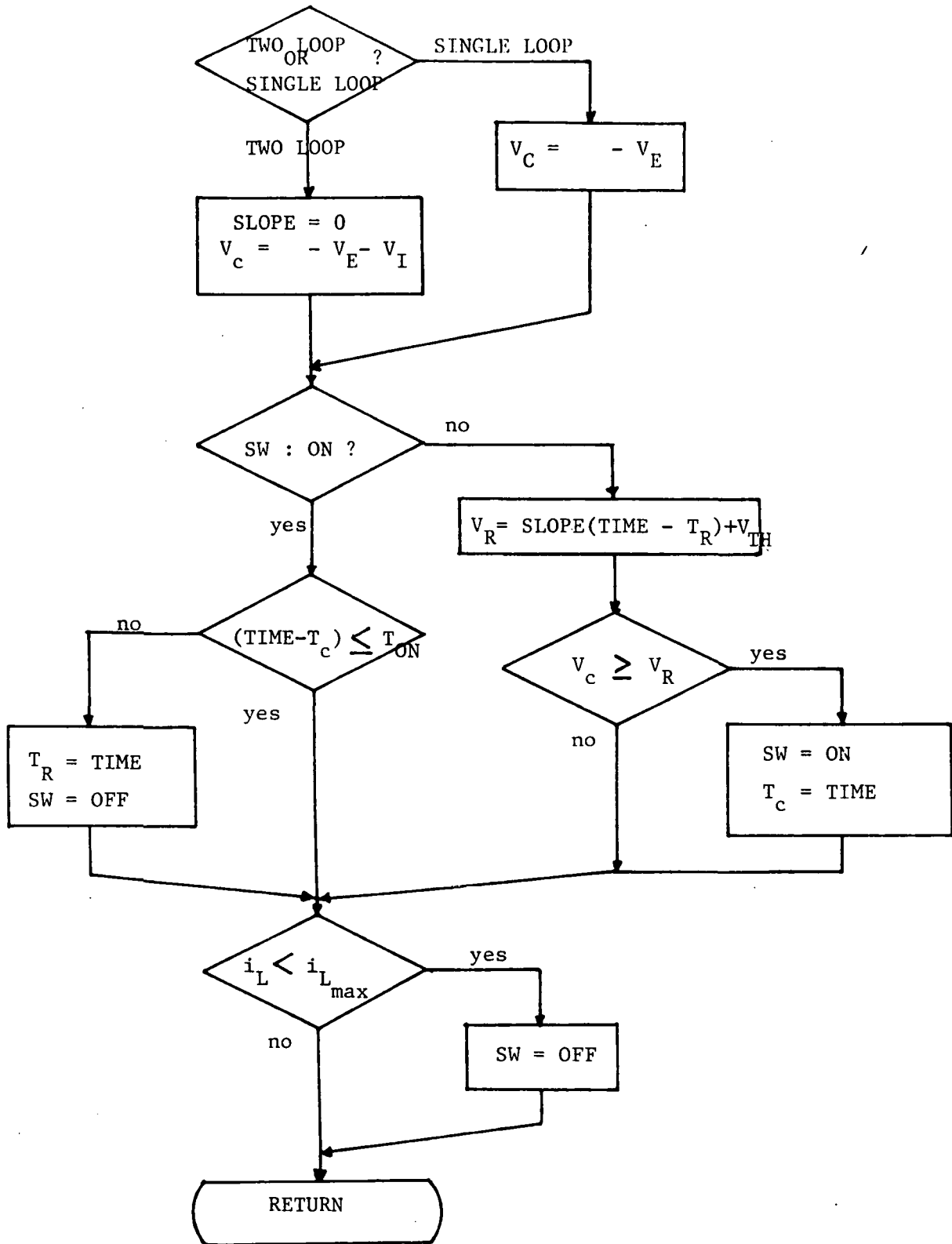
Figure 3.15   Flow-chart for constant ON-time control

51

3.5 SIMULATION EXAMPLES

Since a switching regulator is modeled as an unterminated component to give the maximum flexibility to configure a system, it is necessary to connect a load for the simulation. A simple LCR load model [LO] is developed, as shown in Fig.3.16.

The state equations are

$$\dot{i}_L = (v_1 - v_C) / L$$

$$\dot{v}_C = (i_L - v_C/R) / C$$
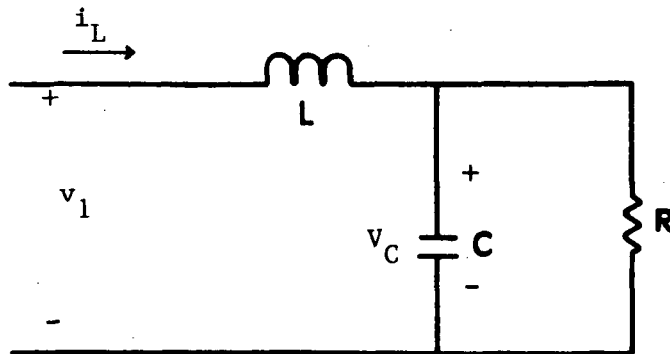
Figure 3.16   *LCR load*

As described in Section 3.1, a complete converter circuit can be configured by arbitrarily choosing a power stage, a analog feedback controller and a digital signal processor. To demonstrate the versatility of this modeling scheme, the following two examples are given:

• Example 1 : Buck regulator employing SCM feedback and a constant-OFF-time duty-cycle control

Following modules are selected to model a switching regulator system as shown in Fig.3.17.

[BC] --- buck power stage

[MP] --- compensator (two-pole one-zero)

[SM] --- SCM (current loop)

[FF] --- PWM (constant-OFF-time control)

[LO] --- load

The EASY5 Model Description Data [BUCKCF.MOD] is shown in Fig.3.18(a). It includes the calling of each module from the Macro-Module Library and the interconnections between the component modules. This is accomplished by matching the port quantities between the input port and the output port. According to the user supplied Model Description Data, the

53
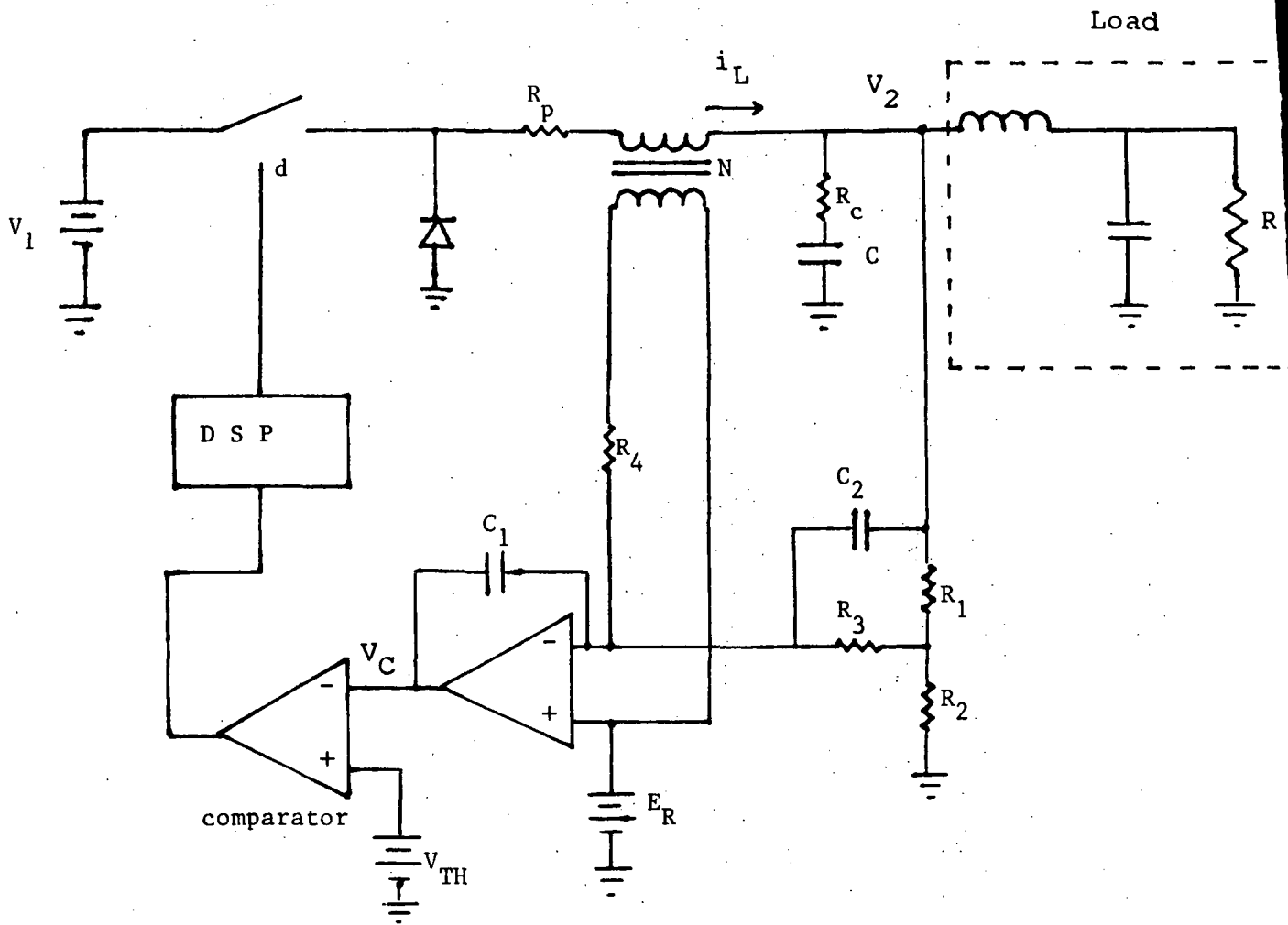
Figure 3.17   Buck regulator employing SCM

EASY5 Model-Generation Program generates the regulator circuit configuration (Fig.3.18(b)) and input data requirement list (Fig.3.19). Figure 3.20 shows the user's input Analysis Program that includes the parameter values, initial conditions of state variables, and various types of analysis commands. Figures 3.21(a)-(c) show the steady-state regulator responses such as the regulator output voltage, the inductor current, and the control voltage vs. threshold voltage. Transient responses when load resistance is increased ten percent at 1ms are shown in Figs.3.22(a)-(b).

```
**********************************************
*** BUCK LARGE SIGNAL(MODULAR APPROACH)
**********************************************
** REVISED 2/4/86
MACRO FILE NAME=MACROS
*LIST MACRO COMPONENTS=BC,LO,FF,SM,MP
MODEL DESCRIPTION
LOCATION=12,BC,  INPUTS=LO(IL=I2),FF(Q=IQ)
LOCATION=17,LO,  INPUTS=BC(V2=V1)
LOCATION=34,SM, INPUTS=BC(VL=VL)
LOCATION=36,MP, INPUTS=BC(V2=VO)
LOCATION=43,FF, INPUTS=SM(VI=VI),MP(VE=VE),BC(IL=IL)
END OF MODEL
PRINT
```

Figure 3.18(a)   User input model description data
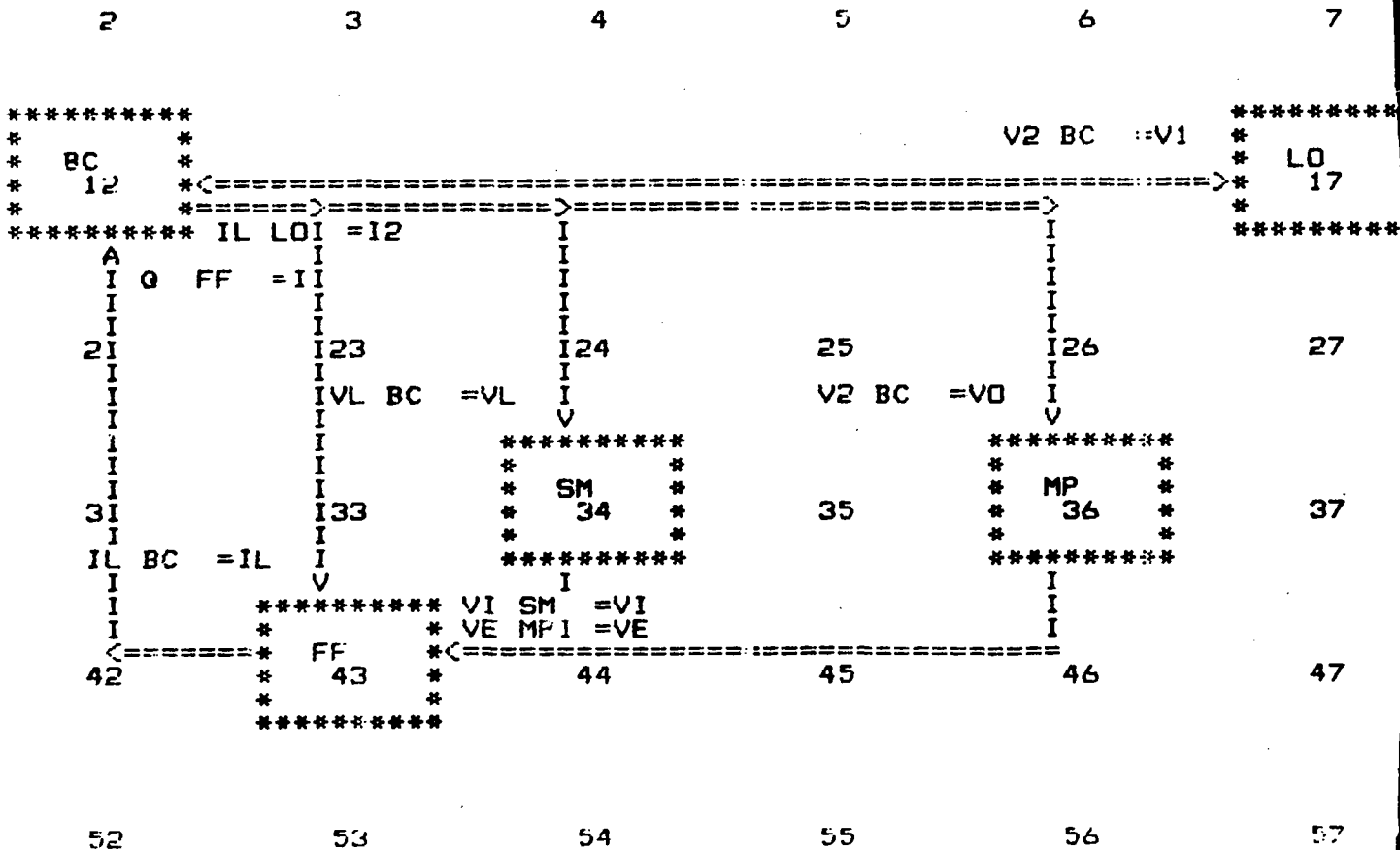
[BUCKCF.MOD]

Figure 3.18(b)   EASY5 generated model configuration

[BUCKCF.MGL]

56

INPUT DATA REQUIREMENTS LIST

PARAMETERS REQUIRED

PARAMETER NAME (AND DIMENSION DATA FOR VECTOR AND MATRIX PARAMETERS)

COMPONENT					
BC	RL BC	RC BC	L BC	C BC	V1 BC
LO	RA LO	TC LO	RE LO	L LO	C LO
SM	NV SM	C SM	R SM		
MP	WA MP	WB MP	K MP	ER MP	GA MP
FF	TI FF	VP FF	VTHFF	ER FF	CICFF
	EPSFF	TOFFF	ILMFF		
	SCMCF				

STATES (INITIAL CONDITIONS AND ERROR CONTROLS REQUIRED)

STATE NAME (AND DIMENSION DATA FOR VECTOR AND MATRIX STATES)

COMPONENT		
BC	IL BC	VC BC
LO	IL LO	VC LO
SM	VI SM	
MP	X1 MP	VE MP

Figure 3.19 Input data requirement list [BUCKCF.MGL]

57

```
TITLE=BUCK, SCM CONST OFF TIME(LARGE SIGNAL)
*REVISED 1/24/86
**BC (POWER STAGE)
INITIAL CONDITIONS
IL BC=10, VC BC=20
PARAMETER VALUES
L   BC=250E-6, C   BC=400E-6
RL  BC=1E-2, RC BC=1E-2
V1 BC=28
**VCG LOOP COMPENSATER
K   MP=.3, ER MP=6
GA MP=4488, WA MP=628, WB MP=1E5
** CURRENT LOOP(SCM)
NV SM=.08, C   SM=7.275E-9, R   SM=3.44E3
** PWM
TI FF=20E-6, VP FF=0, VTHFF=.5
ER FF=6, CICFF=0, SCMFF=1
TOFFF=10E-6, EPSFF=1E-5
ILMFF=15
** LOAD
RA LO=2, RB LO=2.2, TC LO=100E-3
L   LO=1E-6, C   LO=1E-6
INITIAL CONDITIONS
VE MP=0
IL LO=10, VC LO=20
PRINTER PLOTS
ONLINE PLOTS
INT MODE=4
DISPLAY1
V2 BC
DISPLAY2
IL BC
DISPLAY4(OVERPLOT)
VR FF, VC FF
TMAX=10E-3, TINC=5E-7
PRATE=200, OUTRATE=20
*PRATE=100, OUTRATE=4
SIMULATE
XIC-X
PARAMETER VALUES
RB LO=2.2
TC LO=222E-3
DISPLAY1
V2 BC
DISPLAY2
IL BC
DISPLAY4(OVERPLOT)
VR FF, VC FF
TMAX=100E-6, TINC=2E-7
PRATE=10, OUTRATE=5
SIMULATE
XIC-X
PARAMETER VALUES
TC LO=1E-3
DISPLAY1
V2 BC
DISPLAY2
IL BC
DISPLAY3
VL BC, VM SM
DISPLAY4(OVERPLOT)
VR FF, VC FF
TMAX=6E-3, TINC=2E-7
PRATE=200, OUTRATE=10
SIMULATE
```

Figure 3.20   User input analysis program

[BUCKCF.ANC]

58

(a)

(b)

(c)

Figure 3.21   Buck converter steady-state response
              (SCM, constant OFF-time control)

(a)   output voltage v_2

(b)   inductor current i_L

(c)   comparator input voltages v_C & v_R

59

Figure 3.22   Buck converter step-load response
               (SCM, constant OFF-time control)

(a)   load resistance R
(b)   output voltage v_2
(c)   inductor current i_L

60

• Example 2 : Buck/boost (Flyback) regulator employing CIC
   and a constant-frequency control

Following modules are selected to model the circuit shown in
Fig.3.23.

   [FB] --- buck/boost power stage

   [MP] --- compensator (two-pole one zero)

   [CC] --- CIC (current-feedback loop)

   [WM] --- PWM (constant-frequency control)

   [LO] --- load

The EASY5 Model description data and the EASY5 generated
system configuration are shown in Fig.3.24(a) and (b), re-
spectively. The input data requirement list is shown in
Fig.3.25. Figure 3.26 is the user input Analysis Program
list. Figures 3.27(a)-(c) show the simulation results at
steady state. Transient responses when load resistance is
decreased ten percent at 1ms are shown in Figs.3.28(a)-(b)
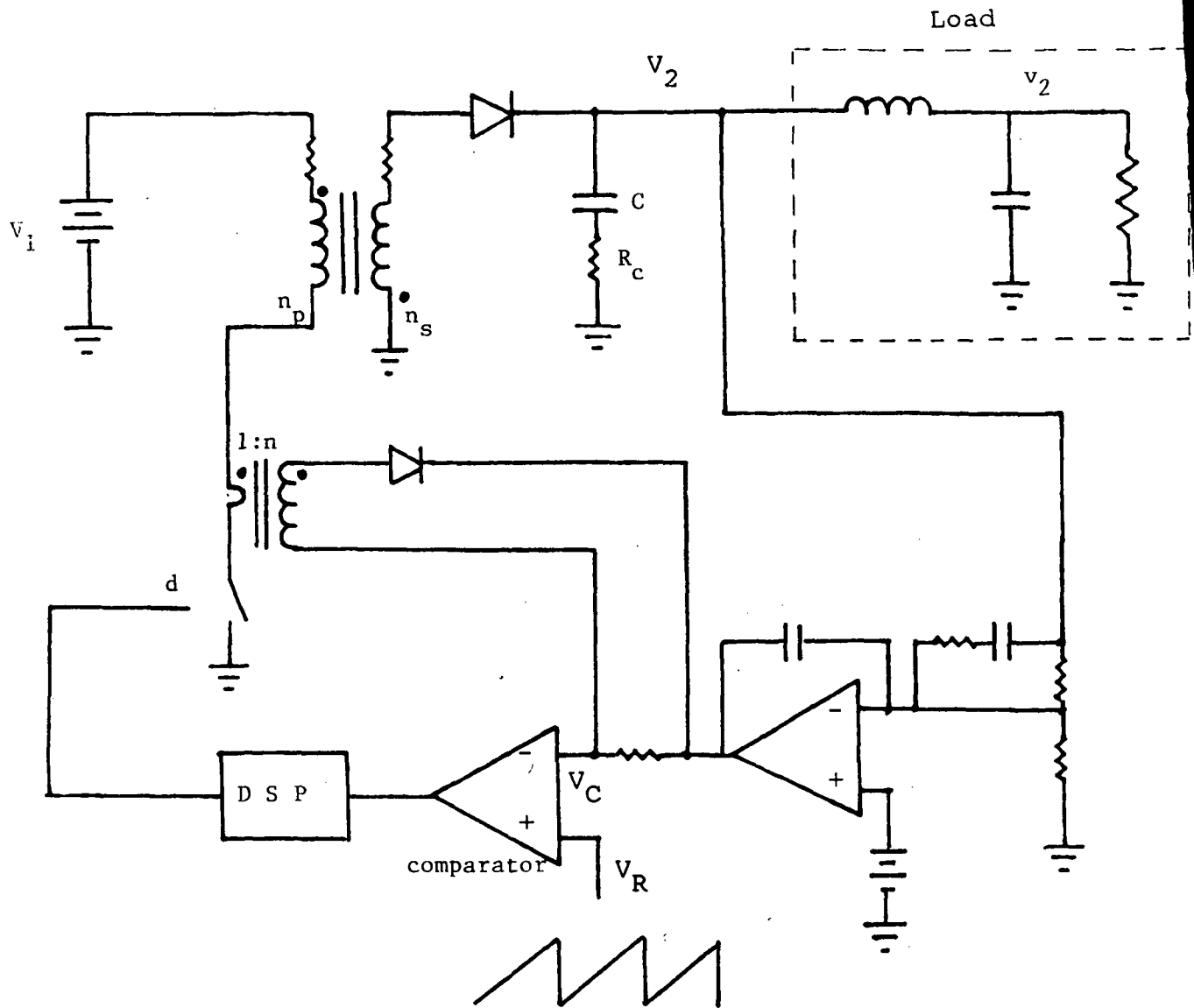
Figure 3.23   Flyback converter employing CIC

```
********************************************
** FLYBACK LARGE SIGNAL(MODULAR APPROACH)
********************************************
** REVISED 12/8/85
MACRO FILE NAME=MACROS
#LIST MACRO COMPONENTS=FB,LO,CC,SM,MP,WM
MODEL DESCRIPTION
LOCATION=12,FB,INPUTS=LO(IL=I2),WM(IQ=QQ)
LOCATION=17,LO,INPUTS=FB(V2=V1)
LOCATION=34,CC,INPUTS=FB(PHI=IL)
LOCATION=36,MP,INPUTS=FB(V2=VO)
LOCATION=43,WM,INPUTS=CC(VI=VI),MP(VE=VE)
END OF MODEL
PRINT
```

Figure 3.24(a)   [FLYBCK.MOD]

63

Figure 3.24(b)   [FLYBCK,MGL]

INPUT DATA REQUIREMENTS LIST

PARAMETERS REQUIRED

PARAMETER NAME (AND DIMENSION DATA FOR VECTOR AND MATRIX PARAMETERS)

COMPONENT					
FB	RS FB / LP FB	RC FB / NP FB	LS FB / VI FB	NS FB / RP FB	C FB
LO	RA LO	TC LO	RE LO	L LO	C LO
CC	NP CC	LP CC	RW CC	NI CC	
MP	WA MP	WB MP	K MP	ER MP	GA MP
WM	TI WM / SCMWM	VP WM	VG WM	ER WM	CICWM

STATES (INITIAL CONDITIONS AND ERROR CONTROLS REQUIRED)

STATE NAME (AND DIMENSION DATA FOR VECTOR AND MATRIX STATES)

COMPONENT		
FB	PHIFB	VC FB
LO	IL LO	VC LO
MP	X1 MP	VE MP

Figure 3.25   [FLYBCK.MGL]

```
TITLE=FLYBACK,CIC(LARGE SIGNAL)
*REVISED 12/8/85
**FB (POWER STAGE)
INITIAL CONDITIONS
PHIFB=.8E-4,VC FB=5.2
PARAMETER VALUES
RS FB=.013,RC FB=.007,LS FB=82.6E-6
NS FB=10,C  FB=330E-6,RP FB=.02
LP FB=400E-6,NP FB=22,V1 FB=23
**VTG LOOP COMPENSATER
K  MP=1,ER MP=5.2
GA MP=952.4,WA MP=348.8,WB MP=13270
** CURRENT LOOP(SCM)
*NV SM=.08,C  SM=7.275E-9,R  SM=3.44E3
** CURRENT LOOP(CIC)
RW CC=53.6,NI CC=100
NP CC=22,LP CC=400E-6
** PWM
TI WM=20E-6,VP WM=0,VQ WM=5.2
ER WM=5.2,CICWM=1,SCMWM=0
** LOAD
RA LO=1.69,RB LO=1.5,TC LO=100E-3
L  LO=1E-6,C  LO=1E-6
INITIAL CONDITIONS
VE MP=-2.54
IL LO=3.077,VC LO=5.2
PRINTER PLOTS
ONLINE PLOTS
INT MODE=4
DISPLAY1
V2 FB,PHIFB
DISPLAY2
IP FB,IS FB
DISPLAY3
PHIFB
DISPLAY4(OVERPLOT)
VR WM,VT WM
TMAX=5E-3,TINC=5E-7
PRATE=500,OUTRATE=10
*PRATE=100,OUTRATE=4
SIMULATE
XIC-X
PARAMETER VALUES
TC LO=222E-3
DISPLAY1
V2 FB
DISPLAY2
IP FB,IS FB
DISPLAY4(OVERPLOT)
VR WM,VT WM
TMAX=80E-6,TINC=2E-7
PRATE=50,OUTRATE=2
*SIMULATE
XIC-X
PARAMETER VALUES
TC LO=1E-3
DISPLAY1
V2 FB
DISPLAY2

DISPLAY3
PHIFB
DISPLAY4(OVERPLOT)
VR WM,VT WM
TMAX=5E-3,TINC=2E-7
PRATE=200,OUTRATE=5
SIMULATE
```
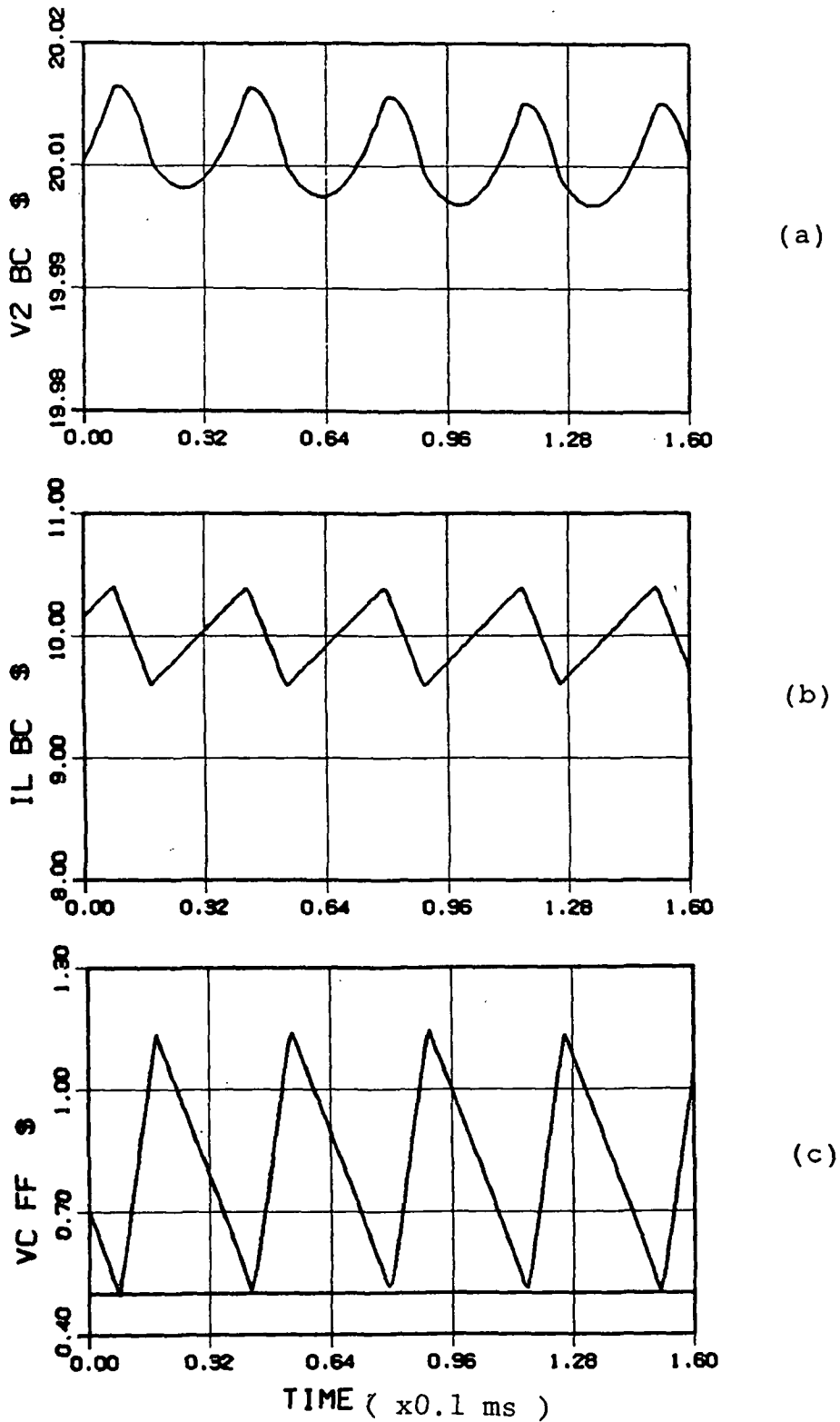
Figure 3.26 [FLYBCK.ANC]
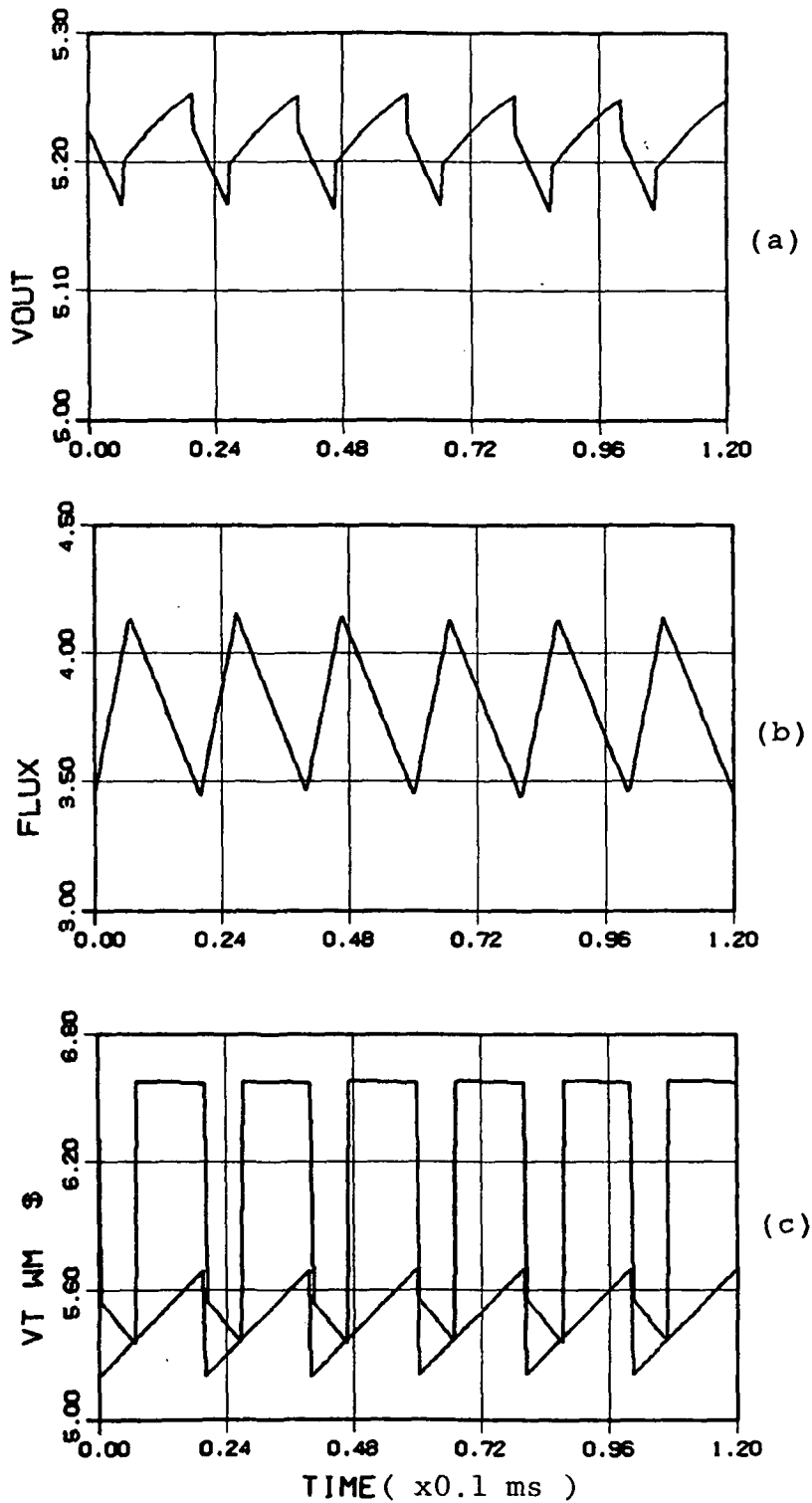
Figure 3.27 Flyback converter steady-state response
(CIC, constant frequency control)

(a) output voltage v_2

(b) inductor current i_L
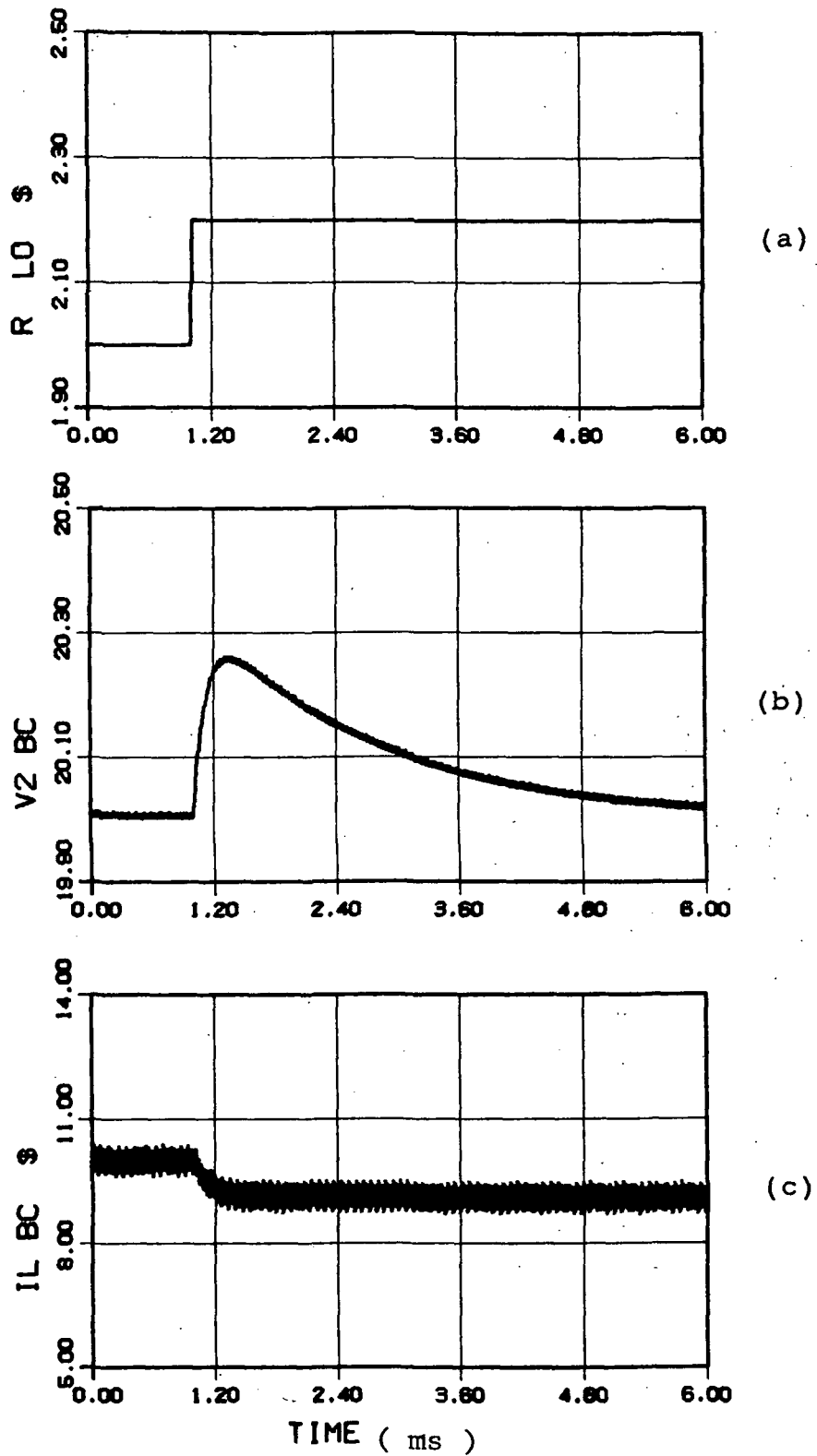
(c) comparator input voltages v_C & v_R

67
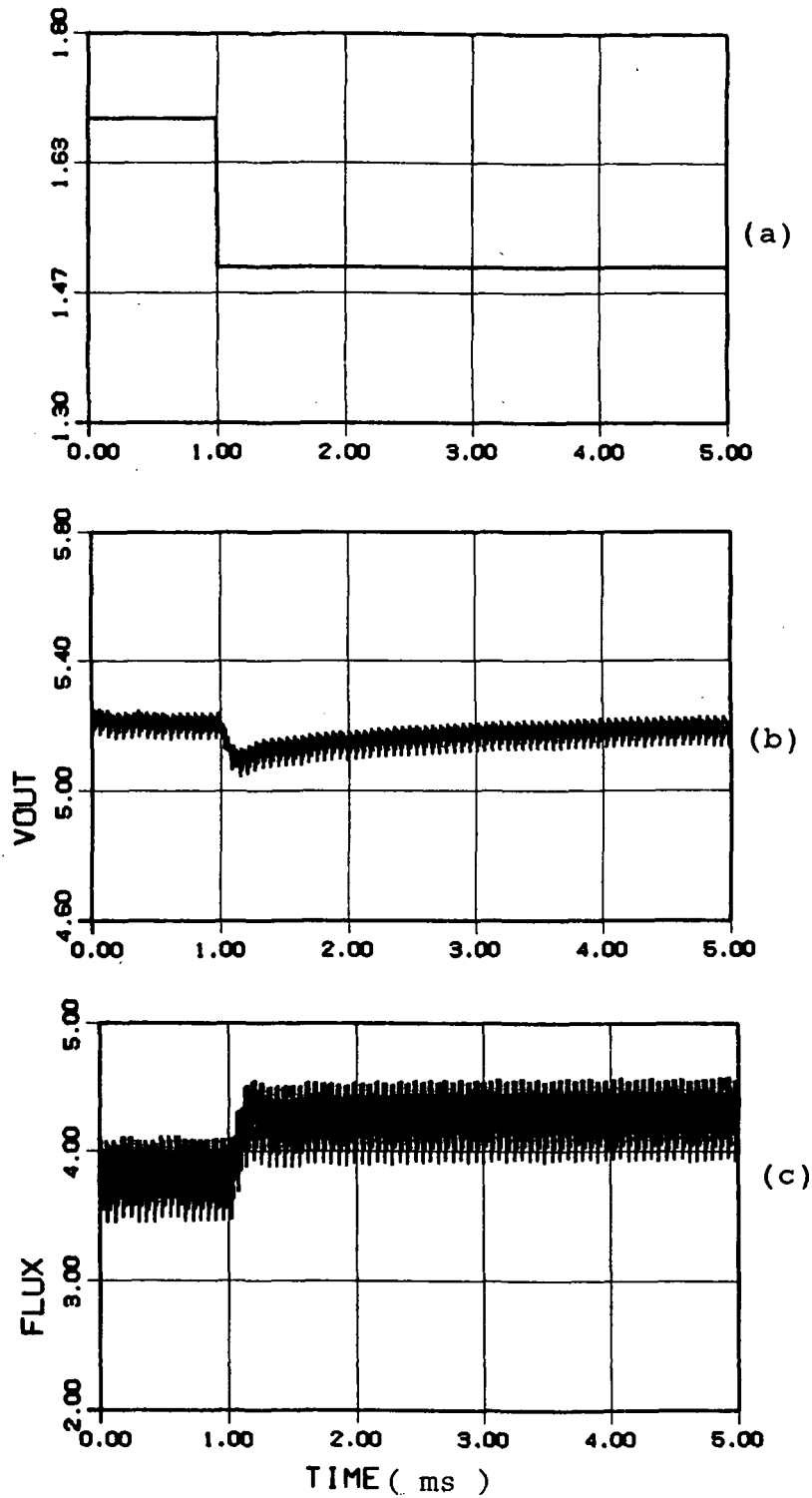
Figure 3.28 Flyback converter step-load response
(CIC, constant frequency control)

(a) load resistance R
(b) output voltage v_2
(c) flux ϕ

68

CHAPTER 4

SOLAR ARRAY MODELING

4.1 SOLAR ARRAY MODEL

4.1.1 INTRODUCTION

Solar arrays, made of silicon solar cells, are the main source of electrical power for spacecraft power systems. Because the individual silicon cell used on these arrays is small and produces very little power, many solar cells are connected in series and parallel combination to provide necessary power to the spacecraft.

Several approaches have been proposed for modeling a solar array [3]. First, it is possible to model an array by an interconnection of individual solar cells (individual cell model approach). Advantages of this approach are: the parameters for the individual cell model are readily obtained using established measurement and calculation procedures and the effects of parameter variation can be easily included. Shadowing effects, as well as cell faults, can easily be inserted into the array. However, the major disadvantage of this approach is that an extremely large amount of computation time is required which might easily exceed the total computer capacity.

Another approach is to use a single-cell model to simulate the entire array (macro model approach). The major advantage of this approach is the ability to minimize computer time and

memory space needed to analyze array behavior. Parameters can be obtained by incorporating the measurement/calculation of the individual cells and their interconnection scheme or simply by making terminal measurements of the array itself. Neither of these methods takes much more effort than would be needed for the individual cell model. One disadvantage of the macro model approach is a new set of macro model parameters needs to be developed for each different array configuration. This tends to make the model less flexible than desired. Furthermore, shadowing and individual cell faults cannot be easily included in the macro model without, again, a redevelopment of model parameters.

An approach which uses a combination of the macro model and the individual cell model could be very advantageous. This approach retains the flexibility of the individual cell model approach while reducing the necessary computer time and capacity. Any fault that occurs in an individual cell can be simulated. Shadowing effects can be accounted for in much the same way as would be done in the individual model. Sensitivity of parameters can also be easily analyzed by varying individual cell parameters. The disadvantage of using the combination model is the need to determine at least two sets of model parameters -- one set for the group of individual cells and one set for the group of macro models.

The choice of modeling approaches depends on the particular modeling objective(s). In the present study, the macro

model approach, shown in Fig.4.1, is used for an overall system analysis. With this type of analysis, it is presumed that the solar array model need not have great detail.

SOLAR ARRAY DC MODEL

For this study, two types of dc models are generated: the analytical macro model and the empirical data model. For the solar array's analytical macro model, the standard solar cell dc model, shown in Fig.4.2, is used [4]. It provides very good first order predictions of the dc behavior of the silicon cell. Literature is available for determining its parameter values. An analytical expression that describes the terminal characteristics of the solar cell model in Fig.4.2 is

$$I_o = I_g - I_{do} [\exp \{ Q (V_0 + I_o \cdot R_s) / kT \} - 1]$$
$$- (V_o + I_o \cdot R_s) / R_{sh} \qquad (4.1)$$

I_o = current output of the cell

I_g = light-generated current

I_{do} = reverse saturation current

Q = magnitude of the electronic charge

k = Boltzmann constant

T = absolute temperature

V_o = output voltage at the cell terminals

R_s = series resistance

R_{sh} = shunt resistance

71
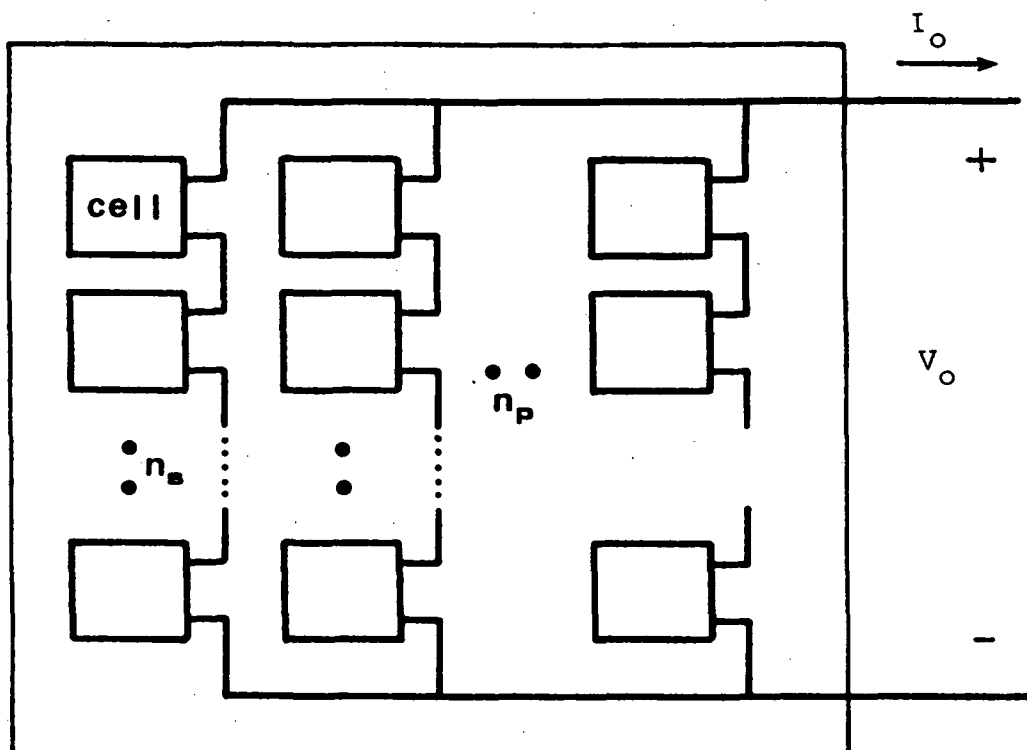
Fig.4.1 Solar Array Macro Model
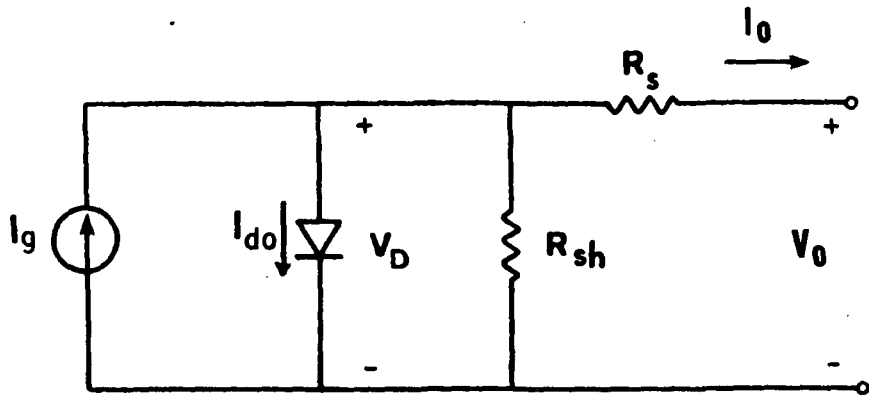
Fig.4.2 DC Model of Solar Cell
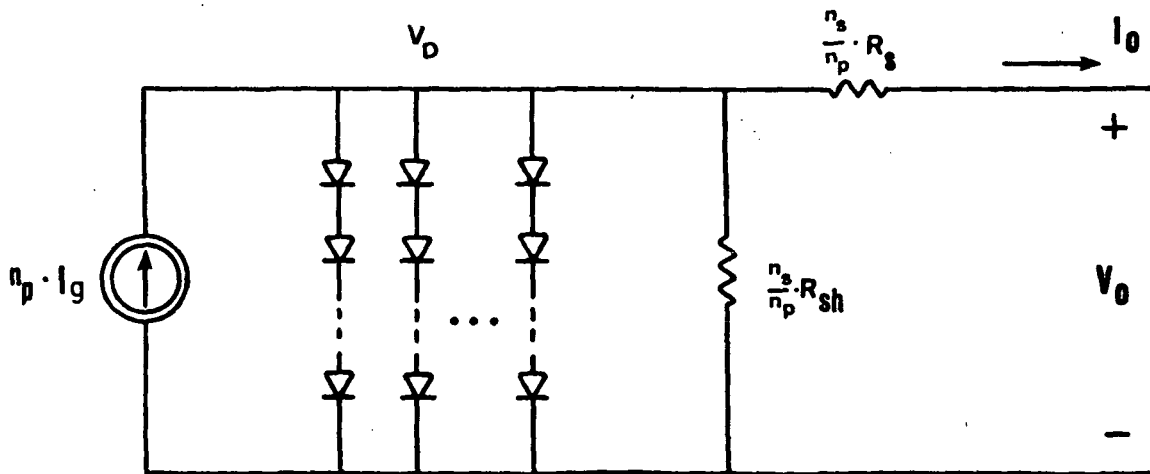
Fig.4.3 DC Macro Model of Solar Array

73

Based on the cell model, a solar array macro model is constructed by assembling solar cells in parallel and series connections as shown in Fig.4.1. In Fig.4.3, the resulting equivalent circuit model is illustrated where its elements are lumped parameters and functions of the number of cells in series, n_s, and the number of parallel strings, n_p.

The analytical expression for the terminal I-V characteristic of the solar array model in Fig.4.3 is then

$$I_o = n_p [I_g - I_{do} \{ EXP (Q (V_o / n_s + I_o \cdot R_s / n_p) / kT) \}$$
$$- (V_o / n_s + I_o \cdot R_s / n_p) / R_{sh}] \qquad (4.2)$$

From Equation (4.2), the solar array operating conditions are set by the load power demand and the shunt regulator's limiting voltage. Other more elaborate, analytical dc models exist, such as multiple-element models which include second order effects [5]. The multiple-element models are used to accurately model the effects of distributed series resistance, complex voltage dependencies and radiation. Due to the complexities of the model it is not practical to incorporate these second order effects in the system study.

The second model generated for this study is based on empirical data about the solar array terminal I-V characteristics. The solar array illumination level and temperature can be chosen as the independent variables. Based on four-dimensional empirical data, both linear and high-order interpolation techniques are employed to define the array I-V

74

characteristic curve for any arbitrary temperature and illumination. Figure 4.8, in Section 4.1.4, shows the interpolated I-V characteristics based on two interpolated empirical data curves for two different illumination levels. In these data, temperature is assumed constant. Other dependent variables for the array characteristics can be added provided their effects can be accounted for by the measurement. If the measurement data is available, this approach is simple and accurate.

4.1.2 MODEL GENERATION [AR]

Equation (4.2) can be rewritten as following.

$$I_o = n_p [I_g - I_{do} \{ EXP (k_o (V_o / n_s + I_o \cdot R_s / n_p)) \}$$
$$- (V_o / n_s + I_o \cdot R_s / n_p) / R_{sh}] \qquad (4.3)$$

where $K_o = Q / AKT_o$

T_o : Nominal temperature ($301^\circ K$)

A : Empirical data-fitting constant

Since the above equation is an implicit function, that is, $V_o = f(I_o, V_o)$, solutions I_o and V_o can be obtained using a numerical iteration method. In this model, the Newton's Method was used. The algorithm of Newton's Method is expressed as

$$X_{n+1} = X_n - f(X_n) / f'(X_n) \qquad n = 0,1,2 \ldots$$

75

To incorporate the solar array model in a complete system, the solar array load current, I_o, is chosen to be the independent variable (input variable) and the output voltage, V_o, to be the dependent variable (output variable) as expressed in Equation (4.4).

$$f(V_o) = n_p [I_g - I_{do} \{ EXP (k_o (V_o / n_s + I_o \cdot R_s / n_p)) \}$$
$$- (V_o / n_s + I_o \cdot R_s / n_p) / R_{sh}] - I_o \qquad (4.4)$$

As shown in Fig.4.4, an LC filter was included in the actual solar array circuit model for the EASY5 program model [AR]. This filter can represent either the output filter of the solar array or the cable impedance. It is also important to note that assigning the output of the solar array model as a state avoids the implicit loop problem in the EASY5 program. With the solar array output voltage (V_o), obtained from the Newton's Method, two state equations can be written to find the bus voltage (V_B) of this model.

$$L (dI_L / dt) = V_o - R \cdot I_L - V_B$$
$$C (dV_B / dt) = I_L - I_x$$

There are several papers [4,5] which describe a method to include the temperature effect in the solar array model.

76
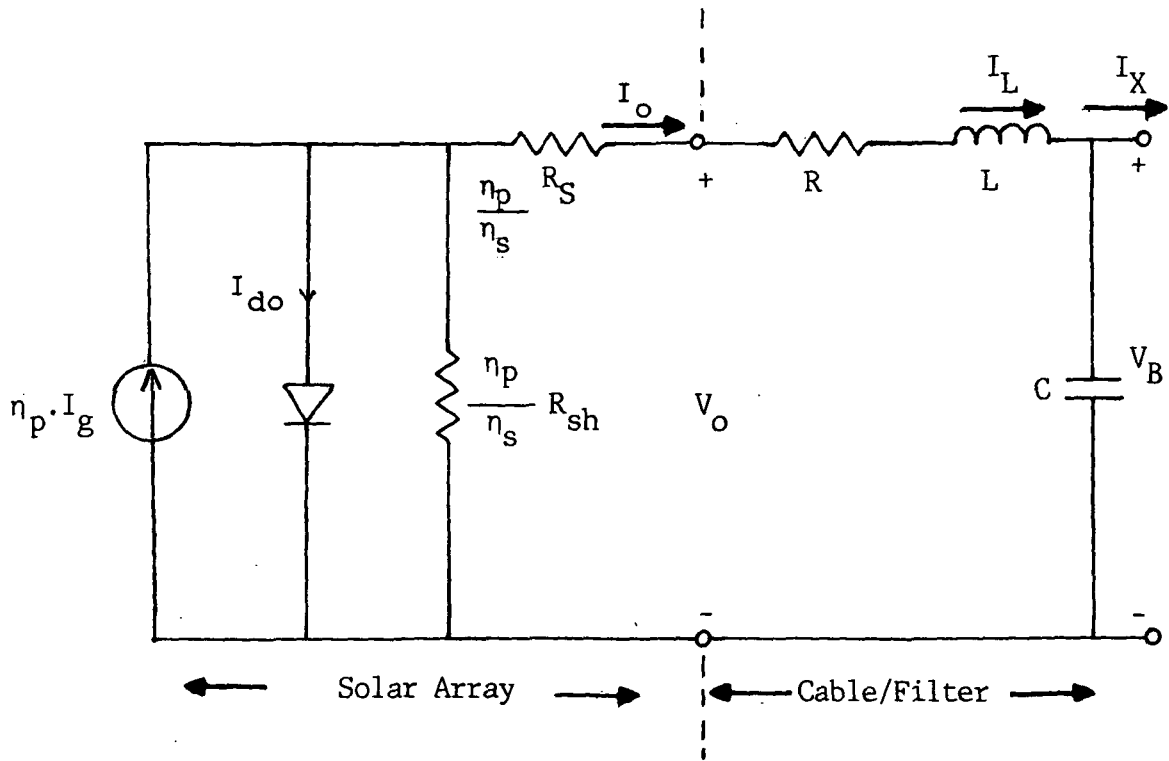
Equations:

$$I_o = \eta_p \left[I_g - I_{do} \left\{ EXP\ K_o \cdot \left(\frac{V_o}{n_s} + I_o \cdot \frac{R_s}{n_p} \right) \right\} \right.$$

$$\left. - \left(\frac{V_o}{n_s} + I_o \cdot \frac{R_s}{n_p} \right) \cdot \frac{1}{R_{sh}} \right]$$

$$L \frac{dI_L}{dt} = V_o - R \cdot I_L - V_B$$

$$C \frac{dV_B}{dt} = I_L - I_X$$

Fig.4.4 Circuit Model of Solar Array and Cable/Filter [AR]

77

One simple expression for the temperature effect is as follows [4]:

$$\Delta I = f_c \cdot \Delta T$$

$$\Delta V = (f_v + f_c \cdot R_s) \Delta T$$

where ΔT, ΔI and ΔV represent the difference between the values at a given temperature and the nominal temperature. The temperature coefficients of current and voltage are f_c and f_v, respectively. The current coefficient, f_c, can be obtained from the empirical data of the solar array I-V curve by comparing the short-circuit currents at a given temperature and the nominal temperature. The f_v is obtained from the open-circuit voltage difference at the two temperatures with the known f_c and R_s.

The illumination change effect of the solar array I-V characteristics is modeled by multiplying an appropriate factor to the light-generated current, I_g, under the assumption that the illumination change affects only the value of I_g.

4.1.3 EXAMPLE OF SIMULATION

Figure 4.5 shows the solar array I-V curves at four temperatures. For this simulation, the model [AR] shown in Fig.4.6 is used. When the model was simulated, the cable/filter section was ignored to obtain the solar cell terminal I-V curve characteristics.
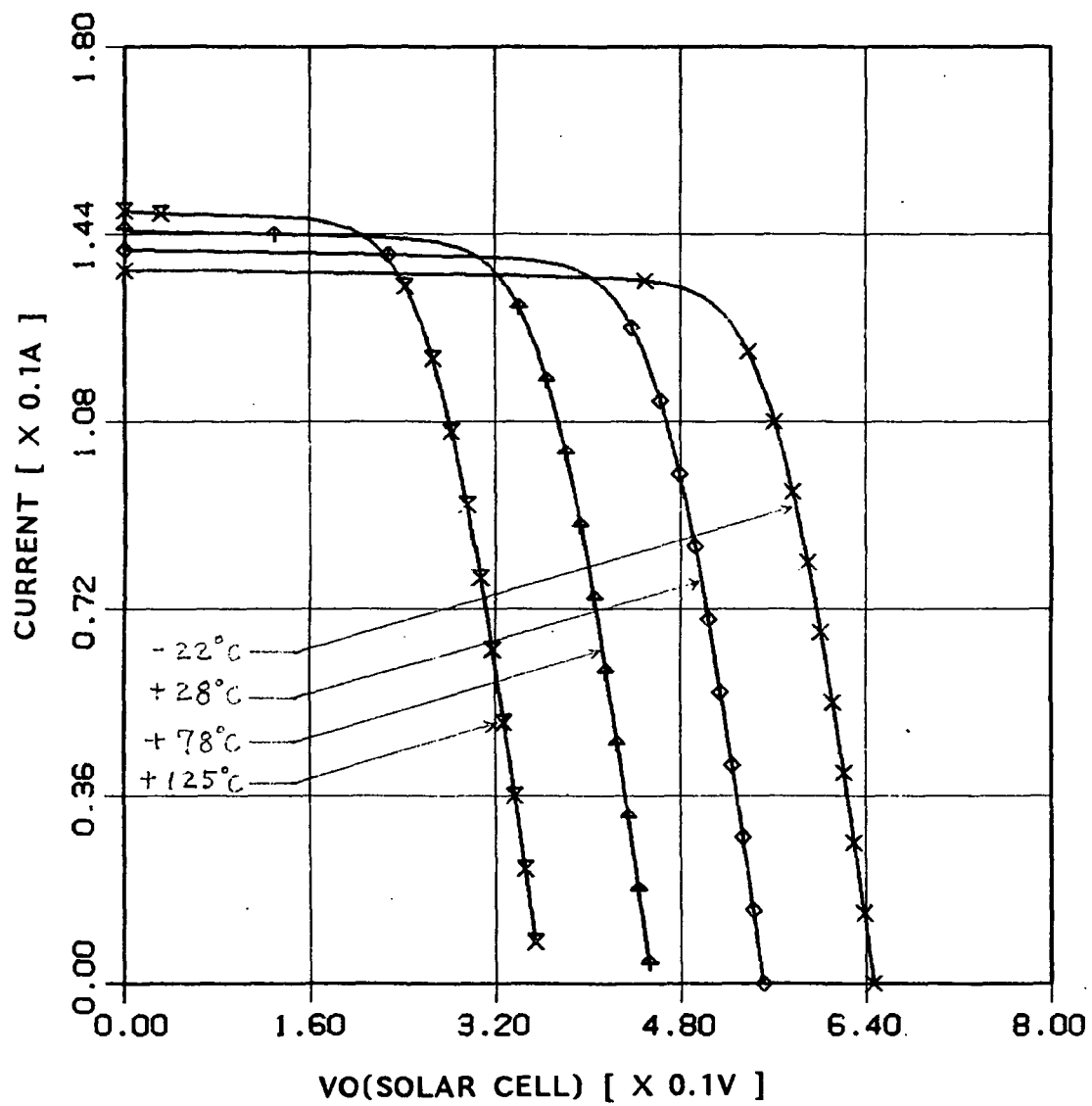
Fig.4.5 Simulation Result of Solar Array Model

```
MACRO FILE NAME = MACROS
DEFINE MACRO = AR
*******************************
**    SOLAR ARRAY MODEL  ******
*******************************

*========> VR

*========< IX

***

MACRO INPUTS = IX      LL        LLS
       R       L        C        TA
       FC      FV       NP       NS
* IX = INPUT CURRENT
* LL = ILLUMINATION LEVEL
* LLS = SLOPE OF ILLUMINATION CHANGE
* R,L,C, : CABLE IMPEDANCE
* TA = AMBIENT TEMPERATURE
* FC,FV : TEMPERATURE COEFFICIENTS
* NP = NO. OF PARALLEL ARRAYS
* NS = NO. OF SERIAL CELLS
* R,L,C, : CABLE IMPEDANCE

MACRO OUTPUTS : VO       IL       VB

* VO = SOLAR ARRAY OUTPUT VOLTAGE
* VB = BUS VOLTAGE

MACRO CODE
MACRO STOP SORT

*** SOLAR CELL PARAMETERS ****
*
* RS = INTERNAL SERIES RESISTANCE
* RSH= INTERNAL SHUNT  RESISTANCE
* XIO= REVERSE SATURATION CURRENT
* TN = NOMINAL TEMPERATURE
* Q  = ELECTRON CHARGE
* XK = BOLTZMANN CONSTANT
* XIG= LIGHT-GENERATED CURRENT
* VOC= OPEN  CIRCUIT VOLTAGE
*
        RS = .42
        RSH = 250.
        XIG = .14115
        XIO = 4.1869E-11
        A = .967
        TN = 301.
        Q = 1.602E-19
        XK = 1.381E-23
        VOC = .5512
*       XKO = Q / ( XK * A * TN )
        XKO=39.3
*
* ILLUMINATION CHANGE WITH A LINEAR SLOPE OF LLS
        FILL = LL AR-- + LLSAR-- * TIME

* EFFECT OF ILLUMINATION CHANGE
```

Fig.4.6 Solar Array Model [AR.MOD]   continued

```
        XIG = XIG * FILL  .
*

        C1 = ( 1. + RS / RSH )
        C2 = NP AR-- / ( NS AR--. * RSH )
        C3 = -NP AR -- * XIG
        A1 = XKD / NS AR--
        A2 = XKD * RS / NP AR--
        IF ( TIME .NE. 0. ) GOTO +++10
*
*  INITIAL GUESS FOR SOLAR ARRAY OUTPUT VOLTAGE
        VO AR-- = VB AR--

*******************************************************
***    NEWTON ITERATION    ****************************
*******************************************************

+++10 CONTINUE
        VOP = VO AR--

        FV = C1 * IL AR-- + C2 * VO AR--- + C3 + NP AR--
     &      * XIO * DEXP ( A1 * VO AR-- + A2 * IL AR-- )
        DFV = C2 + A1 * NP AR-- * XIO * DEXP ( A1 * VO AR---
     &      + A2 * IL AR--)
        VO AR-- = VO AR-- - FV / DFV
        ZZ = ( VO AR-- - VOP ) / VO AR---
        IF ( DABS ( ZZ ) .LE. 1.E-4 ) GOTO +++20
        GO TO +++10

*******************************************************************
*   TEMPERATURE CORRECTION FOR S.A. I-V CURVE              *
*   DEL(I) = FC * DEL(T)                                   *
*   DEL(V) = ( FV + FC * RS ) * DEL(T)                     *
*******************************************************************

+++20 DELI = FC AR-- * ( TA AR-- - TN )
        DELV = ( FV AR-- + FC AR-- * RS ) * ( TA AR-- - TN )
        ILT = IL AR-- + DELI
        VO AR-- = VO AR-- + DELV
*
        VL = VO AR-- - ILT * R  AR-- - VB AR--
MACRO DERIVATIVES, IL AR-- = VL / L  AR--
MACRO DERIVATIVES, VB AR-- = ( IL AR-- - IX AR-- ) / C  AR--
MACRO RESUME SORT
END OF MACRO
*******************************************************************
MODEL DESCRIPTION
LOCATION = 22, AR
END OF MODEL
PRINT
```

Fig.4.6 Solar Array Model [AR.MOD]

This simulation result was similar to the original graph drawn from the experimental data in [6]. The solar cell model's parameter values were obtained from the experimental data of a 2 X 2cm, 10ohm-cm, 8mil silicon cell [4]. The analysis program listing [AR.ANC], including all parameter values, is given in Fig.4.7.

4.1.4 MODEL GENERATION WITH EMPIRICAL DATA [AE]

The empirical data model can be generated using the EASY5 function generator facility. The EASY5 function generator constructs a continuous function from a given data set using the interpolation technique. The function generator can interpolate a set of data which is a function of maximum of 6 independent variables. For instance, the solar array output voltage is chosen to be the dependent variable and the solar array output current to be the independent variable. A continuous I-V curve function can be obtained based on the input data set of V vs. I.

To include the illumination and temperature effect in the solar array model, three-independent variable function generator, that is, EASY5 standard component [F3], is needed.

Figure 4.8 shows an interpolated I-V curve created from two different data sets belonging to two illumination levels of a solar array. In this case, since there are two independent variables, such as the solar array voltage and illumination level, the function generator, [FV], was used.

```
TITLE=NASA(LARGE SIGNAL)
***
*TITLE = SOLAR ARRAY
PARAMETER VALUES
R   AR = .001,  C   AR = 5E-4,    L   AR = 10E-6
NP AR = 1,    NS AR=1,   TA AR = 251,  LL AR = 1
FC AR = 8.E-5,  FV AR = -2.E-3
*********************
INITIAL CONDITIONS
VB AR = 0.5
********
PRINTER PLOTS
ONLINE PLOTS
INT MODE=4
SI MANUAL SCALES
DISPLAY1
IL1AR,  VS,  VO1AR,  XRANGE = 0,.8,  YRANGE = 0,0.16
IL AR,  VS,  VO AR,  XRANGE = 0,.8,  YRANGE = 0,0.16
IL2AR,  VS,  VO2AR,  XRANGE = 0,.8,  YRANGE = 0,0.16
IL3AR,  VS,  VO3AR,  XRANGE = 0,.8,  YRANGE = 0,0.16
TMAX= 0.16 ,  TINC = 0.0005
PRATE =100, OUTRATE=1
*OUTRATE2=1, PRATE2=1
*PRINT2 FROM,.005,TO,.006
SIMULATE
```

Fig.4.7 User's Parameter Values and Analysis Commands [AR.ANC]
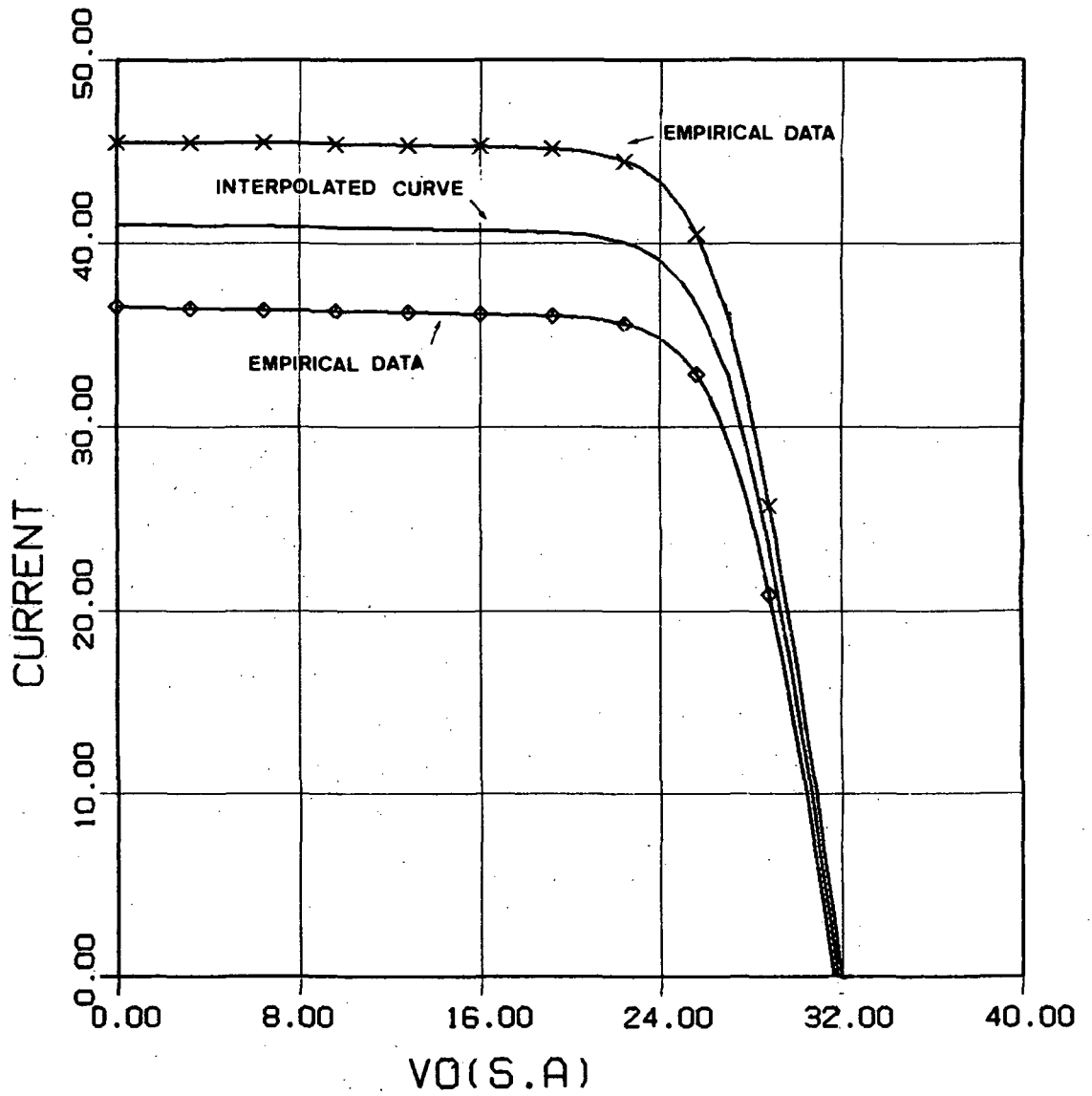
Fig.4.8 Simulation Result of Solar Array's Empirical Data Model

In this model, EASY5 command 'MACRO TABLES' is used to form a tabular function. The interpolated output from the tabular function can be obtained using the following FORTRAN command [2], 'CALL FV (TABNAM,S2,S1,S3,ANX,ANY)' ,where

TABNAM : name of table

S2 : output (e.g. solar array current)

S1 : input (e.g. solar array voltage)

S2 : input (e.g. illumination level)

ANX: degree of interpolation for first independent variable (e.g. 1.0)

ANY: degree of interpolation for second independent variable (e.g. 1.0)

The program listings, [AE.MOD] and [AE.ANC], for this simulation (Fig.4.8) are shown in Figs.4.9-10.

```
MACRO FILE NAME = MACROS
*************************************************
* SOLAR ARRAY MODEL FROM EMPIRICAL DATA          *
*************************************************

DEFINE MACRO = AE

MACRO TABLES = TAE(250)2
MACRO INPUTS = ILL

* ILL = ILLUMINATION LEVEL

MACRO OUTPUTS = IS1      IS2      IS3
               DUM       VS

* IS1 = SOLAR ARRAY CURRENT AT ILLUMINATION LEVEL
*           OF 1.0
* IS2 = SOLAR ARRAY CURRENT AT ILLUMINATION LEVEL
*           OF 0.8
* IS3 = SOLAR ARRAY CURRENT AT ILLUMINATION LEVEL
*           OF INPUT VALUE, ILL.
* DUM = DUMMY STATE FOR AVOIDING ERROR MESSAGE
*           FROM MODEL GENERATION PROGRAM

MACRO CODE
MACRO STOP SORT
        XIN = TIME
        CALL FV ( TAEAE--, OUT, XIN, 1. , 1., 1. )
        IS1AE-- = OUT
        CALL FV ( TAEAE--, OUT, XIN, 0.8, 1., 1. )
        IS2AE-- = OUT
        CALL FV ( TAEAE--, OUT, XIN, ILLAE--, 1., 1. )
        IS3AE-- = OUT
        VS AE-- = TIME


MACRO DERIVATIVES, DUMAE-- = VS AE--
MACRO RESUME SORT
END OF MACRO
MODEL DESCRIPTION
LOCATION = 33, AE
END OF MODEL
PRINT
```

Fig.4.9 Solar Array Empirical Data Model [AE.MOD]

```
TITLE=EMPIRICAL DATA MODEL FOR SOLAR ARRAY
PARAMETER VALUES
ILLAE = 0.9

TABLE, TAEAE, 44, 2
* SECOND INDEPENDENT VARIABLE ( ILLUMINATION )
0.8, 1.0

* FIRST INDEPENDENT VARIABLE ( VOLTAGE )
0.0, 1.0, 5.6, 7.0, 10.,
11.5, 14.5, 15.67 ,18.01, 19.85,
20.65, 21.01, 22.1, 23.01, 24.06,
25.02, 25.52, 26.02, 26.34, 26.7,
27.0, 27.2, 27.41, 27.6, 27.81,
28.0, 28.2, 28.4, 28.6, 28.8,
29.02, 29.21, 29.4, 29.61, 29.81,
30.01, 30.33, 30.54, 30.71, 31.01,
31.15, 31.33, 31.50, 31.63

* DEPENDENT VARIABLE ( CURRENT )
36.55, 36.5, 36.4, 36.35, 36.3,
36.29, 36.2, 36.15, 36.1, 36.02,
35.95, 35.9, 35.7, 35.4, 34.8,
33.8, 33.0, 32.0, 31.2, 30.2,
29.2, 28.5, 27.7, 26.9, 26.,
25.1, 24.1, 23.1, 22.0, 20.9,
19.6, 18.4, 17.2, 15.8, 14.4,
13.0, 10.6, 9.0, 7.7, 5.3,
4.1, 2.6, 1.2, 0.0,
45.5, 45.5, 45.5, 45.5, 45.41,
45.4, 45.31, 45.3, 45.21, 45.1,
45.0, 44.9, 44.6, 44.2, 43.3,
41.8, 40.7, 39.3, 38.2, 36.9,
36.5, 34.8, 33.8, 32.8, 31.7,
30.6, 29.5, 28.3, 27.0, 25.7,
24.3, 22.9, 21.5, 20.0, 18.5,
16.9, 14.3, 12.6, 11.2, 8.6,
7.4, 5.8, 4.3, 3.1
***
PRINTER PLOTS
ONLINE PLOTS
INT MODE = 3
DISPLAY1 (OVERPLOT)
IS1AE, VS, VS AE, XRANGE=0, 31.63
IS2AE, VS, VS AE, XRANGE=0, 31.9
IS3AE, VS, VS AE, XRANGE=0, 31.9
TMAX=31.6, TINC=0.2, PRATE=10
SI MANUAL SCALES
OUTRATE = 1
SIMULATE
```

Fig.4.10 User's Parameter Values and Analysis Commands [AE.ANC]

4.2 SOLAR ARRAY SWITCHING UNIT MODEL

4.2.1 INTRODUCTION

The solar array switching regulation has been proposed as a replacement for conventional regulation techniques to reduce weight, thermal dissipation, and power system complexity for large power spacecraft and advanced space missions.

The solar array switching unit (SASU) contains a voltage and current regulating feedback loop. The SASU differs from the switching regulator in that it controls the bus voltage and battery charge current by switching individual solar array segments as required by the load profile and the state of charge of the battery.

There are two major design parameters for SASU control. One is the size of the array segment switching at each instant. The size of the array segments must be properly chosen to meet dc condition requirements (e.g. voltage regulation specification) of the system. The other design parameter is the frequency of switching. The SASU's ability to respond to perturbations is a function of the switching frequency and the size of the array segment.

There are four basic configurations (Fig.4.11) for the SASU and advantages and disadvantages of each are discussed in [7]. In this study, the series-switching, parallel-array configuration was selected for its low stress on the solar array during shadowing, low wiring complexity and simple switch drive electronics [7].
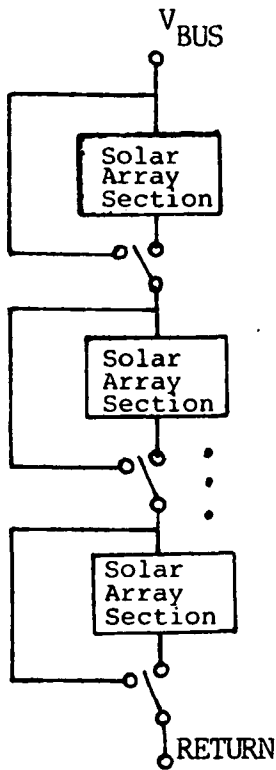
SERIES SWITCHING
SERIES ARRAY
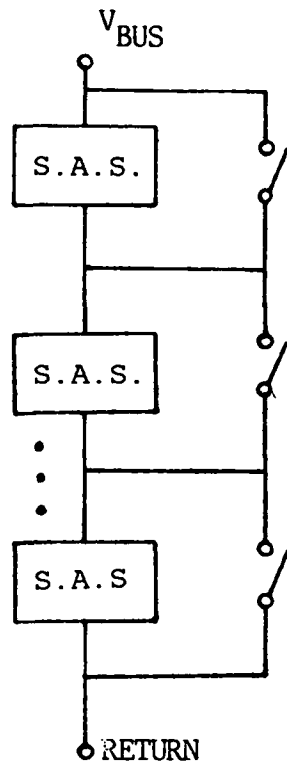
SHUNT SWITCHING
SERIES ARRAY
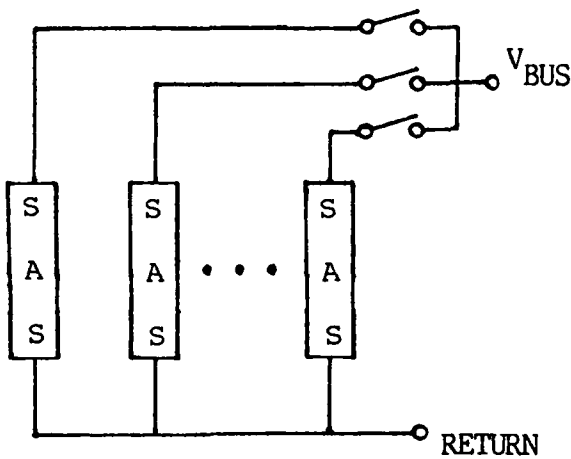
SERIES SWITCHING
PARALLEL ARRAY
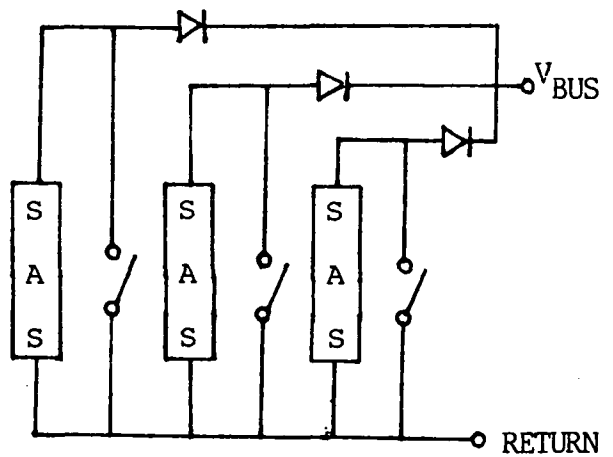
SHUNT SWITCHING
PARALLEL ARRAY

Fig.4.11 Four Basic Configurations of SASU

89

Based on the series-switching, parallel-array configuration, the SASU and control scheme can be constructed as shown in Fig.4.12. The solar array strings, SS1 through SS14, are switched-array sections. There is also an active array section which is connected to the main bus without a switch. This active array section performs fine regulation of the bus voltage while the switched-array sections give coarse regulation.

The combined operation of the active and switched-array sections is described by the operation of the system during exit from an eclipse. When the spacecraft is in an eclipse, the array provides no output and the bus voltage is less than the setting of the shunt regulator. Given these conditions, the shunt is turned off and the current sensors are producing a 'count up' signal so that all of the array are switched on.

As the spacecraft exits eclipse, the full array is on and eventually the output current is sufficient to charge the battery and supply the load demand. The bus voltage rises until it reaches the voltage reference of the shunt regulator and the shunt regulator activates to absorb excess array capacity. When the shunt current increases to a preset value (e.g. 2A), the 'count up' signal is turned off. As the current increases to another preset value (e.g. 5A) the shunt current sensors initiate a 'count down' signal which switches off the array sections, one by one, until the shunt current is stabilized between 2A and 5A. At this time, the switching action stops and the shunt regulator regulates the bus with
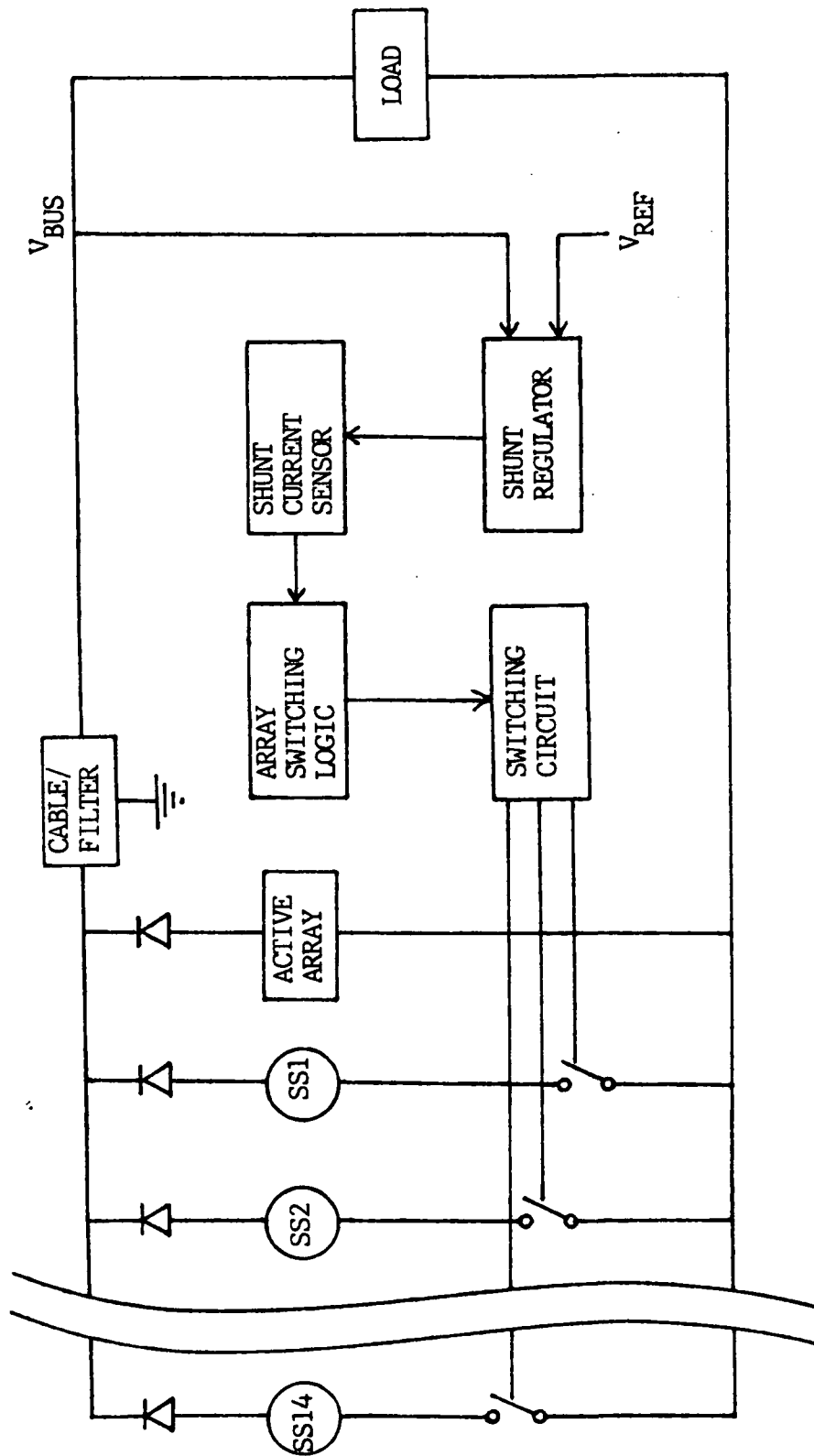
Fig.4.12 Solar Array Switching and Control Configuration

the active array section. Figure 4.13 shows the array characteristic under static conditions.

Circuit operation and model performance are illustrated using the simulation results shown in Fig.4.16 in Section 4.2.3.

4.2.2 MODEL GENERATION [AS]

To generate the solar array switching model, the previous solar array model [AR] was modified to add the array switching effect. Since the number of parallel solar array strings may vary in this model [AS], the solar array I-V curve varies accordingly. The array switching depends on the shunt current level and delay time between switchings. Detailed switching logic of the SASU system is shown in Fig.4.15. The additional capacitor, C1(Fig.4.14), is included to absorb an abrupt step change of the solar array switching dynamics. The parameter values of R1 and C1 must be properly selected to maintain system stability.

The following state equations are used to implement the cable/filter section of the SASU circuit model shown in Fig.4.14.

$$V_L = V_o - R \cdot I_L - V_B$$
$$C_1 \left(dV_{c1} / dt \right) = I_o - I_L$$
$$L \left(dI_L / dt \right) = V_L$$
$$C \left(dV_B / dt \right) = I_L - I_x$$

where $I_x = I_{sh} + I_{load}$
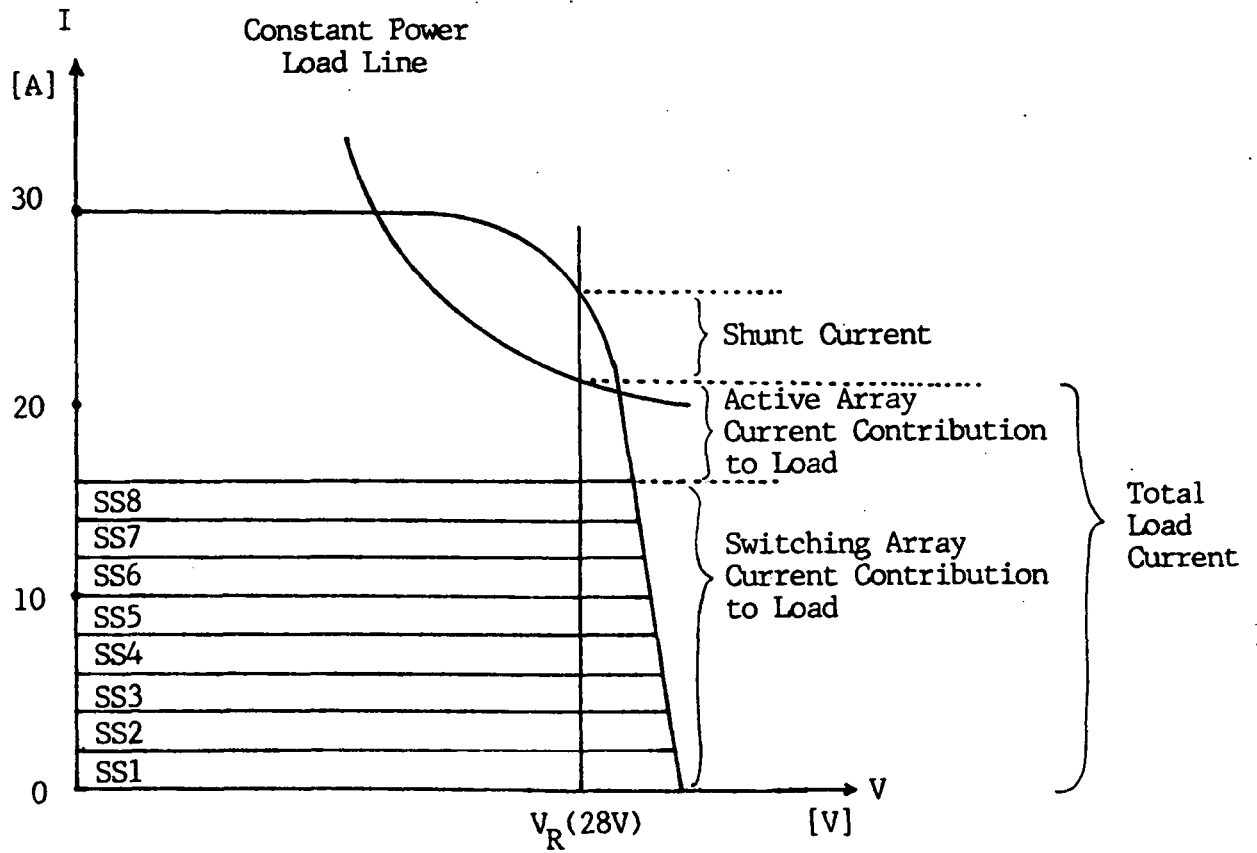
Fig.4.13 SASU System I-V Characteristics

Fig. 4.14 Circuit Model of SASU and Cable/Filter [AS]

Equations:

$$I_o = n_p \left[I_g - I_{do} \left| EXP \; K_o \cdot \left(\frac{V_o}{n_s} + I_o \cdot \frac{R_s}{n_p} \right) \right| \right.$$
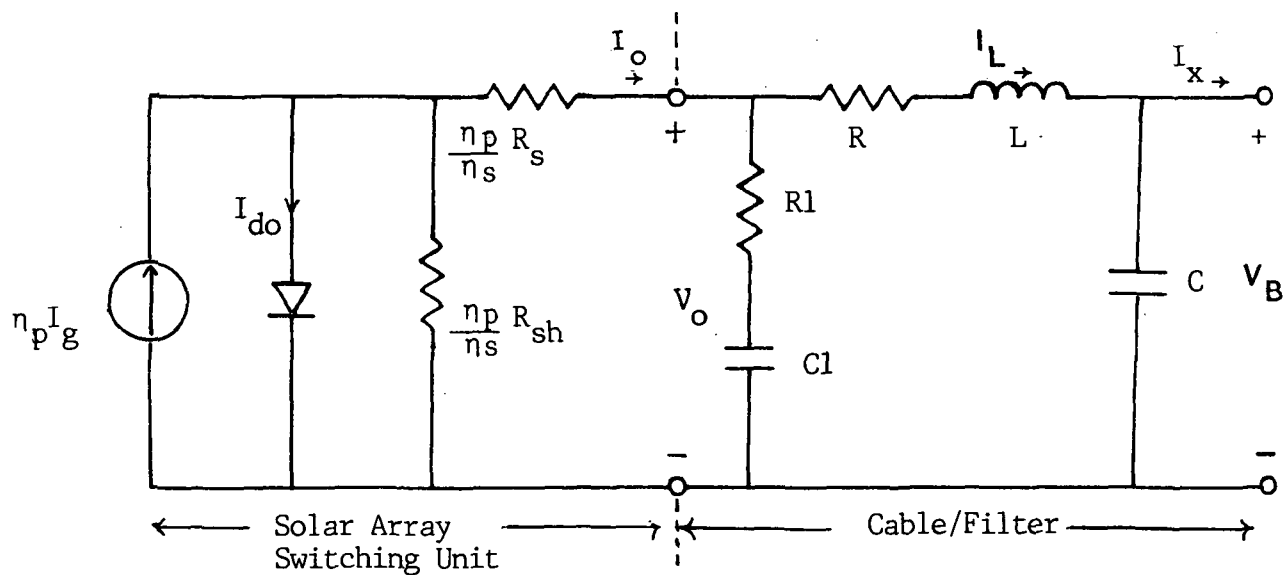
$$\left. - \left(\frac{V_o}{n_s} + I \cdot \frac{R_s}{n_p} \right) \cdot \frac{1}{R_{sh}} \right]$$

$$V_L = V_o - R \, I_L - V_B$$

$$Cl \, \frac{dV_{Cl}}{dt} = I_o - I_L$$

$$L \, \frac{dI_L}{dt} = V_L$$

$$C \, \frac{dV_B}{dt} = I_L - I_X$$

94

START

FTIME = 0

$I_{SH} \geq 5$
AND
NP > 64

NO

$I_{SH} \leq 2$
AND
NP < 324

NO

NO

TIME $\geq$ FTIME + DL

TIME $\geq$ FTIME + DL

NO

NP = NP + 20

FTIME = TIME

NP = NP + 20

FTIME = TIME
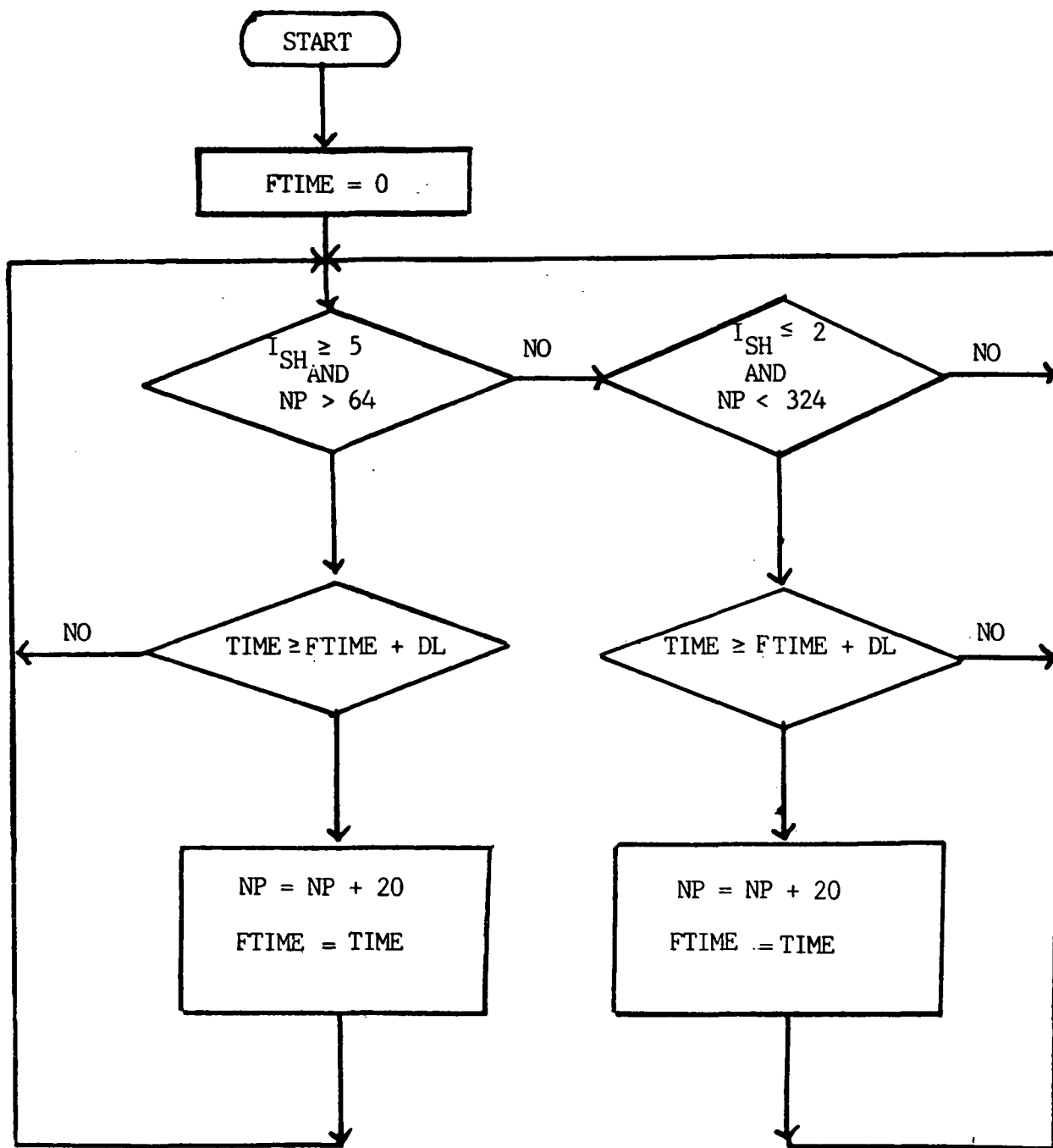
I_{SH} : Shunt Current

NP : No. of Parallel S.A.

DL : Delay Time Between Switchings

C·2

Fig. 4.15 Solar Array Switching Logic

95

4.2.3 EXAMPLE OF SIMULATION

In this simulation, a simple constant-power load model [PT] was used for load variation. A full shunt model [FS] was included to sense the shunt current.

Initially 324 parallel solar array strings, each consisting of 58 solar cells in series, are connected to the main bus. They produce a maximum power of 853 watts. A constant power (500W, in this example) load is applied to the bus. The excess power of the solar arrays will be consumed in the shunt regulator. As the shunt current becomes greater than 5A, the solar arrays are switched off, 20 arrays at a time, with time delay of 1ms. The sharp transients of the bus voltage are observed at the switch-off and the bus voltage approaches the preset value of 28.14V (Fig.4.16). For each switching step, the shunt current drops by 1.88A, which corresponds to the current of 20 arrays, until it becomes less than 5A.   Since the bus voltage is regulated, the load current remains almost constant.   The solar array current, I_{SA}, is the sum of the load current, I_L, and the shunt current, I_{sh}.

When a system with this model [AS] is simulated, numerical integration methods involving variable step-size algorithms should be avoided. Since this model includes a routine for sensing the present time and comparing it with the delay time, the above integration method can not work properly.
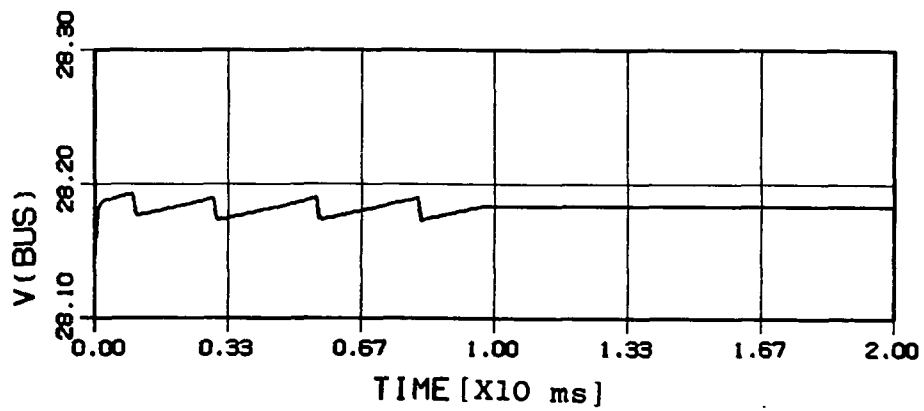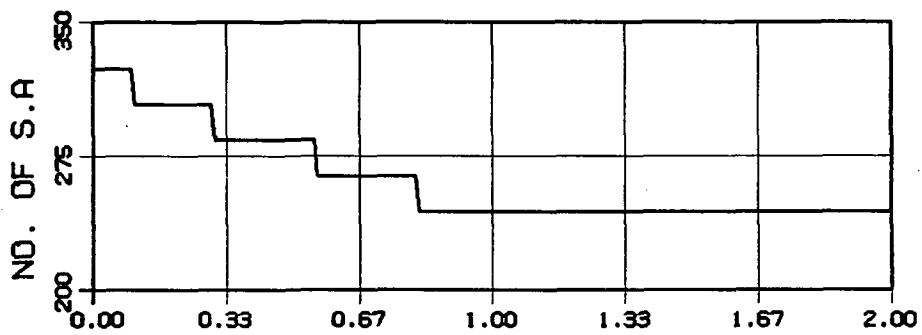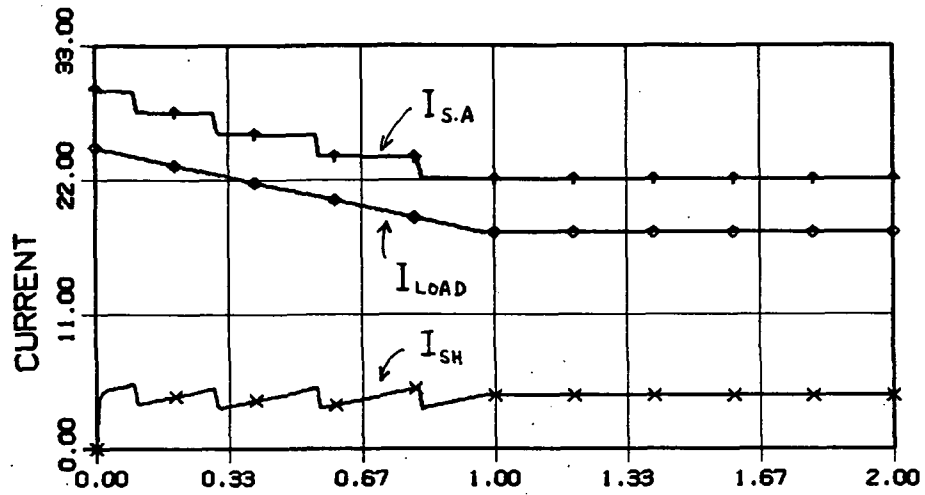
Fig.4.16 Simulation Results of Solar Array Switching System

The fixed-step integration methods, such as mode 3 or 4 in the EASY5 User's Guide [2], are recommended for simulation of this model.

The system model description program [PSS2.MOD], schematic diagram, input data requirements list and analysis program [PSS2.ANC] are shown in Figs.4.17-20.

```
MACRO FILE NAME = MACROS

*******************************************************
* SASU SYSTEM WITH SHUNT REGULATOR AND                *
* CONSTANT POWER LOAD                                 *
*******************************************************
* REVISED ON 3/3/86

LIST MACRO COMPONENTS = AS,FS,PT
MODEL DESCRIPTION
LOCATION=1,   AS,  INPUTS = FS(IH=IH),  MC(S,2=IX)
LOCATION=23,  FS,  INPUTS = AS(VB=VB)
LOCATION=5,   PT,  INPUTS = AS(VB=VL)
LOCATION=41 ,MC,  INPUTS = FS(IH=S,1),  PT(IL=S,4)
END OF MODEL
PRINT
```

Fig.4.17 System Model Generation Using SASU [PSS2.MOD]
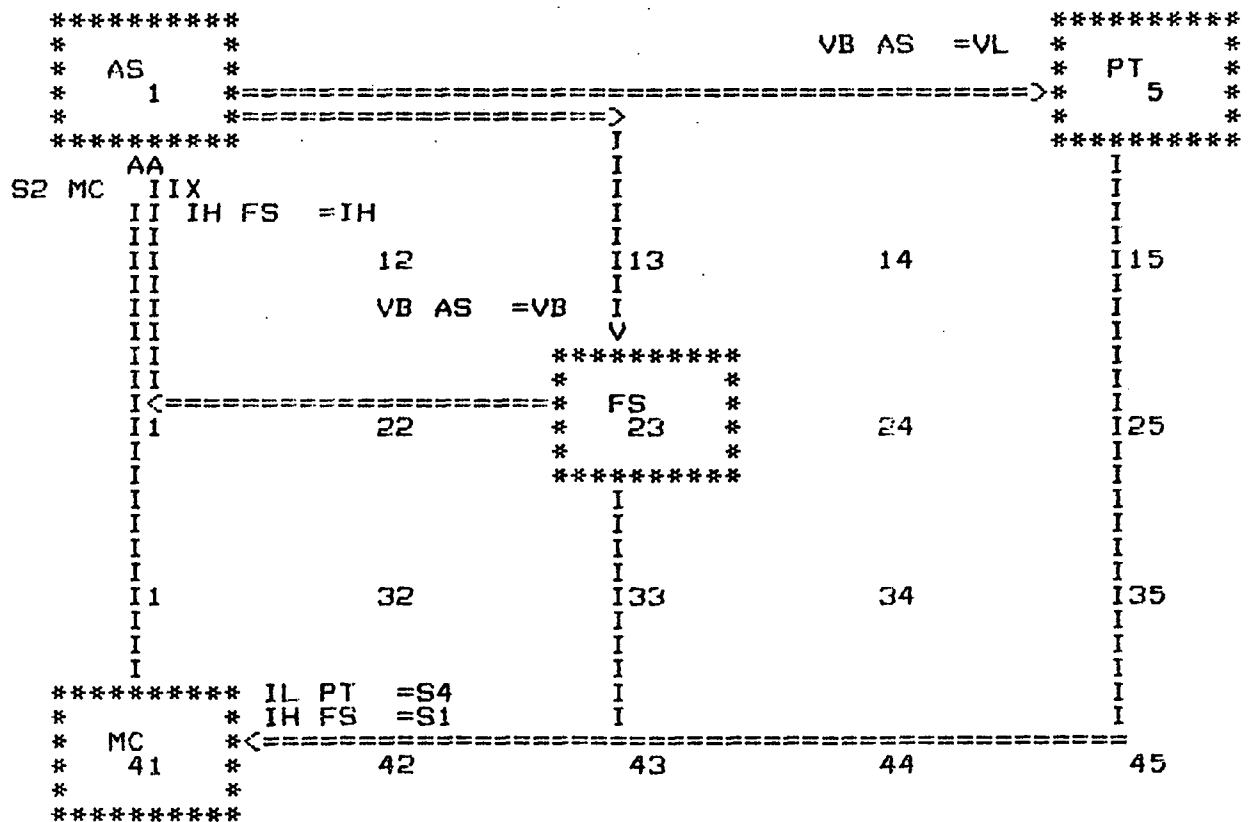
Fig.4.18 Schematic Diagram of [PSS2.MOD]

INPUT DATA REQUIREMENTS LIST

PARAMETERS REQUIRED

PARAMETER NAME (AND DIMENSION DATA FOR VECTOR AND MATRIX PARAMETERS)

COMPONENT						
AS	NP AS L AS	DL AS C AS	NNPAS R1 AS	NS AS	R AS	C1 AS
FS	VR FS VSAFS	R1 FS ILMFS	R2 FS	R3 FS	GM FS	VTHFS
PT	PC PT T1 PT	SW PT PW3PT	TC PT T2 PT	PW1PT PW4PT	PW2PT T3 PT	VR PT PW5PT
MC	S3 MC	C1 MC	C2 MC	C3 MC	C4 MC	

STATES   (INITIAL CONDITIONS AND ERROR CONTROLS REQUIRED)
STATE NAME (AND DIMENSION DATA FOR VECTOR AND MATRIX STATES)

COMPONENT			
AS	VC1AS	IL AS	VB AS

Fig.4.19 Input Data Requirements List

100

```
TITLE=NASA(LARGE SIGNAL)

****************************************************
* SOLAR ARRAY SWITCHING UNIT SYSTEM WITH SHUNT *
* REGULATOR AND CONSTANT POWER LOAD            *
****************************************************
PARAMETER VALUES
R   AS = .001,  C  AS = 5E-5,    L  AS = 1E-6,   C1 AS = 1.E-3
R1 AS = 1.0
NP AS = 324,   NS AS=58,   NNPAS =20,  DL AS = .001
***********************

INITIAL CONDITIONS
VB AS = 28.14
IL AS = 29.565
VC1AS = 28.140
********

PARAMETER VALUES
VR FS = 28.14,   VSAFS = 15.
R1 FS = 12400,   R2 FS = 2200000,   R3 FS = 1.78419
GM FS = 4.,      VTHFS = 3.,        ILMFS = 45.
********

PARAMETER VALUES
VR PT=15
SW PT=20000
PW1PT=694, PW2PT=500
TC PT=5E-1, PC PT=2

C1 MC=1, C2 MC=0, C3 MC=1, C4 MC=0
*
PRINTER PLOTS
ONLINE PLOTS
INT MODE=4
DISPLAY1(OVERPLOT)
VB AS
DISPLAY2 (OVERPLOT)
IH FS, IL PT, IO AS
DISPLAY3, NPPAS
TMAX = 20E-3,  TINC=1E-6
PRATE = 200, OUTRATE = 80.
SIMULATE
```

Fig.4.20 User's Parameter Values and Analysis Commands [PSS2.ANC]

CHAPTER 5

SHUNT REGULATOR MODELING

5.1 FULL SHUNT MODEL

5.1.1 INTRODUCTION

Shunt regulators are used to clamp the power bus voltage when excess solar array power is available. There exist basically two types of shunt regulator circuits, linear type and PWM type. Modeling techniques for the PWM type have received a great deal of attention in the last two decades. A discussion of the modeling and analysis of the PWM regulator is found in the chapter on The Switching Regulator Model. The shunt regulator configurations can also be categorized by their functions: full shunt and partial shunt. In a full shunt configuration, the shunt elements are placed in parallel with the load. In a partial shunt configuration, the shunt elements only shunt part of the solar array cells. Each solar array segment is tapped by a shunt element. In this study, the full shunt and partial shunt configurations are modeled in detail.

Figure 5.1 illustrates the simplified block diagram of a typical shunt regulator. The basic circuit functions are as follows. A divided-down sensed bus voltage is compared to a reference voltage. The error voltage is then amplified to control the current through the shunt elements. A suitable resistor (dependent on the shunt's maximum design current)
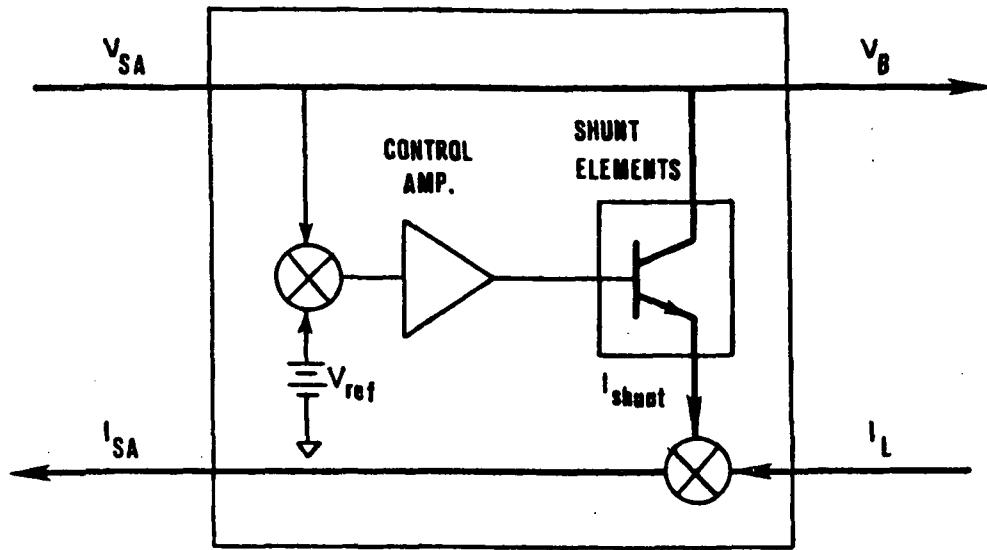
Fig.5.1 Simplified Block Diagram of Shunt Regulator

is used in the shunt current path to monitor current flowing through the shunt elements.

To illustrate shunt regulator modeling techniques, typical shunt regulators are modeled in detail in the following sections. The circuit diagram and the block diagram are shown in Figs.5.2 and 5.3. These models take into account salient dynamics and nonlinearities including Op-Amp feedback, Op-Amp saturation and darlington cut-off. All diodes, including the transistor base-to-emitter junctions, have an infinite reverse impedance. The first order model is used for transistors.

Most shunt regulators are composed of two major function blocks, the error amplifier (EA) block and the shunt element block.

In some applications, the EA block is implemented with three identical amplifier circuits and a majority voting circuit for redundancy. Also, the shunt element block is mostly composed of parallel, identical, shunt transistor circuits or sequentially turn-on shunt transistor circuits. Since it is not practical to generate a generalized model which fits any shunt regulator circuit, two typical shunt circuits (Type-1 and Type-2) are modeled to demonstrate modeling procedures. These two circuits represent the most commonly used linear shunt regulators in spacecraft power systems.
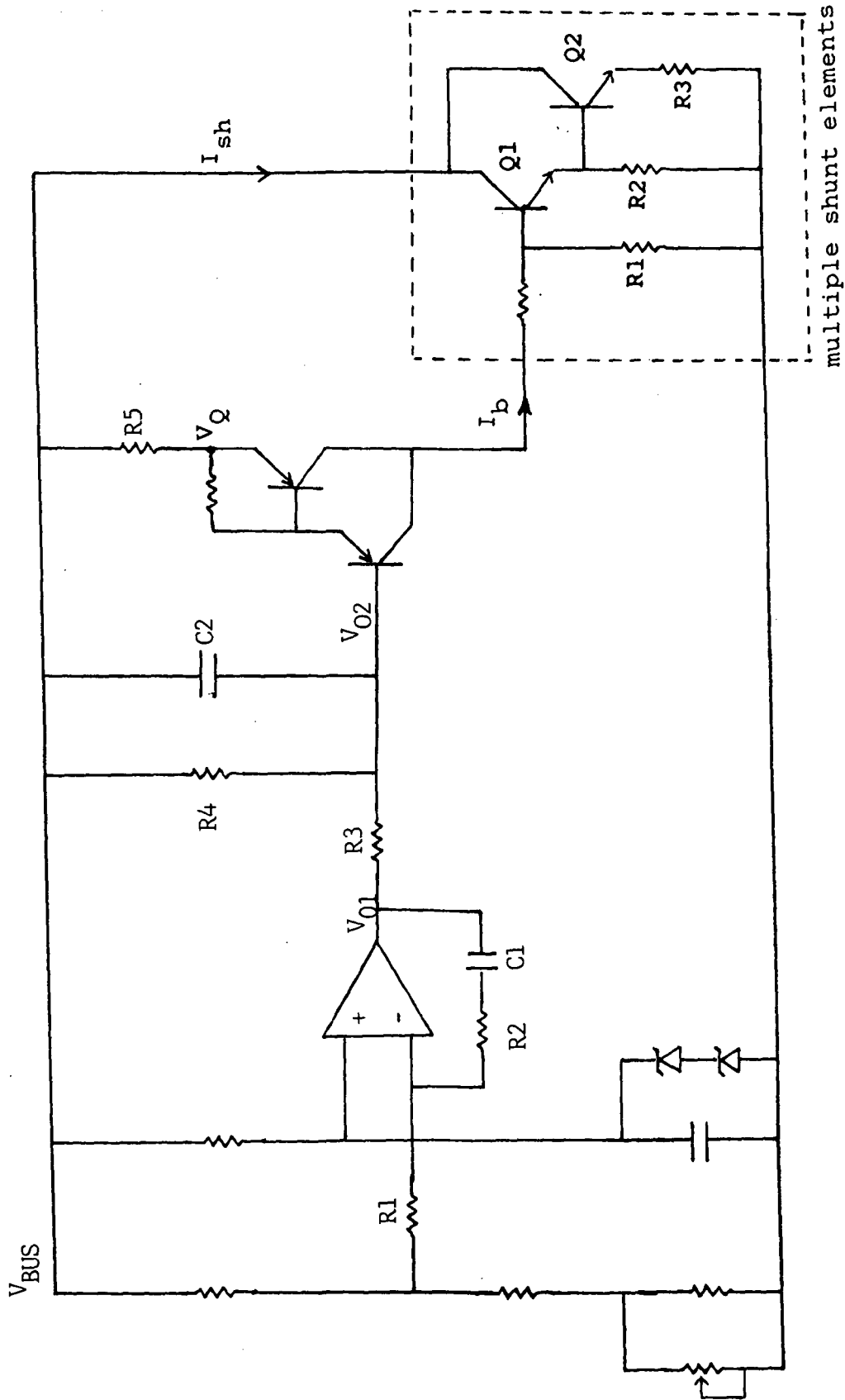
Fig. 5.2   Shunt Regulator Circuit Diagram (Type 1)
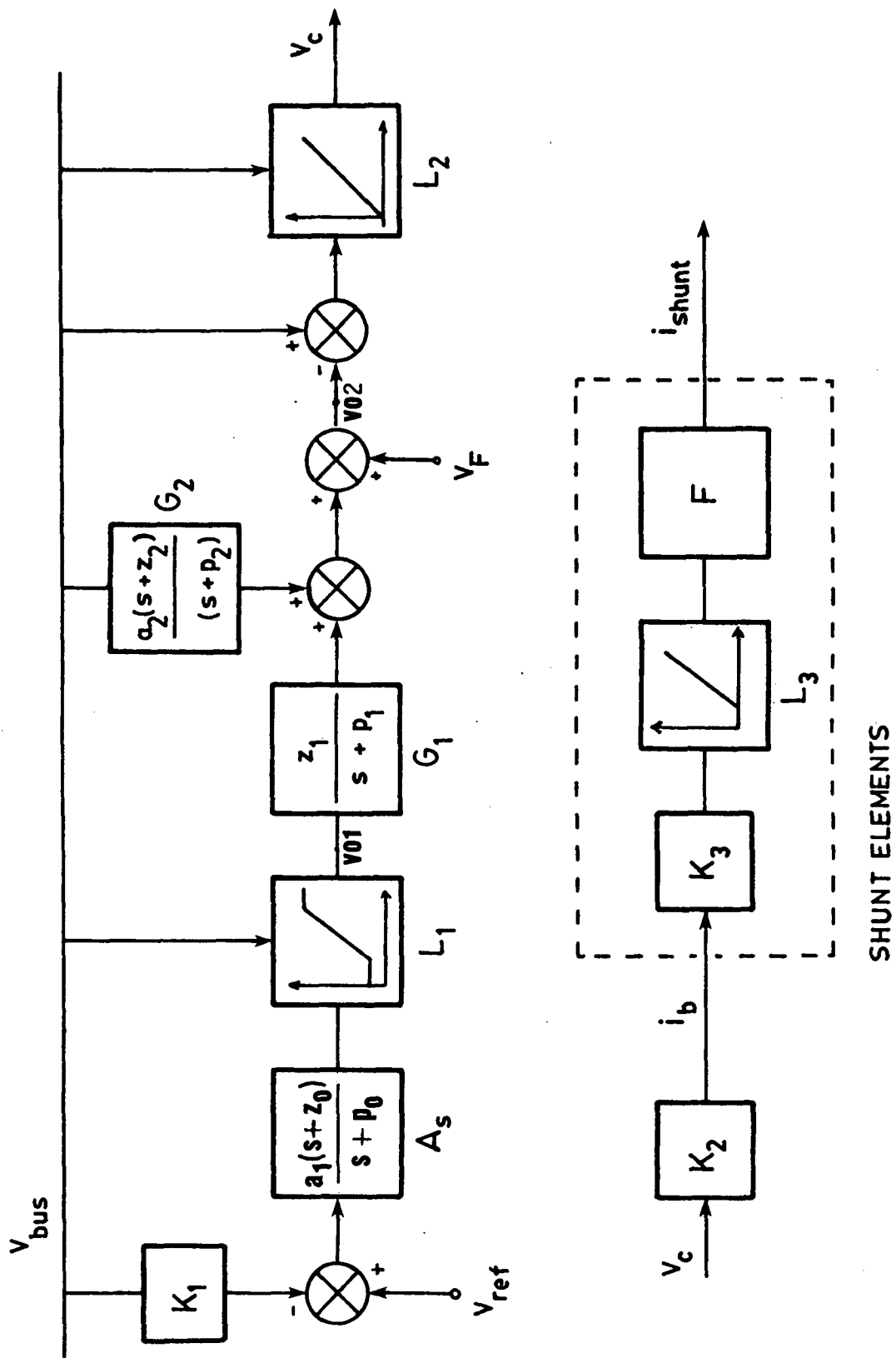
Fig. 5.3 Type-1 Shunt Regulator Circuit Block Diagram

5.1.2 MODEL GENERATION FOR A TYPE-1 SHUNT

A. MODELING WITH TRANSFER FUNCTIONS

A shunt regulator circuit, Fig.5.2, is modeled through the block diagram shown in Fig.5.3. The block diagram shows the transfer function representation of each functional block of the circuit. This transfer function model is useful when creating a generalized model to handle different circuits belonging to the same type shunt. The transfer function model is particularly useful for the frequency response analysis. By providing the values of gains, poles, and zeros, the user can implement the corresponding models for different circuits.

Although the model is implemented based on transfer functions, the transfer functions are programmed with state equations in the model when the functional block diagram is actually modeled. The A_s block, in Fig.5.3, can be expressed in state equations as

$$S2 = A1 \cdot S1 + X1$$
$$\overset{\circ}{X1} = A1 \cdot S1 \ Z0 - S2 \cdot P0$$

The above state variable equations were converted from a transfer function which had one pole and one zero. The input (S1) of this block is an error voltage between the K1, V(bus) product and V_r, and the output voltage (V_{o1}) is the sum of the dc voltage component and the ac voltage component (S2) of the A_s block.

$$S1 = K1 \cdot V_B - V_r$$
$$V_{ol} = S2 + V_r$$

The dummy state variable, X1, which is not a capacitor voltage, is introduced by converting the transfer function into state equations. Similarly, the G1 and G2 blocks are expressed in state equations. However, in this case, the inputs (S1,S3) of these blocks are V_{ol} and V(bus), respectively, and the outputs (S2,S4) are directly fed to the summer in order to obtain V_{o2}. The L1 block represents the Op-Amp saturation. This limiting function can be easily implemented by using FORTRAN 'IF' statements (Refer to program listing). The V_F is needed to include the base-emitter junction voltage drop of the darlington circuit. The L2 block represents the limiting of control voltage, V_c, to a positive value. The K2 block is a gain of control voltage to base current of the transistor driver circuit and K3 is a factor from the number of multiple shunt elements. The L3 block represents the I_c vs. V_{be} characteristic of the shunt transistor. The F block represents the functional expression of the shunt current, I_{sh}, with respect to base current, I_b.

$$I_{sh} = f(I_b) = C1 \cdot I_b + C2$$

$$C1 = \frac{\beta 1 \cdot \beta 2 \cdot R1 \cdot R2}{\beta 1 \cdot \beta 2 \cdot R2 \cdot R3 + \beta 2 \cdot R1 \cdot R3 + R1 \cdot R2} \qquad (5.1)$$

$$C2 = -\frac{0.7 \, \beta 2 \, (R1 + \beta 1 \, R2)}{\beta 1 \cdot \beta 2 \cdot R2 \cdot R3 + \beta 2 \cdot R1 \cdot R3 + R1 \cdot R2} \qquad (5.2)$$

where $\beta 1$ and $\beta 2$ are the current gains of transistors Q1 and Q2, respectively, and V_{be} of Q1 and Q2 is assumed as 0.7V.

B. MODELING WITH STATE EQUATIONS

The same shunt regulator circuit, Fig.5.2, is modeled directly from the state equation representation of the circuit without transfer function blocks. This is a more convenient way of modeling a specific circuit since it is not necessary to calculate transfer functions. The state variable represents the actual capacitor voltage or inductor current. This circuit can be divided into three function blocks, i.e., error amplifier circuit, error amplifier output circuit and shunt element circuit, as shown in Fig.5.4a-c.

1) Error amplifier circuit

If the Op-Amp is assumed to be ideal, then the output voltage (V_{o1}) can be expressed in terms of the inputs $(K1*V_B$ and $V_r)$ and the state variable, V_{c1}, by the following equation.

$$V_{o1} = -\frac{R2}{R1} \left(K_1 \cdot V_B \right) + \left(1 + \frac{R2}{R1} \right) \cdot V_r + V_{c1}$$

The state variable, V_{c1}, is expressed as
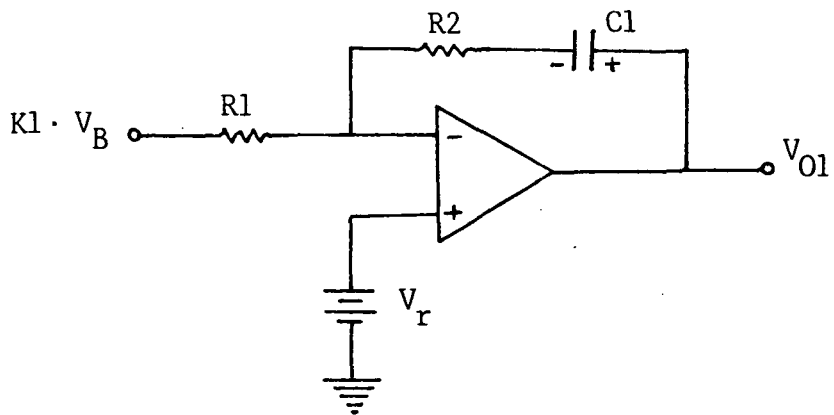
Fig. 5.4 (a) Error Amplifier Circuit
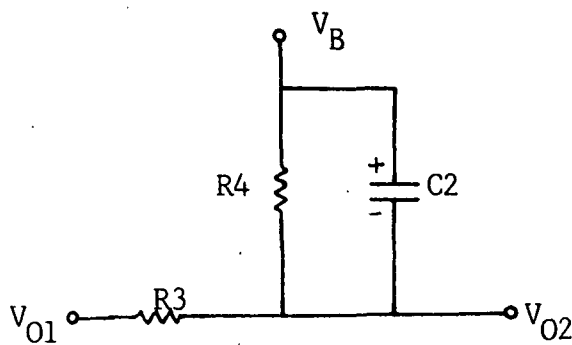
Fig. 5.4 (b) Error Amplifier Output Circuit

multiple shunt elements
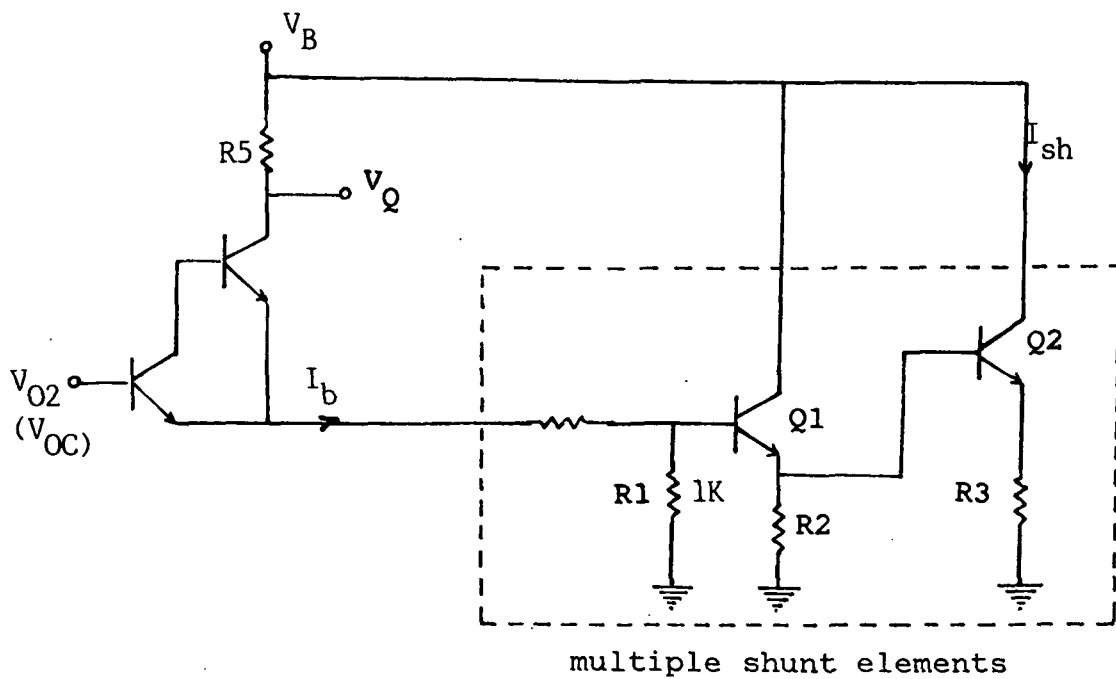
Fig. 5.4 (c) Shunt Element Circuit

110

$$\frac{dV_{c1}}{dt} = \frac{V_{o1} - V_r - V_{c1}}{C1 \cdot R2}$$

since the current through capacitor C1 is

$$C1 \frac{dV_{c1}}{dt} = \frac{V_{o1} - V_r - V_{c1}}{R2}$$

In order to take into account the saturation effect of Op-Amp, the output voltage (V_{o1}) is limited to a voltage between the supply voltage (V_{bus}) and the ground.

2) Error amplifier output circuit

Since the error amplifier circuit, shown in Fig.5.4b, is a simple linear circuit, the following output voltage equation and capacitor-voltage state equation are easily obtained to model this circuit.

$$V_{o2} = V_B - V_{c2}$$

$$C2 \frac{dV_{c2}}{dt} = -\frac{V_B}{R4} - \frac{V_{o1}}{R3} + \frac{(R3 + R4) \cdot V_{o2}}{R3 \, R4}$$

3) Shunt element circuit

This circuit is basically a shunt transistor circuit with a base-drive circuit. If the upper darlington is not in cut-off, then the emitter current, I_b, to transistor Q1 is

$$I_b = \frac{V_B - (V_{o2} + 1.4)}{R5 \, N}$$

111

where 1.4V is a darlington base-emitter voltage drop and N represents the number of multiple shunt elements. The shunt current flows only when V_Q, which is equal to $V_B - (V_{o2} + 1.4V)$, is positive. Also, before there is any shunt current, the voltage across the 1KΩ resistor must be at least 1.4V or I_b must be greater than 1.4mA. Once I_b is determined, the shunt current can be expressed in terms of I_b through manipulation of transistor circuit equations. As a result,

$$I_{sh} = f(I_b) = C1 \cdot I_b + C2$$

where C1 and C2 are described in Equations (5.1) and (5.2). Finally, the shunt current is limited to the maximum current capacity of the solar array current.

$$0 < I_{sh} < I_{SA}(max)$$

5.1.3 MODEL GENERATION FOR A TYPE-2 SHUNT

Another typical shunt regulator circuit uses a FET instead of a BJT as the shunt element. The following procedures use the state equation method for modeling the circuit shown in Fig. 5.5.
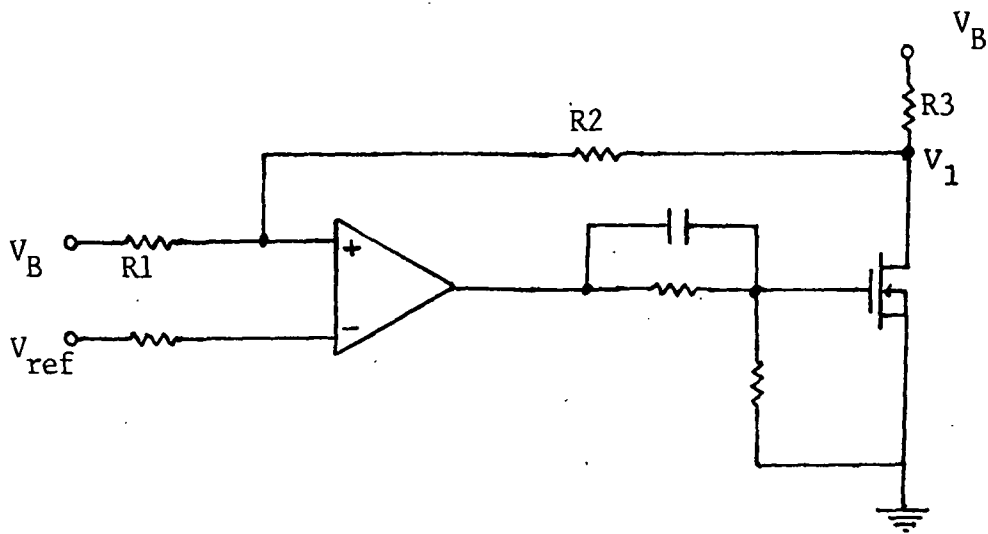
Fig.5.5 Shunt Regulator Circuit Diagram (Type 2)
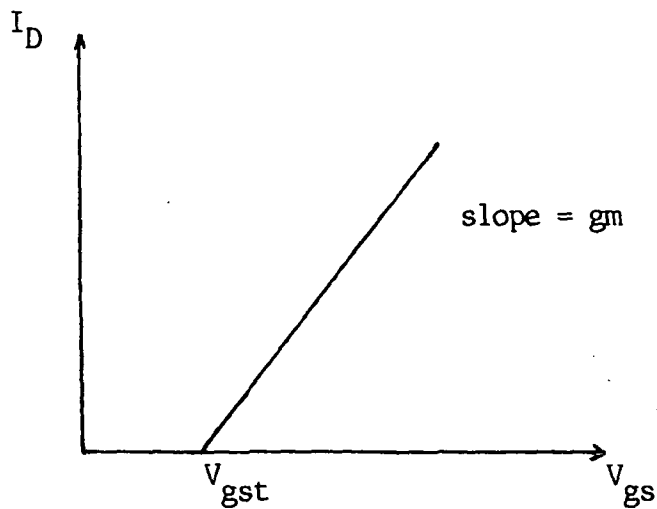
Fig.5.6 Transfer Curve of MOSFET

From Fig.5.5, two equations can be written assuming the operational amplifier is ideal.

$$\frac{V_B - V_r}{R1} = - \frac{V_1 - V_r}{R2} \qquad (5.3)$$

$$V_1 = V_B - \left(gm \cdot V_{gs} + \frac{V_1 - V_r}{R2} \right) \cdot R3 \qquad (5.4)$$

From Equation (5.4), V_1 can be expressed in terms of V_{gs}, V_B and V_r resulting in an explicit expression for V_1 with an assumption of R2 >> R3.

$$V_1 = V_B - gm \cdot V_{gs} \cdot R_3 \qquad (5.5)$$

By substituting Equation (5.5) into Equation (5.3),

$$gm \cdot V_{gs} = \frac{(R1 + R2)}{R1 \cdot R3} (V_B - V_r) \qquad (5.6)$$

The power MOSFET is modeled on the assumption that this device is operated in a linear region as shown in Fig.5.6. The drain current is expressed as

$$I_d = gm \cdot (V_{gs} - V_{gst})$$

where I_d = drain current

gm = forward transconductance of MOSFET

V_{gst} = gate threshold voltage

If this MOSFET characteristic is included in Equation (5.5),

$$V_{gs} = \frac{(R1 + R2)}{gm \cdot R1 \cdot R3} (V_B - V_r) + V_{gst}$$

The saturation effect of the Op-Amp is implemented by limiting the maximum output voltage of the Op-Amp using a FORTRAN 'IF' statement. The shunt current should be limited from zero to the maximum solar array's output current.

5.1.4 EXAMPLE OF SIMULATION

For simulation of the Type-1 shunt regulator, system [SIML1.MOD](FIG.5.8) is configured as shown in Fig.5.9. The system consists of the transfer-function shunt model [HA], a solar array model [AR] and a constant power model [PT].

In this simulation (Fig.5.7), a constant-power load of 800W is applied to the solar array which has an output power capacity of 853W. After the system reaches a steady state, the load step changes from 800W to 750W at 2ms. The decrease in the load power causes the shunt current to rise. The shunt current is added to the load current so the solar array output current remains almost constant after a small transient. As a result, the bus voltage recovers its specified voltage (28.14V) after a transient period. The input data requirements list and analysis program are given in Figs.5.10-11.

The same system, using the state-equation model [HB] for the Type-1 shunt regulator, is also simulated.
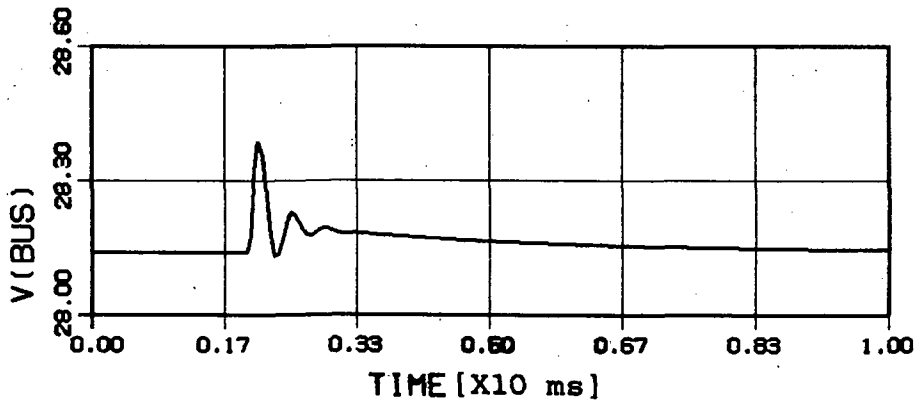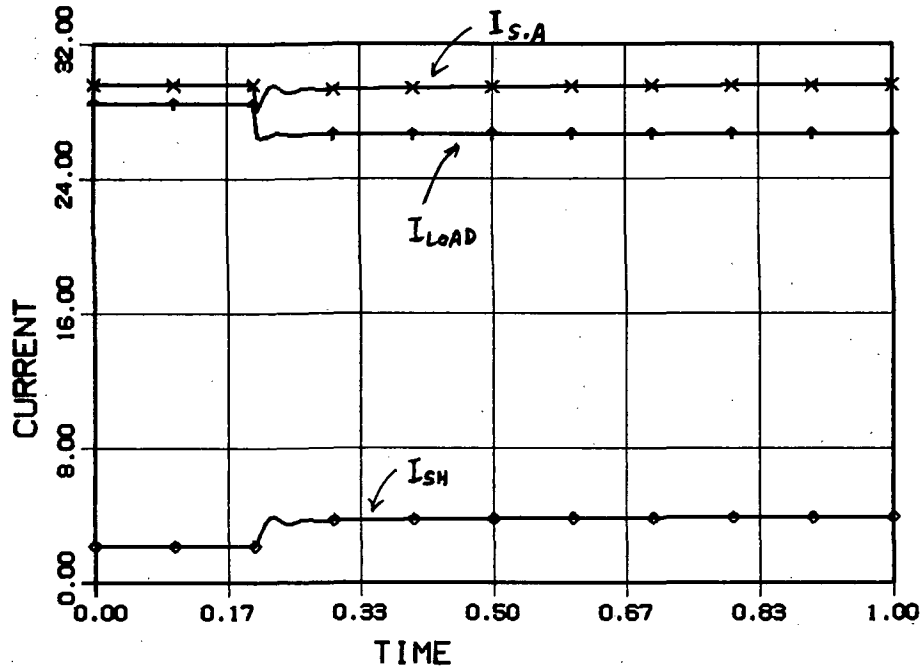
Fig.5.7 Simulation Results of Type-1 Shunt Regulator Model

116

```
MACRO FILE NAME = MACROS

****************************************************
* SOLAR ARRAY SYSTEM WITH TYPE 1 FULL SHUNT       *
* REGULATOR AND CONSTANT POWER LOAD               *
****************************************************

LIST MACRO COMPONENTS = AR, HA, PT
MODEL DESCRIPTION
LOCATION=1,  AR, INPUTS = MC(S, 2=IX)
LOCATION=23, HA, INPUTS = AR(VB=VB)
LOCATION=5,  PT, INPUTS = AR(VB=VL)
LOCATION=41, MC, INPUTS = HA(IH=S, 1), PT(IL=S, 4)
END OF MODEL
PRINT
```

Fig.5.8 System Model Generation Using Type-1 Shunt [SIML1.MOD]
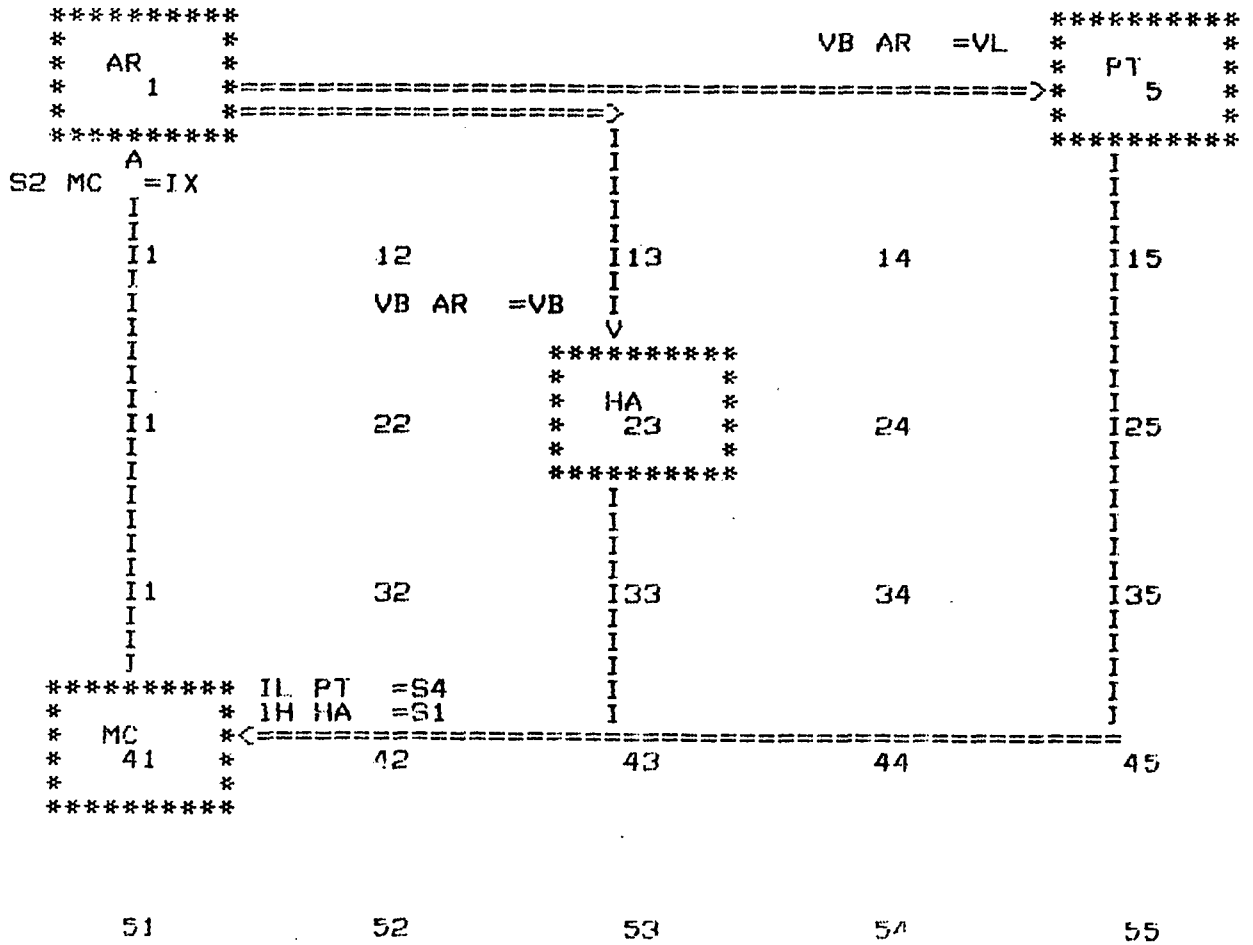
Fig.5.9 Schematic Diagram of [SIML1.MOD]

117

INPUT DATA REQUIREMENTS LIST

PARAMETERS REQUIRED

PARAMETER NAME (AND DIMENSION DATA FOR VECTOR AND MATRIX PARAMETERS)

COMPONENT						
AR	LL AR FV AR	LLSAR R AR	NP AR L AR	NS AR C AR	FC AR	TA AR
HA	A1 HA Z1 HA K2 HA	K1 HA P1 HA K3 HA	VR HA A2 HA L3 HA	ZO HA Z2 HA C1 HA	PO HA P2 HA C2 HA	L1 HA VF HA IMAHA
PT	PC PT T1 PT	SW PT PW3PT	TC PT T2 PT	PW1PT PW4PT	PW2PT T3 PT	VR PT PW5PT
MC	S3 MC	C1 MC	C2 MC	C3 MC	C4 MC	

STATES (INITIAL CONDITIONS AND ERROR CONTROLS REQUIRED)

STATE NAME (AND DIMENSION DATA FOR VECTOR AND MATRIX STATES)

COMPONENT		
AR	IL AR	VB AR
HA	X1 HA	S2 HA	X2 HA

Fig.5.10 Input Data Requirements List

```
TITLE=NASA(LARGE SIGNAL)
***************************************************
*TITLE = SOLAR ARRAY SYSTEM WITH SHUNT REGULATOR *
*          AND CONSTANT POWER LOAD                *
***************************************************

PARAMETER VALUES
R   AR =  .001,  C   AR = 5E-4,  L   AR = 10E-6,  LL AR = 1.
LLSAR = 0.,     TA AR = 301.,  FC AR = 8E-5,  FV AR = -2E-3
NP AR = 324,    NS AR = 58
***************************

INITIAL CONDITIONS
VB AR = 28.141
IL AR = 29.694
********
***********

INITIAL CONDITIONS
X1 HA = 10.678
S2 HA = 18.499
X2 HA = -21.650

PARAMETER VALUES
VR HA = 12.8
L1 HA = 1.5,   K1 HA = 0.4548685
A1 HA = -6.03652
Z1 HA = 2280.,  P1 HA = 2900.
A2 HA = 1.  ,72 HA = 667.,  P2 HA = 2900.
ZO HA = 539.1978,  PO HA = 0.
VF HA = 1.4
K2 HA = 0.0150376,   K3 HA = 0.083333
L3 HA = 1.4E-3,  C1 HA = 5450.  ,  C2 HA = -9.72
IMAHA = 40.

********
VR PT=15
PWOPT= 0, SW PT=50000
PW1PT=800
TC PT=5E-1, PC PT=1
C1 MC=1, C2 MC=-1, C3 MC=1, C4 MC=0
*
PRINTER PLOTS
ONLINE PLOTS
TMAX=10E-3, TINC=1E-6
PRATE=100, OUTRATE=50
SIMULATE
*****************************************

XIC-X
PARAMETER VALUES
PW2PT=750, SW PT=50000
PW1PT=800
TC PT=2E-3, PC PT=1
C1 MC=1, C2 MC=-1, C3 MC=1, C4 MC=0
*
PRINTER PLOTS
ONLINE PLOTS
*INT MODE=4
DISPLAY1(OVERPLOT)

VB AR
DISPLAY2 (OVERPLOT)
S2 MC, IH HA, IL PT
TMAX=10E-3, TINC=1E-6
PRATE=100, OUTRATE=50
SIMULATE
```

Fig.5.11 User's Parameter Values and Analysis Commands [SIML1.ANC]

The simulation results are identical to those of the previous simulation, shown in Fig.5.7.

For simulation of the Type-2 shunt regulator, the shunt regulator model [FS] replaces the Type-1 shunt model [HA] in the previous system configuration. This system model [SIML3.MOD] and schematic diagram are shown in Figs.5.13-14. In this simulation (Fig.5.12), the constant power load decreases linearly from 800W to 500W at a given rate (50W/ms). As the load current decreases, the shunt current increases accordingly. As a result, the solar array output current, again, becomes almost constant so the bus voltage remains within the specified voltage range.

The difference between the bus voltage at 800W and the bus voltage at 500W results from the shunt current being a linear function of the bus voltage. The input data requirements and the analysis program [SIML3.ANC] used in this simulation are given in Figs.5.15-16.
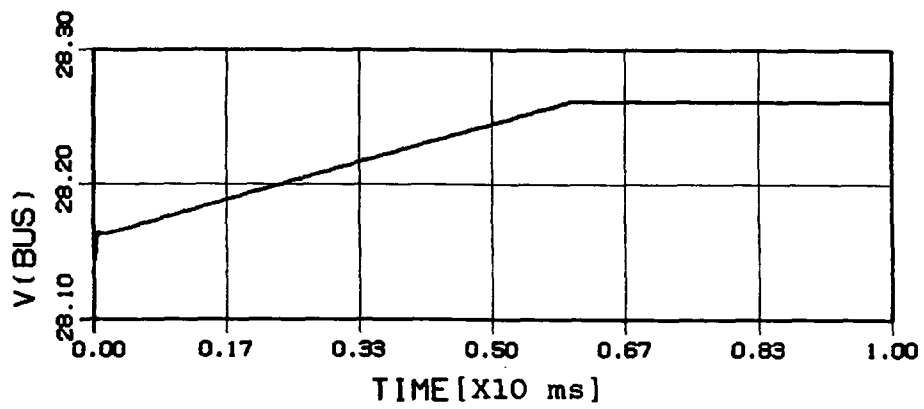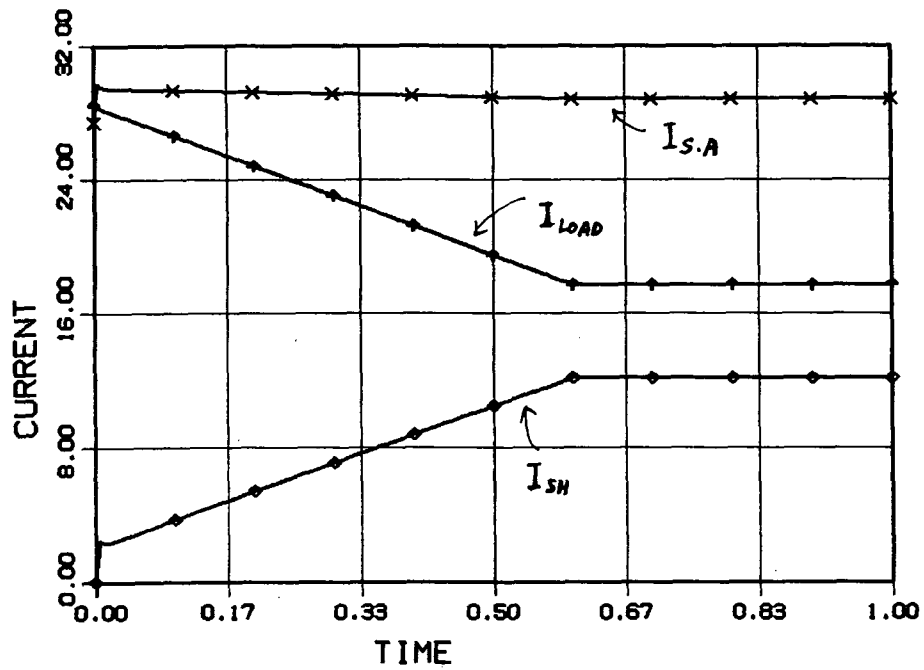
Fig.5.12 Simulation Results of Type-2 Shunt Regulator Model

```
MACRO FILE NAME = MACROS

************************************************
*  SOLAR ARRAY SYSTEM WITH TYPE 2 SHUNT        *
*  REGULATOR AND CONSTANT POWER LOAD           *
************************************************

LIST MACRO COMPONENTS = AR,FS,PT
MODEL DESCRIPTION
LOCATION = 1,  AR, INPUTS = MC(S,2=IX)
LOCATION = 22,FS, INPUTS = AR(VB=VB)
LOCATION = 6,  PT, INPUTS = AR(VB=VL)
LOCATION = 11,MC, INPUTS = FS(IH=S,1),PT(IL=S,4)
END OF MODEL
PRINT
```

Fig.5.13 System Model Generation Using Type-2 Shunt [SIML3.MOD]
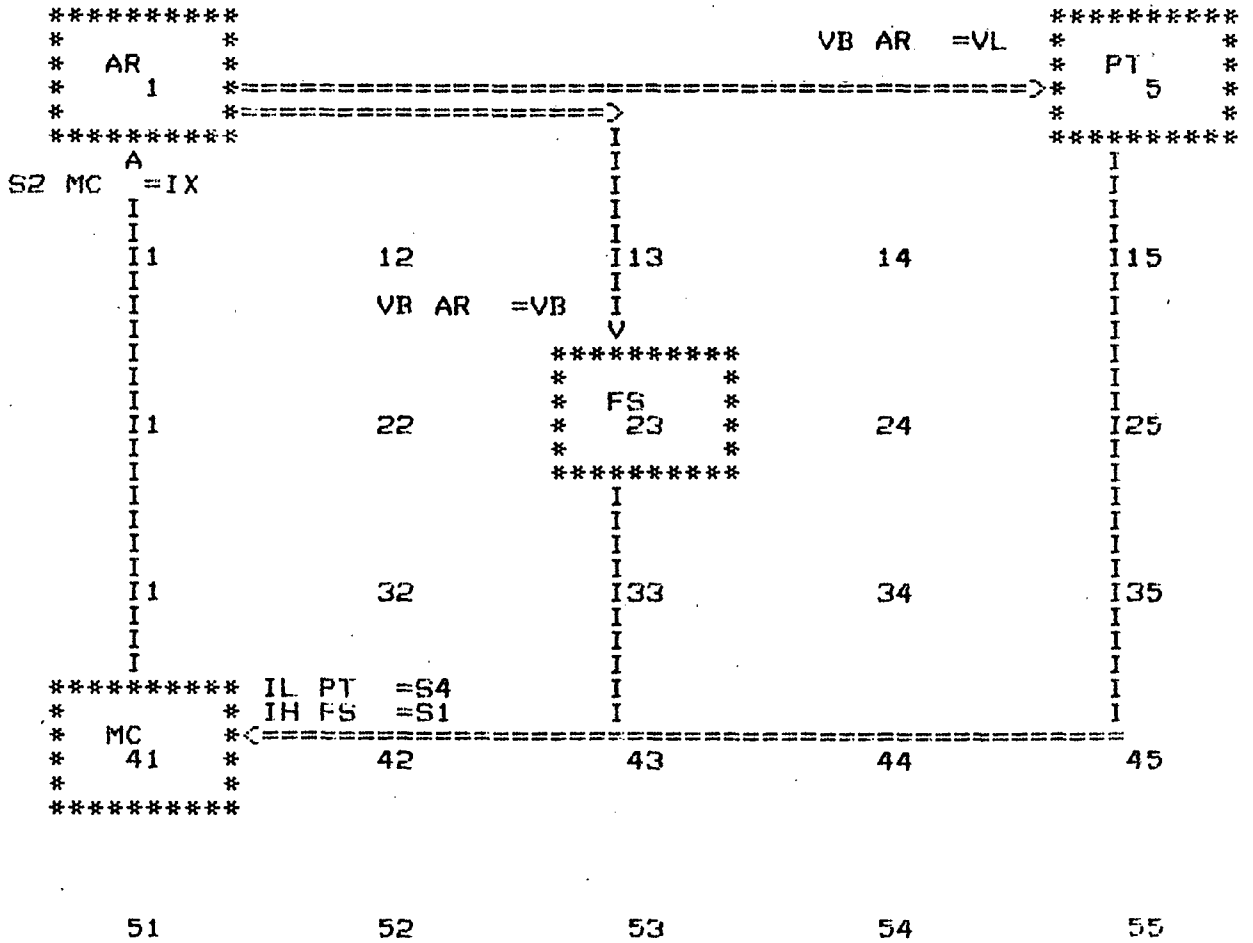
Fig.5.14 Schematic Diagram of [SIML3.MOD]

INPUT DATA REQUIREMENTS LIST

PARAMETERS REQUIRED

PARAMETER NAME (AND DIMENSION DATA FOR VECTOR AND MATRIX PARAMETERS)

COMPONENT						
AR	LL AR / FV AR	LLSAR / R AR	NP AR / L AR	NS AR / C AR	FC AR	TA AR
FS	VR FS / VSAFS	R1 FS / ILMFS	R2 FS	R3 FS	GM FS	VTHFS
PT	PC PT / T1 PT	SW PT / PW3PT	TC PT / T2 PT	PW1PT / PW4PT	PW2PT / T3 PT	VR PT / PW5PT
MC	S3 MC	C1 MC	C2 MC	C3 MC	C4 MC	

STATES (INITIAL CONDITIONS AND ERROR CONTROLS REQUIRED)

STATE NAME (AND DIMENSION DATA FOR VECTOR AND MATRIX STATES)

COMPONENT		
AR	IL AR	VB AR

Fig.5.15 Input Data Requirements List

123

```
TITLE=NASA(LARGE SIGNAL)

*************************************************************
*   SOLAR ARRAY SYSTEM WITH TYPE 2 SHUNT REGULATOR       *
*   AND CONSTANT POWER LOAD                              *
*************************************************************
PARAMETER VALUES
R   AR = .001,  C   AR = 5E-4,    L   AR = 10E-6, LL AR = 1.
LLSAR = 0.,  TA AR = 301.,  FC AR = 8E-5,    FV AR = -2E-3
NP AR = 324,   NS AR = 58
**************************
INITIAL CONDITIONS
VB AR = 28.14
IL AR = 30.138
********
***********
PARAMETER VALUES
VR FS = 28.02,  VSAFS = 15
R1 FS = 12400,  R2 FS =2.2E6,  R3 FS = 1.78419
GM FS =4,          VTHFS = 3,       ILMFS = 45
********
VR PT=15
PWOPT=700, SW PT=50000
PW1PT=800, PW2PT= 500, PW6PT = 500
TC PT=5E-1, PC PT=02
C1 MC=1, C2 MC=-1, C3 MC=1, C4 MC=0
*
PRINTER PLOTS
ONLINE PLOTS
*INT MODE=4
DISPLAY1
VB AR
DISPLAY2 (OVERPLOT)
S2 MC, IH FS, IL PT
DISPLAY3
PW PT
TMAX=10E-3, TINC=1E-6
PRATE=10, OUTRATE=50
SIMULATE
```

Fig.5.16 User's Parameter Values and Analysis Commands [SIML3.ANC]

124

5.2 PARTIAL SHUNT REGULATOR/SOLAR ARRAY MODEL

5.2.1 INTRODUCTION

The full shunt regulator has been widely used in space power systems. One disadvantage is that under a zero load condition it must dissipate the entire array output power. This complicates the thermal design and increases its size and weight. The partial shunt regulator reduces the peak power dissipation to 30 to 50 percent of the amount dissipated in a functionally equivalent full shunt.

As in a full shunt, there is a control circuit that performs the same basic function and there are sections intended to dissipate or bypass some of the excess power. In a partial shunt system, the power sections are placed across only part of the total number of series-connected solar cells. Thus the shunt circuit is used to absorb part of the output of the solar array. The design of a partial shunt is greatly dependent on the type of solar cells used, the degradation encountered, and the temperature extremes to which the cells are subjected in orbital flight.

As shown in Fig.5.17, the total number of series solar cells is expressed as

$$N_S = N_U + N_L \qquad\qquad (5.7)$$

where N_U = the number of upper series cells

N_L = the number of lower series cells
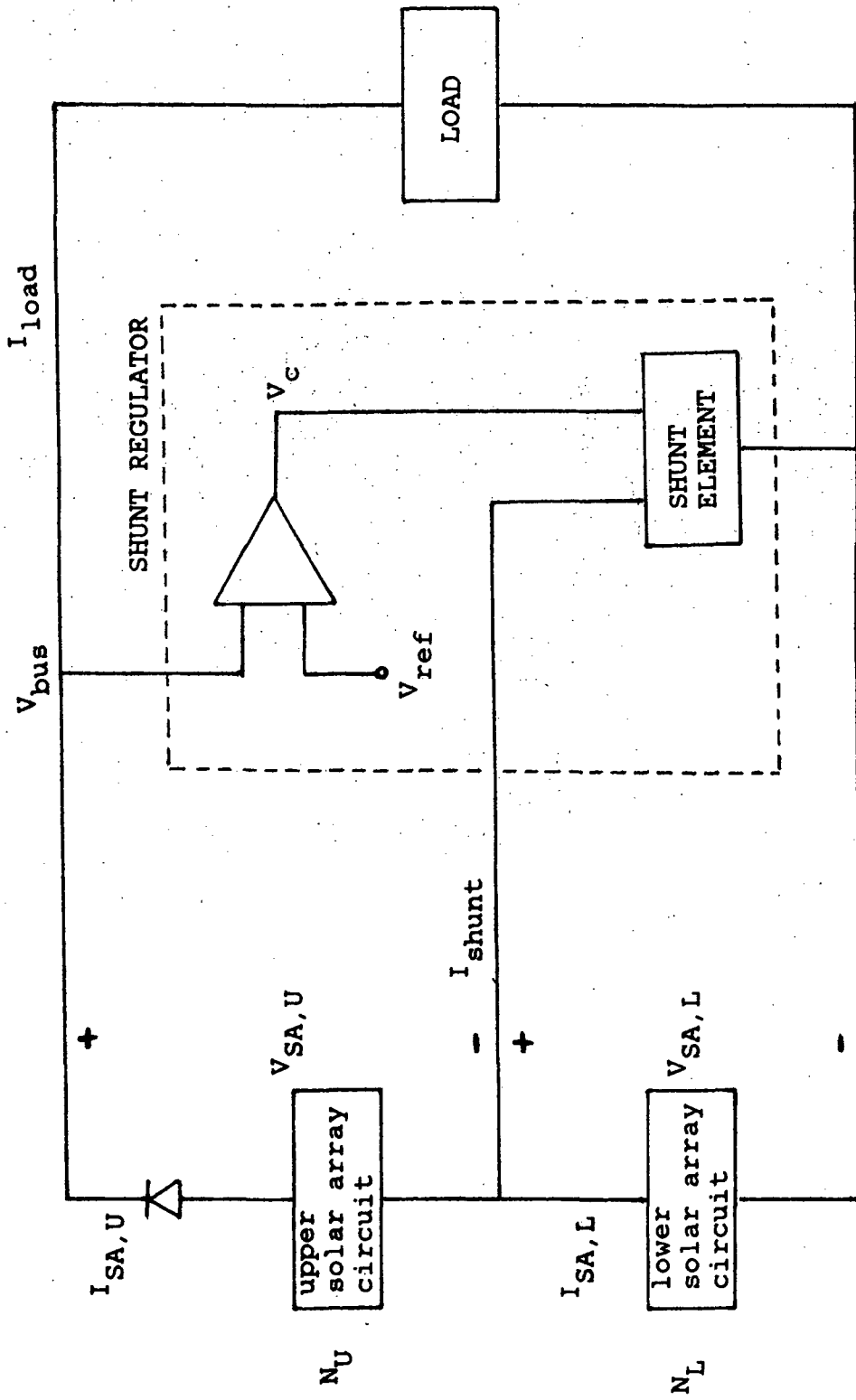
Fig.5.17 Partial Shunt Configuration

126

The number of series cells, N_s, is selected to deliver a given fixed array's output voltage, $V_{bus} = V_r$, throughout the life of the system [8].

$$N_S \cdot d_v \cdot V_{mp} = V_r \qquad (5.8)$$

where d_v is a voltage degradation factor equal to the ratio of the end-of-life to beginning-of-life voltage at the array's maximum power point, and at a steady-state array temperature. However, the array output voltage is lower than V_{mp} at the beginning-of-life if N_s is chosen using Equation (5.8). This is not a proper region of operation since the system can easily become unstable. Therefore, the factor, $\alpha < 1$, must be applied to N_s to ensure the system is operating in the stable region. When the solar array output voltage for normal operation is greater than V_{mp},

$$N_S \cdot d_v \cdot V_{mp} = \alpha \cdot V_r \qquad (5.9)$$

In partial shunt configuration, the array is electrically split into two sections: upper and lower. The partial shunt element is placed across a part of the total number of series cells defined by the fraction m:

$$m = N_L / (N_L + N_U) \qquad (5.10)$$

When the shunt transistor is saturated ($V_{sh} = 0$ assumed), the highest possible voltage which the upper bank of N_U cells can deliver must not exceed V_r.   This will occur when the array is completely unloaded and the solar cells are at their lowest temperature, at the beginning-of-life.

$$N_U \cdot V_{oc}(max) \quad < \quad V_r \qquad\qquad (5.11)$$

By substituting Equations (5.7),(5.9) and (5.10) into equation (5.11),

$$m \quad > \quad 1 - [\ \alpha \cdot d_v \cdot V_{mp}\ /\ V_{oc}(max)\ ] \qquad\qquad (5.12)$$

Thus, the location of the array tap-off point is seen to be dependent on the values of α, d_v, V_{mp} and $V_{oc}(max)$.

5.2.2 MODEL GENERATION [AP]

For the partial shunt configuration, as shown in Fig.5.18, another solar array model has been developed to provide the tap-off point of the solar array for the shunt regulator. The control voltage, V_c, is generated by sensing the main bus voltage to control the shunt current.   In this model, two solar array models are connected in series.   The lower solar array supplies the shunt current to regulate the bus voltage. As a result, Newton iteration routines are included in the model and the output current of the upper solar array is

128
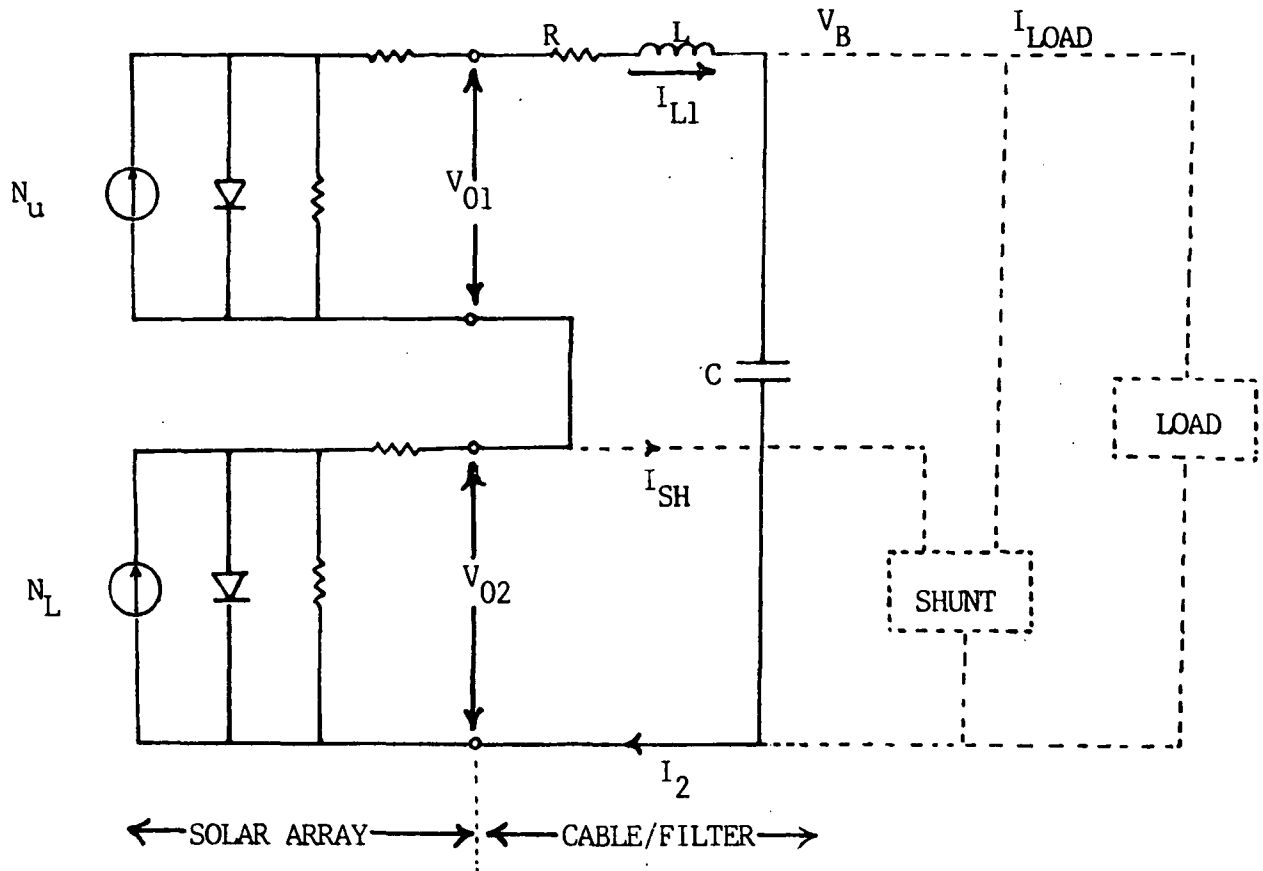
STATE EQUATIONS

$$I_2 = I_{L1} + I_{SH}$$

$$V_L = V_{01} + V_{02} - R \cdot I_{L1} - V_B$$

$$L \frac{dI_L}{dt} = V_L$$

$$C \frac{dV_C}{dt} = I_{L1} - I_{LOAD}$$

Fig.5.18 Circuit Model of Solar Array/Partial Shunt [AP]

equal to the inductor current, I_{L1}. The output current of the lower solar array is the sum of the shunt current and the inductor current. With the known upper and lower solar array output voltages, V_{o1} and V_{o2}, two state equations exist:

$$L_1 \frac{dI_{L1}}{dt} = V_{L1} \qquad \text{where } V_{L1} = V_{o1} + V_{o2} - R1 \cdot I_{L1} - V_B$$

$$C_1 \frac{dV_B}{dt} = I_{L1} - I_L$$

5.2.3 EXAMPLE OF SIMULATION

For simulation of the partial shunt model [AP], system [PSS5.MOD] (Fig.5.20) is configured as shown in Fig.5.21. The system consists of the partial shunt model [AP], the full shunt model [FS] and a constant power model [PT]. As shown in the schematic diagram (Fig.5.21), the solar array model (partial shunt model) [AP] is connected with a full shunt model [FS] and a constant power model [PT].

As shown in Fig.5.19, as the load power decreases at a certain rate, the solar array output voltage increases. The bus voltage increases accordingly and becomes greater than V_r (28.14V) which causes the shunt current to flow. As shown in Fig.5.18, the upper solar array carries only the load current and the lower solar array carries both the load current and shunt current.

130
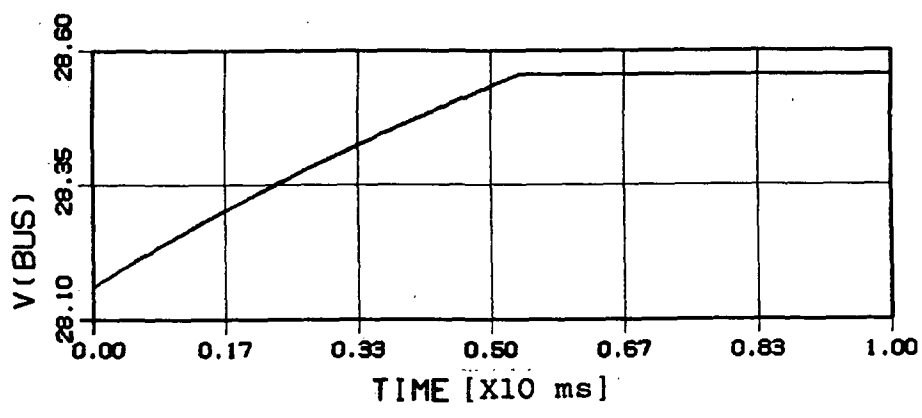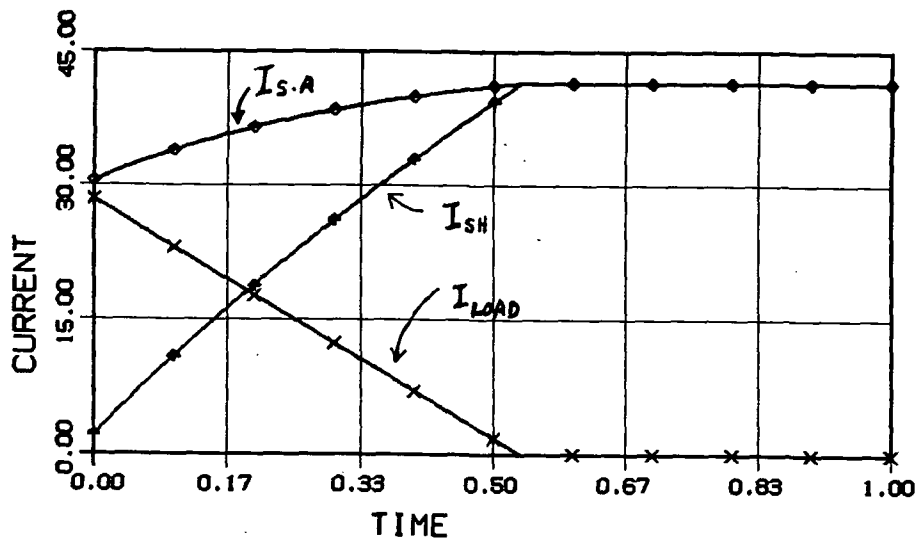
Fig.5.19 Simulation Results of Partial Shunt System

```
MACRO FILE NAME = MACROS

**********************************************
* PARTIAL SHUNT SYSTEM WITH CONSTANT POWER  *
* LOAD                                      *
**********************************************
* REVISED ON 3/3/1986

LIST MACRO COMPONENTS = AP,FS,PT
MODEL DESCRIPTION
LOCATION=1,  AP, INPUTS = FS(IH=IH),  PT(IL=IL)
LOCATION=33,FS, INPUTS = AP(VB=VB)
LOCATION=5,  PT, INPUTS = AP(VB=VL)
END OF MODEL
PRINT
```

Fig.5.20 System Model Generation Using Partial Shunt [PSS5.MOD]

Fig.5.21 Schematic Diagram of [PSS5.MOD]

Since the load current continues to decrease, the upper solar array output voltage increases. The lower array current, the sum of the load and shunt currents, increases so the lower solar array output voltage decreases. The sum of lower and upper solar array voltages becomes the bus voltage.

As a result, the bus voltage could be regulated within the specified range. The input data requirement list and analysis program used for this simulation are given in Figs.5.22-23.

PARAMETERS REQUIRED

PARAMETER NAME (AND DIMENSION DATA FOR VECTOR AND MATRIX PARAMETERS)

COMPONENT						
AP	LL AP	NP AP	NS1AP	NS2AP	ILMAP	VIHAP
	VILAP	V2HAP	V2LAP	R AP	C AP	L AP
FS	VR FS	R1 FS	R2 FS	R3 FS	VTHFS	
	VSAFS	ILMFS		GM FS		
PT	PC PT	SW PT	TC PT	PW1PT	PW2PT	VR PT
	T1 PT	PW3PT	T2 PT	PW4PT	T3 PT	PW5PT

STATES   (INITIAL CONDITIONS AND ERROR CONTROLS REQUIRED)

STATE NAME (AND DIMENSION DATA FOR VECTOR AND MATRIX STATES)

COMPONENT		
AP	VB AP	IL1AP

Fig.5:22 Input Data Requirements List

```
TITLE=NASA(LARGE SIGNAL)
******************************************************
*TITLE = PARTIAL SHUNT SYSTEM WITH CONSTANT       *
*            POWER LOAD                           *
******************************************************
PARAMETER VALUES
R   AP =  .001,  C   AP = 500E-6,      L   AP = 1E-6
NP AP = 324,   NS1AP = 29,    NS2AP = 29,   LL  AP =1.
ILMAP = 45,     V1HAP = 15.976, V1LAP = 12.57
V2HAP = 15.976, V2LAP = 12.57
*************************

INITIAL CONDITIONS
VB AP = 28.161
IL1AP = 28.409
********

PARAMETER VALUES
VR FS = 28.14,   VSAFS = 15.
R1 FS = 12400,  R2 FS = 2.2E6, R3 FS = 1.78419
GM FS = 4.   ,  VTHFS = 3.,    ILMFS = 45.
********

VR PT=15
SW PT=150000
PW1PT=800,  PW2PT=0
TC PT=5E-3,  PC PT=2
*
PRINTER PLOTS
ONLINE PLOTS
*INT MODE=4
DISPLAY1(OVERPLOT)
VB AP
DISPLAY2 (OVERPLOT)
IL1AP,  I2 AP,  IH FS
DISPLAY3 (OVERPLOT)
VO1AP,  VO2AP
DISPLAY4 (OVERPLOT)
PW PT
*************
TMAX=10E-3, TINC=1E-6
PRATE=200,  OUTRATE=50
SIMULATE
```

Fig.5.23 User's Parameter Values and Analysis Commands [PSS5.ANC]

CHAPTER 6

BATTERY-DISCHARGER MODELING

6.1 INTRODUCTION

The basic functional requirement of the battery discharger is to regulate the bus voltage when the solar array is incapable of meeting the load demand. In this mode both the solar array and the battery function as power sources. Figure 6.1 shows the system operating in the battery discharge mode. When the bus voltage drops below a certain magnitude, the control signal activates the battery-discharge converter in order to maintain regulation of the bus voltage.

In the Direct Energy Transfer (DET) system, when the solar array output power decreases due to the weakening of the illumination level, the battery discharger operates from no-load condition through the converter discontinuous-conduction mode (DCM) of operation and ultimately to the continuous-conduction mode (CCM). Since the steady-state and dynamic behaviors of switching regulators for these two modes of operation are quite different, the design of the feedback controller must take into consideration the two modes of operation.
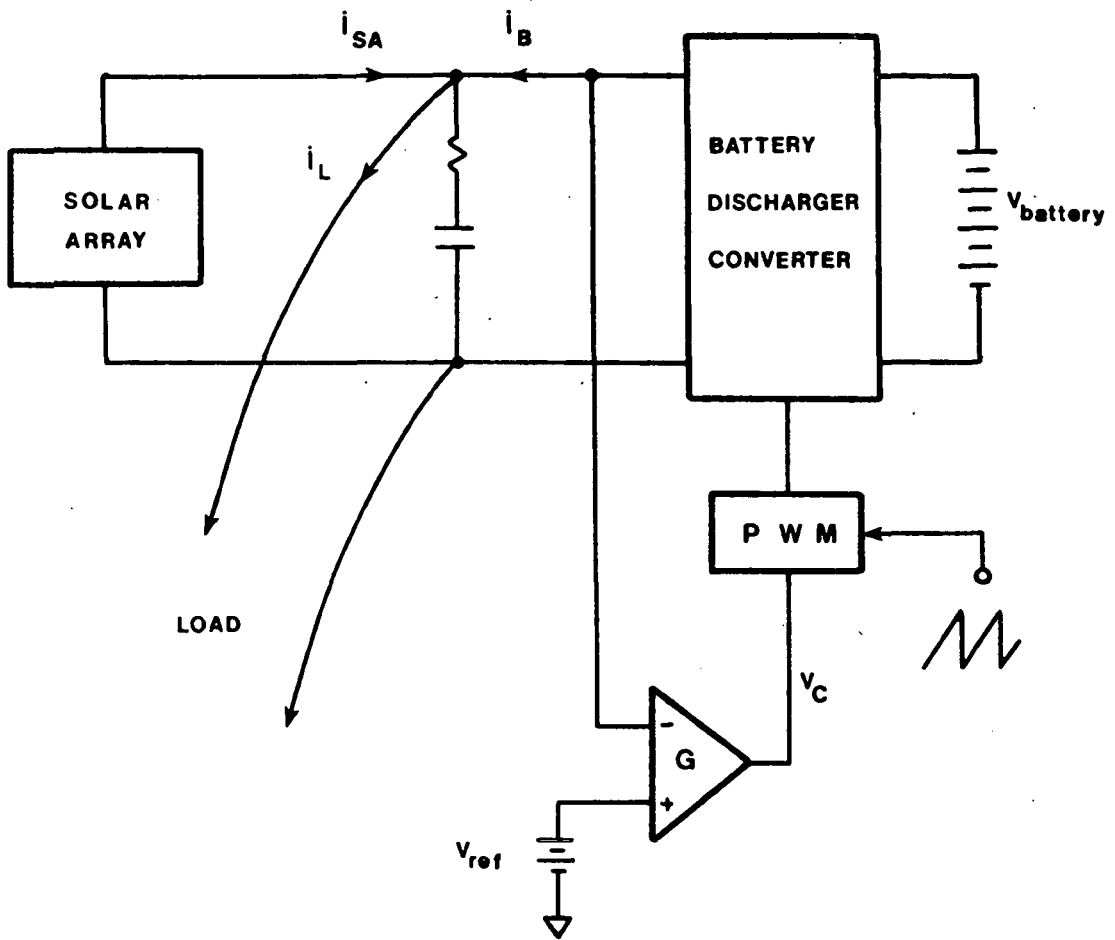
Figure 6.1 *System in the battery discharge mode*

137

6.2 BATTERY-DISCHARGER MODELING AND ANALYSIS

The power stage of the battery-discharge-converter used in the DET system is shown in Fig.6.2. The circuit basically operates as a buck-type regulator operating in a push-pull mode. Since the terminal voltage of the battery is between 17 and 25 volts, an auto-transformer is used to boost the voltage to 28V. In this study, a simplified circuit is used as shown in Fig.6.3(a). The two sources in Fig.6.3(a) represent the transformer action between the power switches' ON and OFF intervals.

6.2.1 ANALYSIS OF BATTERY-DISCHARGE CONVERTER IN DCM

As illustrated in Fig.3.2, there exist three intervals, d_1T_s, d_2T_s and d_3T_s. While the first interval, d_1T_s, (inductor charging) is dictated by the "ON" time of the switching function and is a known quantity, the second interval, d_2T_s, (inductor discharging) is unknown and depends in general on both the length of the first interval and circuit parameters.

Using ideal elements in the circuit in Fig.6.3(a) and ignoring load dynamics, three switched networks in the discontinuous-conduction mode are shown in Fig.6.3(b). For the choice of the state vector, $x = [i \quad v]^T$, the state-space equations of the three switched networks become:
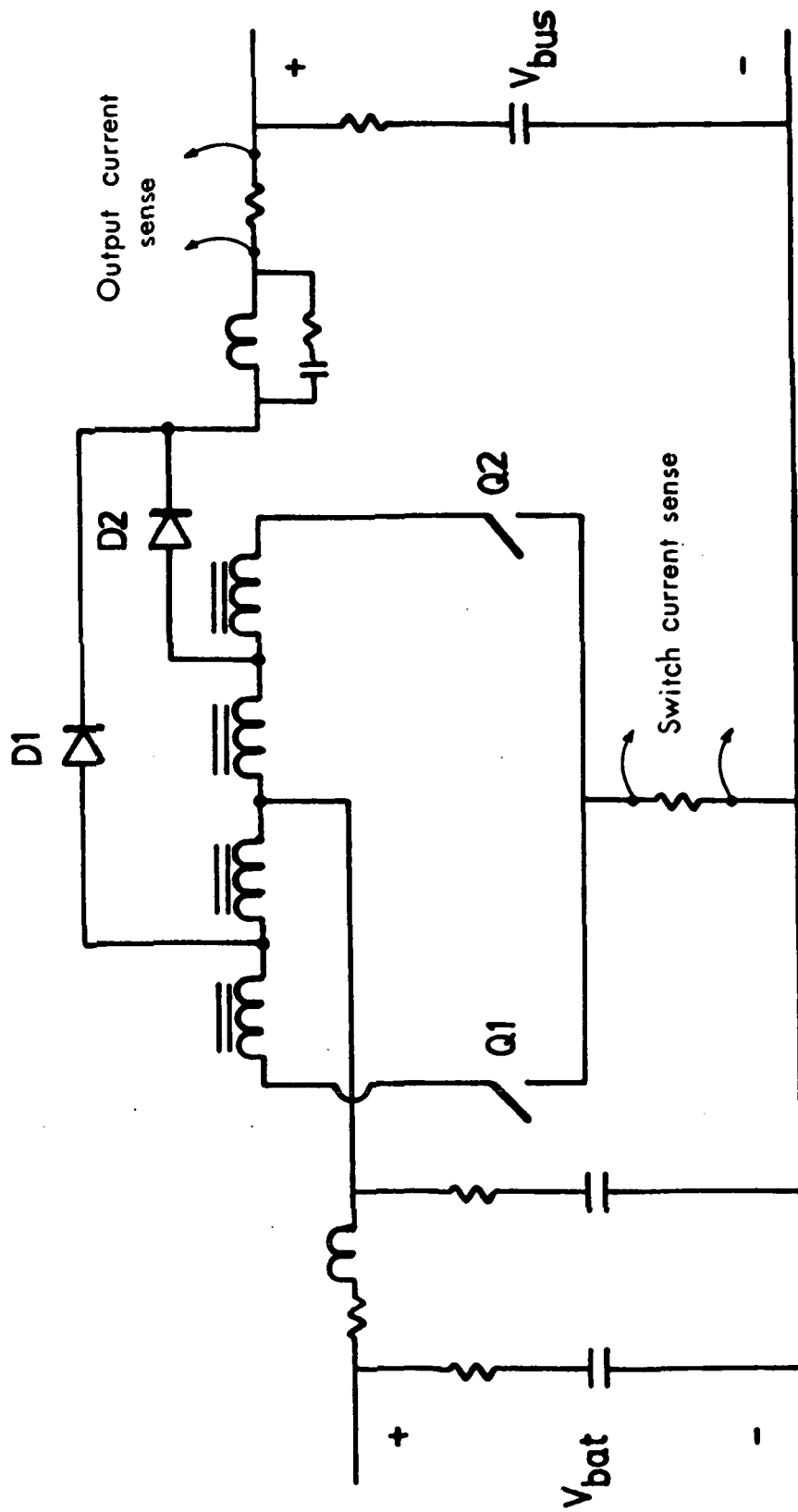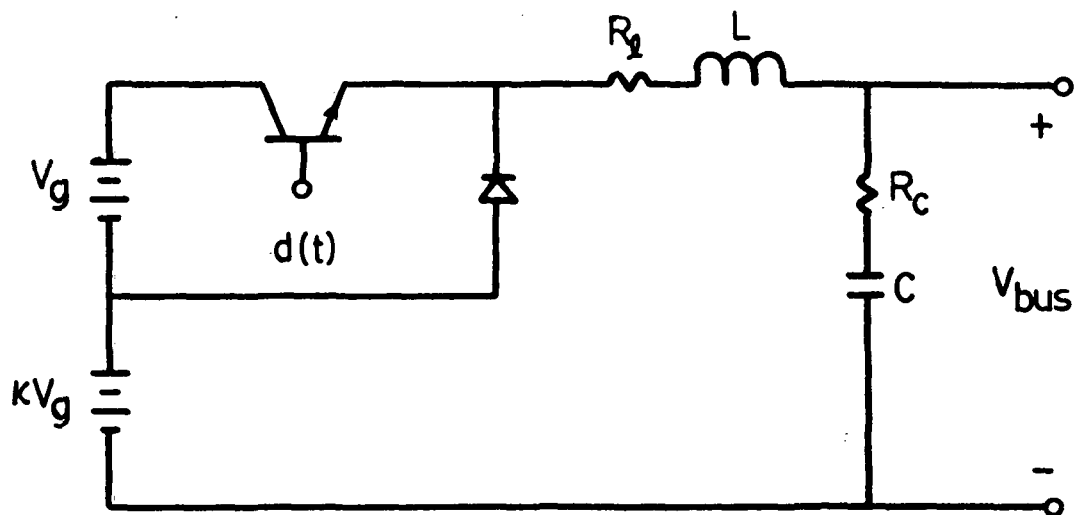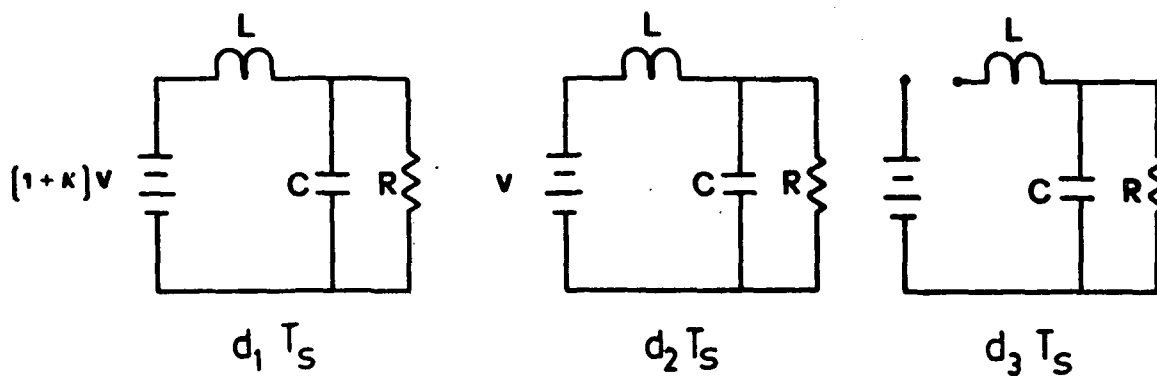
Figure 6.2 Battery discharger converter circuit

139

Figure 6.3 (a) Simplified circuit of the converter in Fig.6.2

(b) Three switched circuits

$$\dot{x} = A_1 x + B_1 v_g \qquad \text{for interval } d_1 T_s$$

$$\dot{x} = A_2 x + B_2 v_g \qquad \text{for interval } d_2 T_s \qquad (6.1)$$

$$\dot{x} = A_3 x + B_3 v_g \qquad \text{for interval } d_3 T_s$$

where

$$A_1 = A_2 = \begin{bmatrix} 0 & -\dfrac{1}{L} \\ \dfrac{1}{C} & -\dfrac{1}{CR} \end{bmatrix}, \qquad A_3 = \begin{bmatrix} 0 & 0 \\ 0 & -\dfrac{1}{CR} \end{bmatrix}$$

$$B_1 = \begin{bmatrix} \dfrac{(1+\kappa)}{L} \\ 0 \end{bmatrix}, \qquad B_2 = \begin{bmatrix} \dfrac{\kappa}{L} \\ 0 \end{bmatrix}, \qquad B_3 = 0 \qquad (6.2)$$

By averaging equation (6.1), the following linear, algebraic, static equations result.

$$\underbrace{\begin{bmatrix} 0 & -\dfrac{D_1+D_2}{L} \\ \dfrac{D_1+D_2}{C} & -\dfrac{1}{CR} \end{bmatrix}}_{A} \underbrace{\begin{bmatrix} I \\ V \end{bmatrix}}_{X} + \underbrace{\begin{bmatrix} \dfrac{D_1(1+\kappa)+\kappa D_2}{L} \\ 0 \end{bmatrix}}_{B} V_g = 0 \qquad (6.3)$$

141

Then the steady-state solution of Eq.(6.3) is

$$\frac{V}{V_g} \equiv M = \frac{D_1(1+\kappa) + \kappa D_2}{D_1 + D_2}$$

$$I = \frac{V}{R} \frac{1}{(D_1 + D_2)} \tag{6.4}$$

Hence, the dc conditions depend not only on D_1 and R, as in the continuous-conduction mode, but also on D_2. Using the additional constraint on the average of the inductor current for $(D_1 + D_2)T_s$,

$$I = \frac{(1+\kappa)V_g - V}{2L} D_1 T_s \tag{6.5}$$

The dc conditions are determined with the known quantities D_1 and R. For example, substitution of Eq.(6.5) into Eq.(6.3) results in

$$D_2 = \frac{1}{2} \left[\left(\frac{\kappa \tau_n}{D_1} - D_1 \right) + \left[\left(\frac{\kappa \tau_n}{D_1} - D_1 \right)^2 + 4\tau_n(1+\kappa)\right]^{\frac{1}{2}} \right] \tag{6.6}$$

where

$$\tau_n \equiv 2L \, / \, (R \, T_s) \; ; \quad \text{normalized time constant.}$$

The boundary condition between the two conduction modes is

$$D_2 < 1 - D_1 \quad ; \quad \text{discontinuous conduction mode}$$

$$D_2 > 1 - D_1 \quad ; \quad \text{continuous conduction mode} \quad (6.7)$$

Using Eqs.(6.6), the critical value of τ_n can be determined by solving $D_2 = 1 - D_1$.

$$\tau_{ncrit} = \frac{1 - D_1}{1 + \kappa + \kappa(1 - D_1)/D_1} \quad (6.8)$$

Suppose that the output voltage is regulated with a proper feedback circuit, then the dc voltage gain, M, can be treated as a constant for a fixed input voltage. The duty ratio, D_1, in the discontinuous-conduction mode can be derived as a function of M, or as a function of τ_n.

$$D_1 = \left[\frac{\tau_n M(M-\kappa)}{1 + \kappa - M} \right]^{\frac{1}{2}} \quad (6.9)$$

Using the results in Eqs.(6.4) through (6.9), the dc behavior of the battery discharger is illustrated in Fig.6.4. In Fig.6.4(a), the boundary condition, τ_{ncrit}, between the two modes is plotted as a function of D_1. The dc voltage gain, M, as a function of D_1 for different values of τ_n, is shown in Fig.6.4(b).
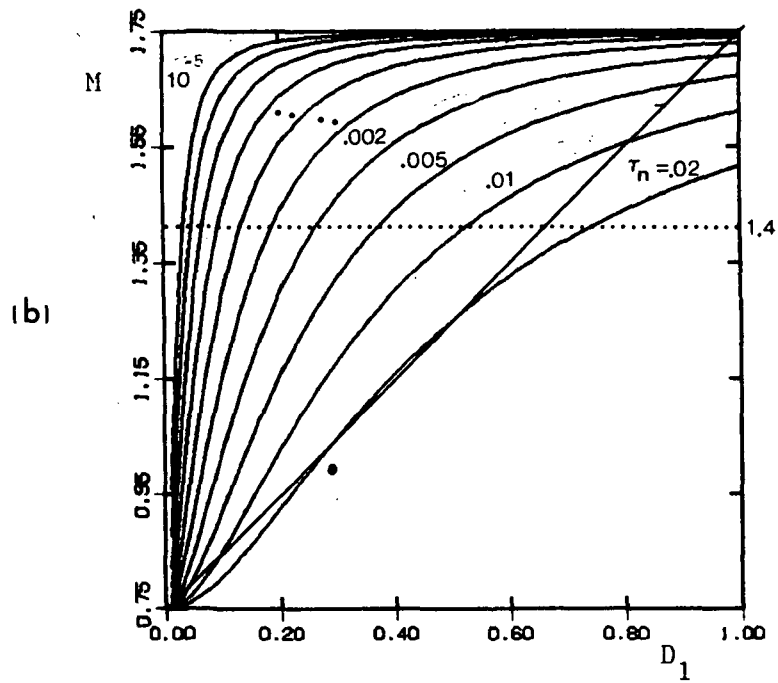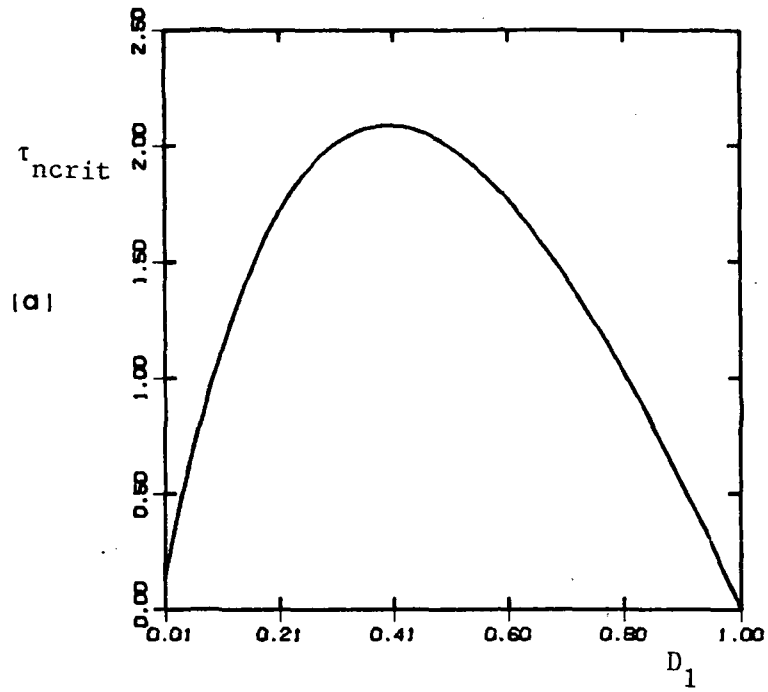
143

Figure 6.4   DC characteristics of the battery discharger converter

(a) τ_{ncrit} vs D_1

(b) M vs D_1

6.2.2 COMPENSATOR DESIGN FOR BATTERY DISCHARGER

Since the battery discharger operates from no-load to full-load, it is important to understand the start-up behavior of the converter. Suppose now that the solar array output power gradually decreases. Initially the battery-discharging current is zero (i.e., $\tau_n=0$) and the duty ratio $D_1=0$. As the solar array output power decreases, the operating point moves along the solar array curve which causes the bus voltage to drop. This activates the battery-discharger electronics via an error amplifier. In this start-up mode, it is very important to design a proper error amplifier circuit for the following reasons.

Since the sensitivity of the dc voltage gain, with respect to the duty ratio, is very high in the light-load condition (start-up mode), as shown in Fig.6.4(b), any delay in the logic circuitry or the false triggering due to noise will cause a high-frequency oscillation in the bus voltage. While in a low-gain feedback system the controller may not act quickly enough to regulate the bus voltage, since the plant time constant of the output capacitor and load resistance is very slow. This may cause a large-amplitude, low-frequency oscillation. This is especially critical when the output voltage of the battery-discharge converter is set such that it operates close to the solar array maximum power point. Since the low-gain controller allows the bus voltage to drop before the controller starts correcting the error, it is

possible that the system may move into the unstable region as discussed previously. Since the battery discharger operates from the discontinuous-conduction mode to continuous-conduction mode, the error amplifier should be able to stabilize the system in both modes.

Small-signal analysis of the battery discharger in discontinuous-conduction mode shows that the transfer functions have a single pole and no zero[9]. Any converter that can be described with two state variables, one of them being an inductor current, has a single-pole transfer function in the discontinuous conduction mode. Thus, the dynamic behavior of the converter, operating in the discontinuous-conduction mode, is completely different from that of the continuous-conduction mode where the system has a complex pole pair. Therefore, the feedback controller should compensate the plant dynamics in both modes of operation. Figure 6.5 illustrates the root-locus diagram of the open-loop converter as a function of load resistance. Without a compensator, the system eigenvalue is close to the origin, thus, the system response should be very slow in the discontinuous-conduction mode as predicted in the dc analysis. Decreasing the load resistance beyond R_{crit}, the converter will operate in the continuous-conduction mode, and the open-loop eigenvalues become complex. In this range, the response is slow and oscillatory. A further decrease of the load resistance will move the locus toward the circle with
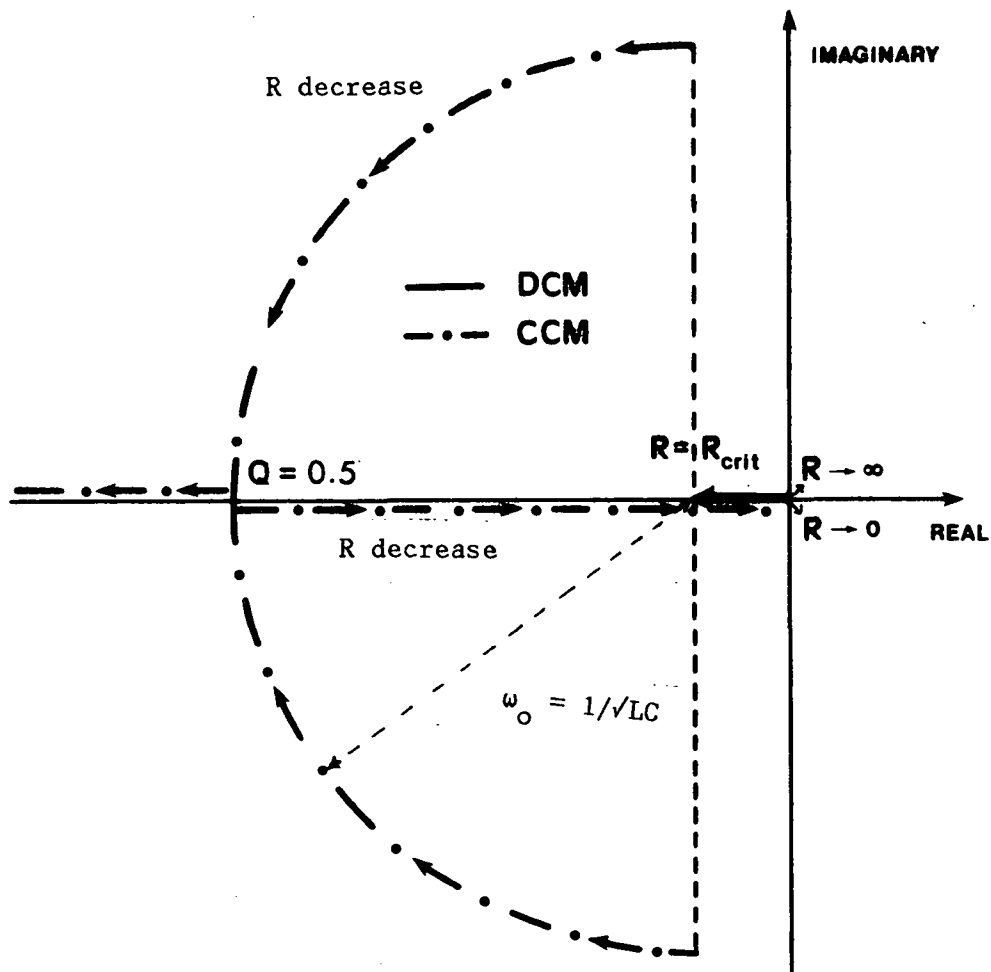
Figure 6.5   Root locus of the open loop buck-type converter as
a function of load resistance, R for DCM and CCM

the radius of $\omega_o = 1/\sqrt{LC}$, and finally approaches to the real axis again.

Figure 6.6 illustrates the root-locus diagrams for different compensators in both DCM and CCM. Let us first consider the converter operating in DCM. Since the open-loop characteristics have a single pole near the origin, to speed-up the response a simple proportional gain controller can be used to move the eigenvalue away from the origin. This is shown in Fig.6.6(a). However, this gain also moves the eigenvalues to the imaginary-axis in the CCM operation. A lower gain may stabilize the system in CCM, but the slow response in DCM may cause a severe, bus voltage droop during transient.

A typical integrator and lead-lag compensator as illustrated in Fig.6.6(b) is examined next. The integrator is used for the tight regulation of the output voltage. The zero compensates the excessive phase lag due to the presence of an integrator, and the pole attenuates the high-frequency switching noise. Since the integrator slows down the system response in DCM, the roots stay near the imaginary axis in DCM.

Therefore, to achieve an optimum response for both CCM and DCM operations, a compensator must include a proportional gain to speed up the system response in DCM and the lead-lag type compensator for stable operation in CCM. This is illustrated in Fig.6.6(c).
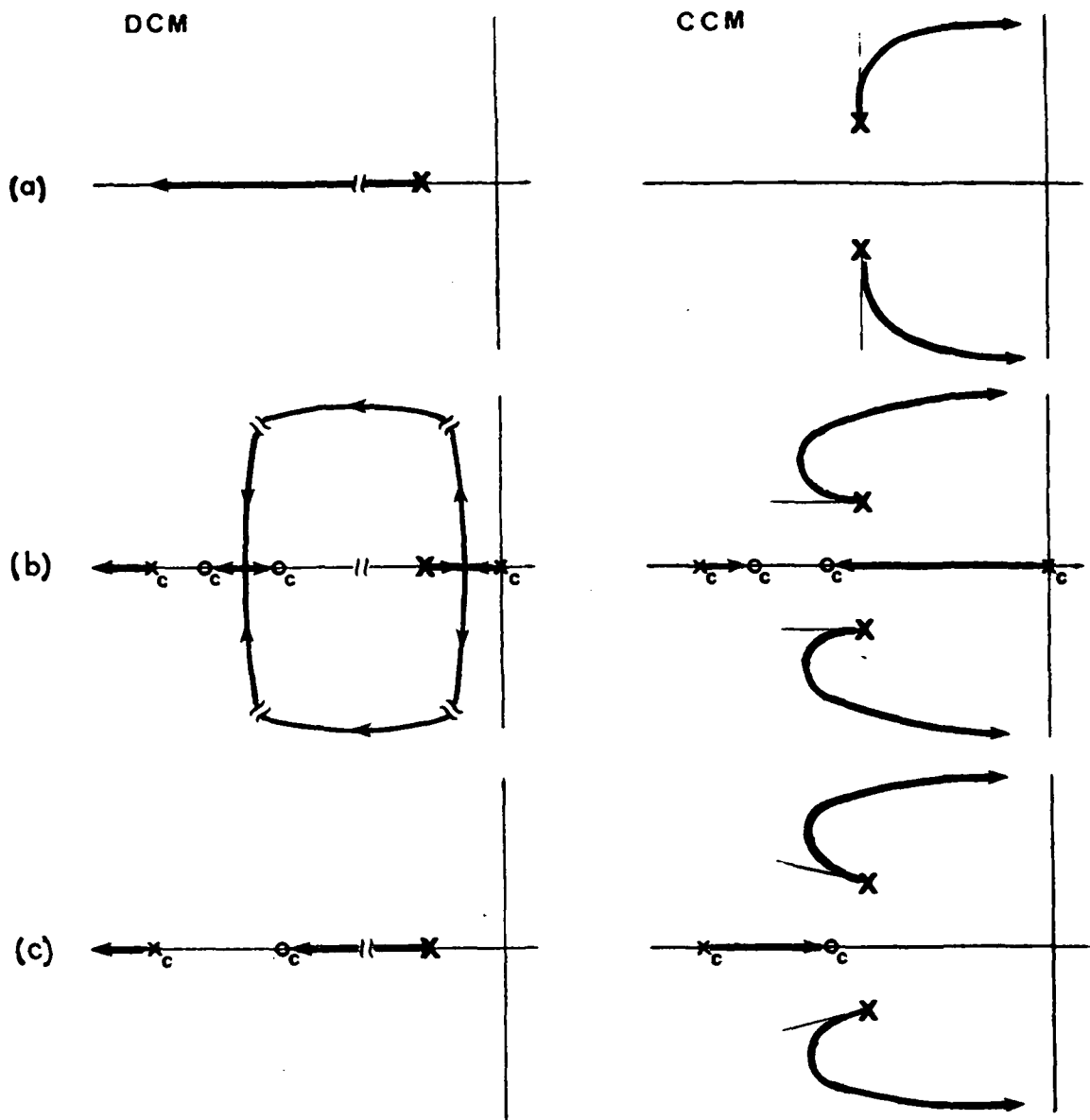
148

Figure 6.6   Root loci of the closed loop buck-type converter
in DCM and CCM for three compensators

(a) proportional gain
(b) integrator plus lead-lag
(c) proportional plus lead-lag

x_c : compensation pole

o_c : compensation zero

149

6.3 EASY5 MODELING FOR THE BATTERY-DISCHARGE CONVERTER [BP]

In the DET system, as shown in Fig.6.1, the output capacitor of the battery discharger is shared with the output-filter capacitor of the solar array. Thus, the capacitor is not included in the power stage model. Since only one state variable, inductor current (i_L), is needed in the power-stage model, the state equation for each interval is as follows.

For $D_1 T_s$ (switch is on),

$$\dot{i}_L = [(1 + \kappa)v_1 - i_L R_c - v_2]/L$$

For $D_2 T_s$ (switch is off, i_L 0),

$$\dot{i}_L = [v_1 - i_L R_c - v_2]/L$$

For $D_3 T_s$ (switch is off, $i_L = 0$),

$$\dot{i}_L = 0$$

For the feedback control, macro modules developed in Chapter 3 can be used.

6.4 BATTERY DISCHARGER MODEL SIMULATION

To simulate the performances of the battery discharger, a simplified DET system is configured using the following modules.

- [AR] --- solar array

- [FS] --- full shunt regulator

- [BP] --- battery-discharger power stage

- [PT] --- constant power load

- [WM] --- PWM(constant frequency control)

- [MC] --- summer(EASY5 standard module)

- various compensator modules [MP],[PZ],[DG]

Figure 6.7 shows the EASY5 generated system configuration [SIM.MGL]. The following simulations are done with the single-loop control employing constant-frequency PWM. Two compensators are employed, as shown in Fig.6.8, to verify the previous analysis. Figure 6.9 shows the step-load transient response from 1300W to 1400W when the battery discharger operates in the continuous-conduction mode. As shown in the figure, the system behaves equally well for both

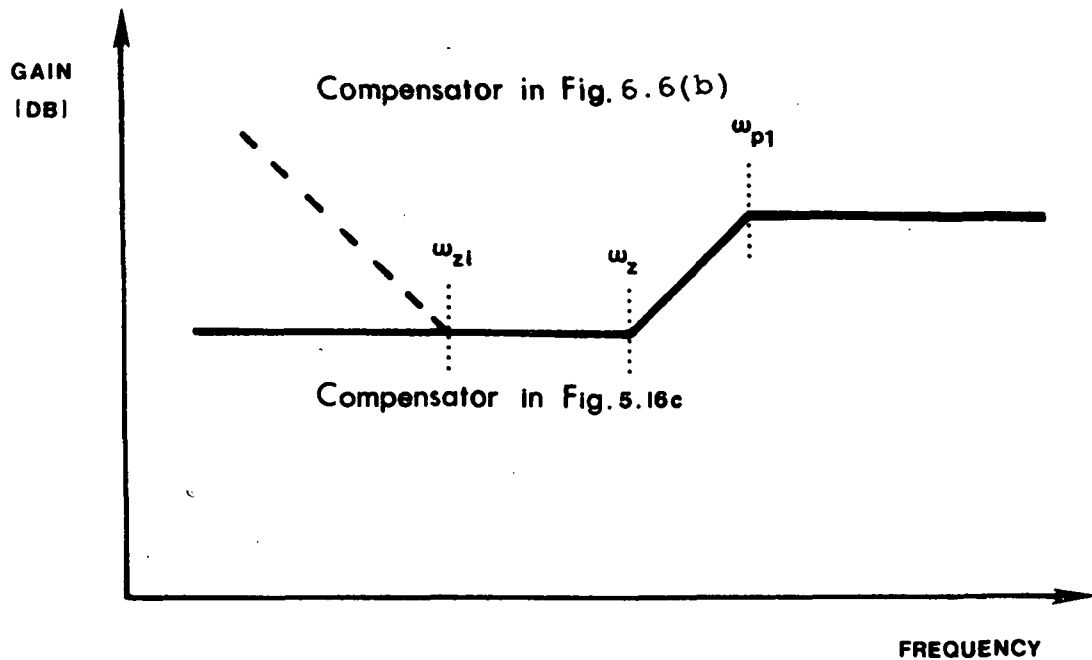Figure 6.7 EASY5 generated system configuration

Figure 6.8   Two compensators used for the simulation

Power stage : $\omega_o = 3000$ in CCM

$0 < \omega_p < 12.4$ in DCM

Compensator : $\omega_{zi} = 1000$

$\omega_{z1} = 6000$

$\omega_{p1} = 50000$

compensators. In Fig.6.10, the load power (i_{load}) is gradually increasing and various modes are illustrated. The system initially operates in the shunt mode until 0.6 ms, then it gets into the dead-band mode where the solar array solely supplies the load power. The operating point moves along the solar array curve as the load power increases. The battery discharger, employing the proportional-gain feedback (Fig.6.6(c)), starts regulating the bus voltage at t=1ms as shown in Fig.6.10(a). While using the integrator feedback, it starts to operate at t=2ms and slowly creeps up to reach the output-voltage regulation, as shown in Fig.6.10(b). As shown in this figure, the slow response in DCM of the integrator- type controller causes severe droop in the bus voltage.

The results in Figs.6.9 and 6.10 show that a compensator designed for the CCM operation may not be suitable for the DCM operation, and consequently, the compensator design for the boost converter must be done more carefully. This is because such a converter has a single pole in the discontinuous-conduction mode, and a complex-pole pair and a right-half-plane zero in the continuous-conduction mode.
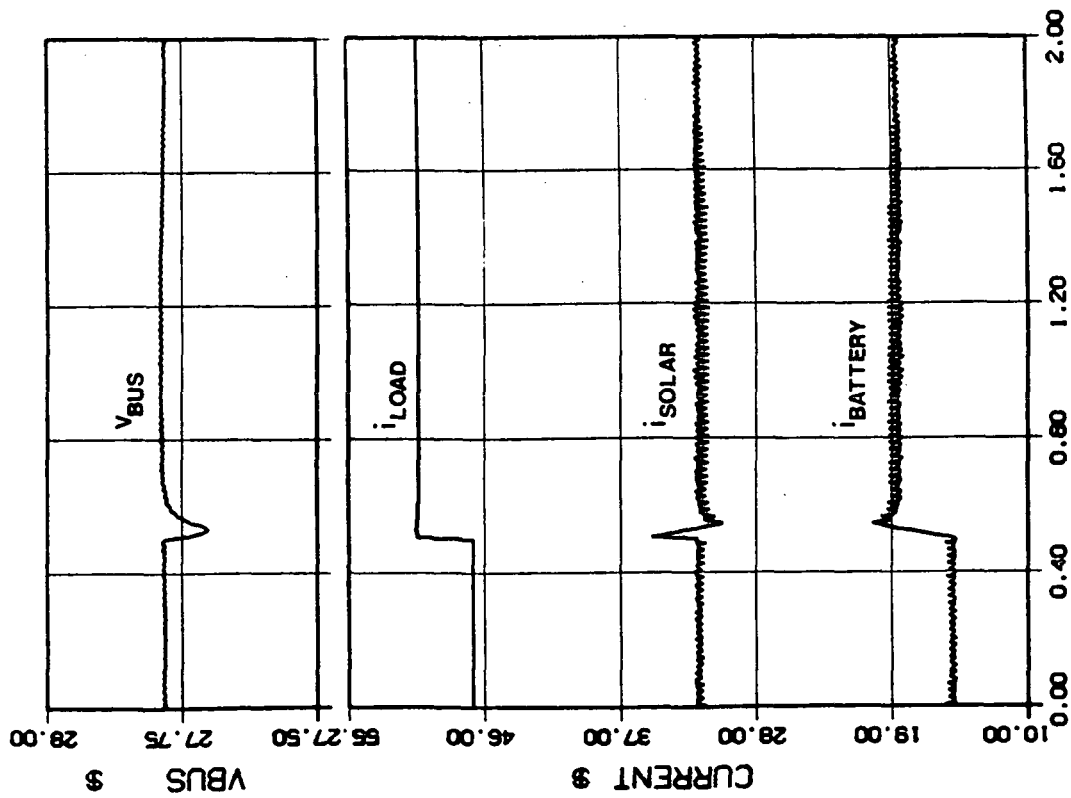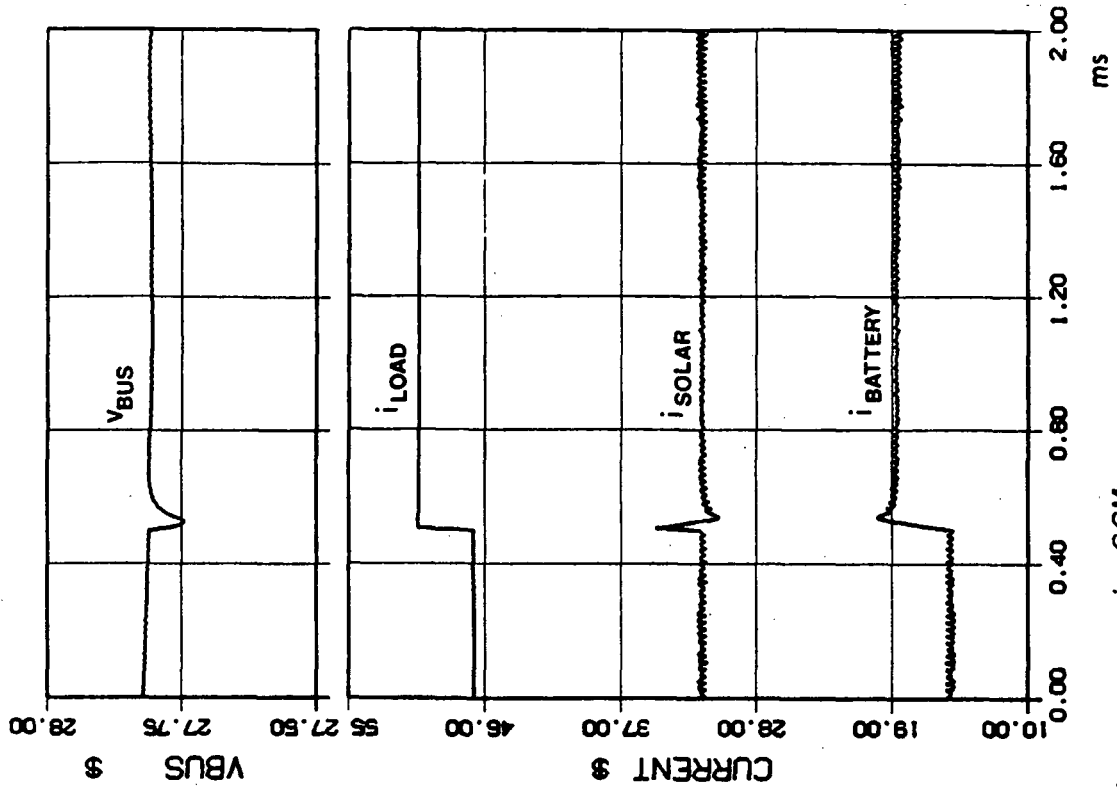
Figure 6.9   Step load transient responses in CCM

(a)   using the compensator shown in Fig.6.6(c)
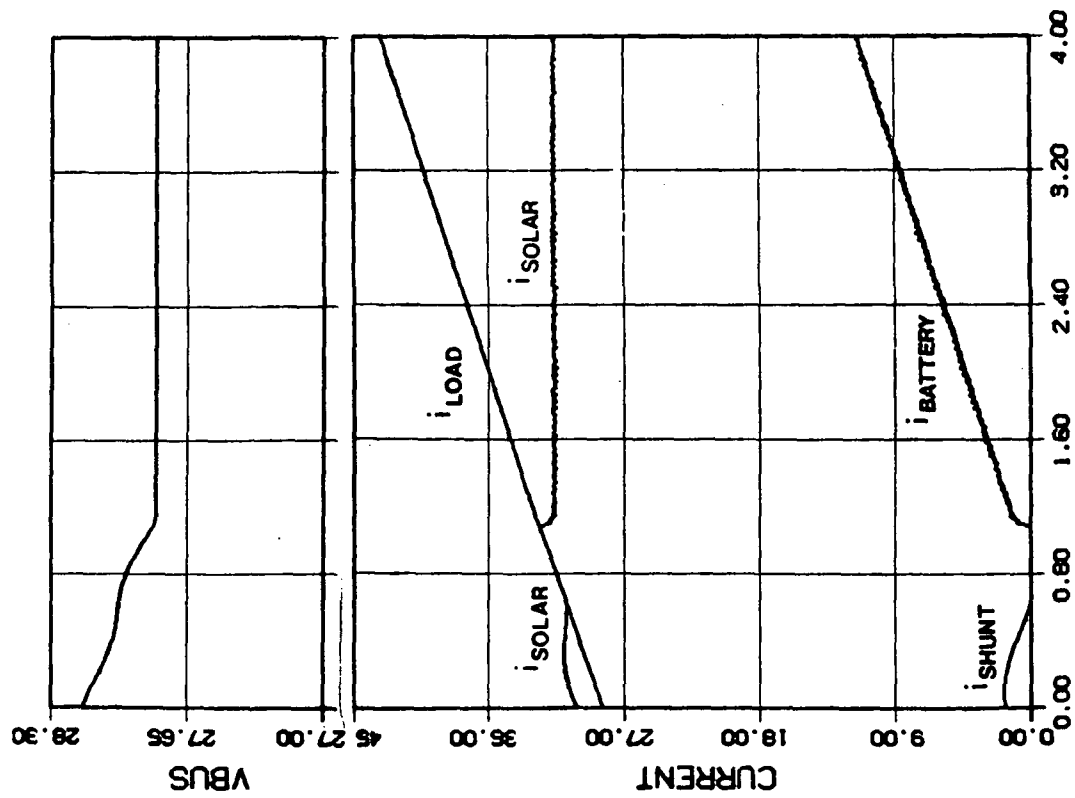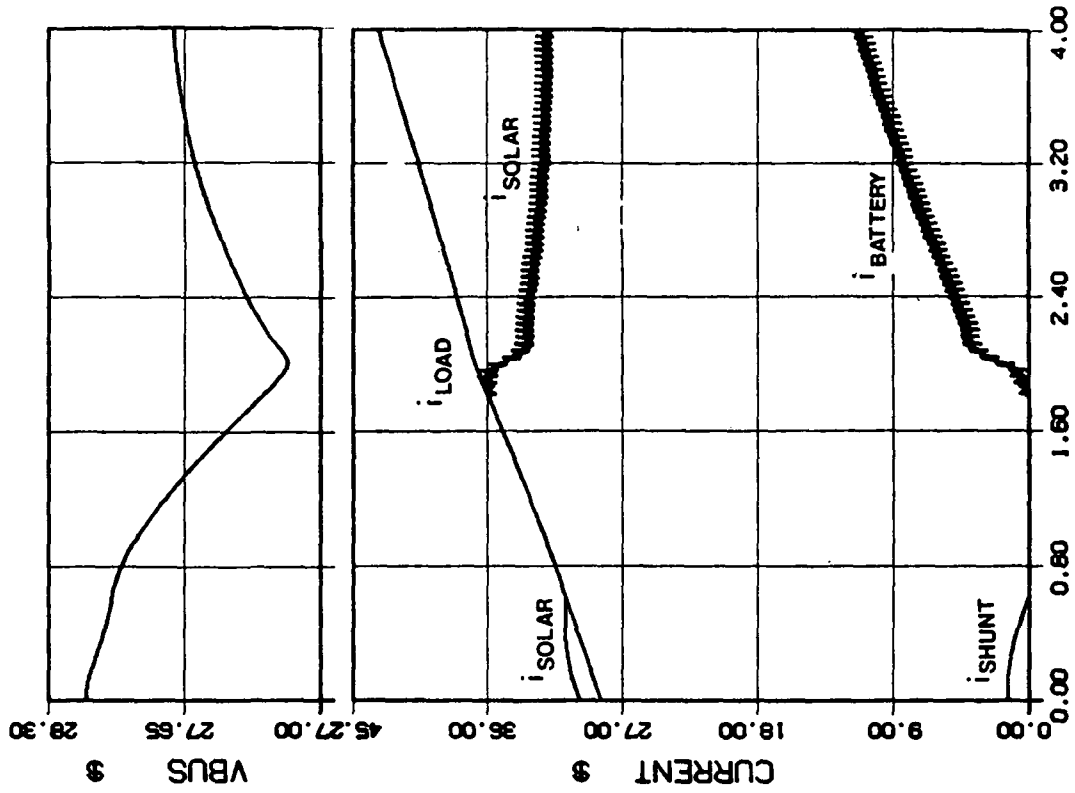(b)   using the compensator shown in Fig.6.6(b)

155

Figure 6.10 System responses in the transition mode (DCM)

(a) using the compensator shown in Fig.6.6(c)
(b) using the compensator shown in Fig.6.6(b)

CHAPTER 7

SYSTEM LEVEL MODELING, ANALYSIS AND SIMULATION

7.1 INTRODUCTION

Solar arrays, as the primary power source for spacecraft, generate electrical power proportional to the illumination level. The operating point of the solar arrays is determined by the power conditioning equipment and the load characteristic. The power conditioning equipment consists of a shunt regulator, a battery bank and its charging and discharging electronics. When the output power of the solar array exceeds the load demand, a portion of the excess power is used to charge the battery bank, the secondary power source, and the rest dissipated in the shunt regulator. When the load-power demand is higher than the solar array output power, the battery bank supplies the additional load-power demand through the battery discharging electronics. Since the solar array output power varies over a wide range according to the changes in the illumination level, several modes of operation exist depending on the characteristics of the solar array, the power-conditioning equipment, and the load.

As described in Chapter 4, the solar array output characteristic is nonlinear. This nonlinear-source coupled with nonlinear load characteristics may result in multiple equilibrium points under a given operating condition. The actual equilibrium state that the system resides on is determined

by the stability nature of the equilibrium points and its past history. Thus, it is necessary to analyze the stability of the equilibrium points and to understand various modes of operation.

In Section 7.2, stability of the equilibrium points of a solar array system with a nonlinear load is analyzed. The behavior of different solar array operating points are plotted as trajectories on the state plane. Stability and transient responses of the system operating near the solar array maximum-power point is considered in Section 7.3.

In Section 7.4, various modes of operation of the DET system are described. The solar array switching system and the partial shunt system with a buck converter are simulated in Section 7.5. Conclusions are presented in Section 7.6.

7.2 LARGE-SIGNAL BEHAVIOR OF THE SOLAR ARRAY OPERATING POINT

Fig.7.1 illustrates a solar array power system, in which the static load line represents a typical regulator load-line characteristic. The voltage V_R in the figure is the minimum solar array output voltage above which the converter is able to regulate its output voltage. When the converter is regulating, the solar array sees a constant power. Note that the converter exhibits a negative-resistance characteristic in this mode. Below V_R, the converter behaves as a resistive load to the solar array.

As shown in Fig.7.1, there exist three equilibrium points in the system. The large-signal behavior of a solar array operating point depends on the stability nature of each equilibrium point. The qualitative large-signal analysis can be carried out by considering a second-order system as shown in Fig.7.2. The solar array output and the load characteristics are replaced by nonlinear functions. The LC low-pass filter in the model represents actual physical elements in the system such as an input filter of the switching regulator or the cable impedance between the solar array and the load.

Let us first consider the stability nature of each equilibrium point. Defining the states $x = [i_L \ \ v_C]^T$, the system state equations are

$$\frac{di_L}{dt} = \frac{1}{L} (v_S - v_C) = \frac{1}{L} (-f(i_L) - v_C) \quad (7.1)$$
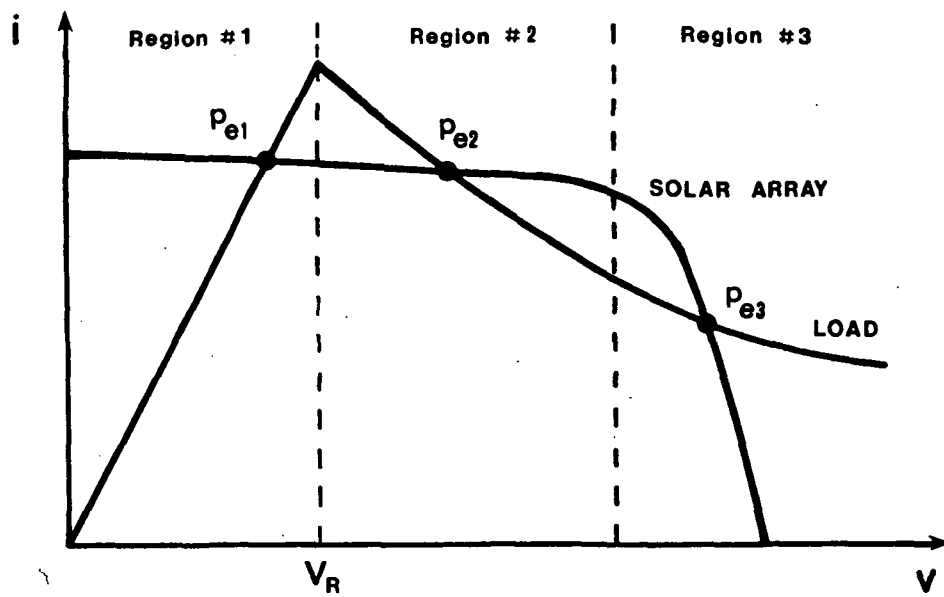
159

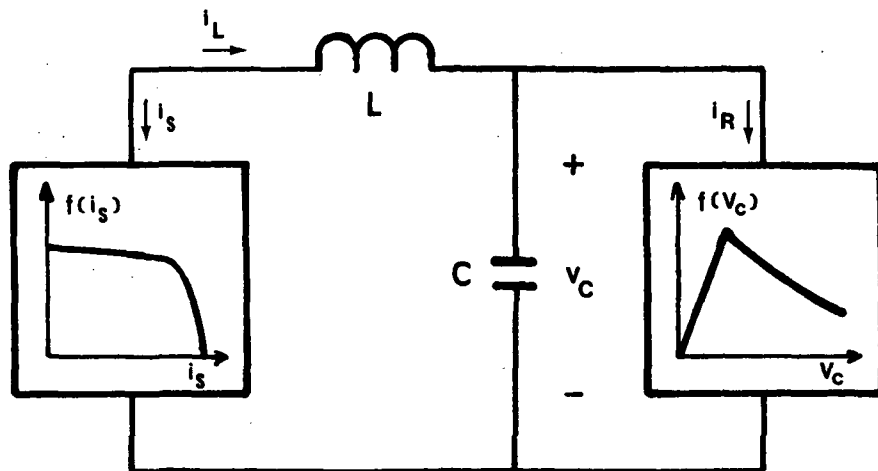Figure 7.1 *Representation of a solar array power system with a switching regulator load line*

Figure 7.2 *Equivalent circuit model of the system in Fig.7.1 including LC filter*

160

$$\frac{dv_C}{dt} = \frac{1}{C} (i_L - i_R) = \frac{1}{C} (-f(v_C) - i_L) \quad (7.2)$$

where v_S and i_R are defined in Fig.7.2.

From Eqs.(7.1) and (7.2), the equilibrium points in Fig.7.2 are

$$V_C = -f(I_L) \quad (7.3)$$

$$I_L = f(V_C) \quad (7.4)$$

The behavior of the trajectories in the neighborhood of an equilibrium point can be found by linearizing Eqs.(7.1) and (7.2) about an equilibrium point. The nature of these equilibrium points is analyzed by introducing small perturbations about the equilibrium points.

$$i_L = I_L + i_\ell \quad (7.5)$$

$$v_C = V_C + v_c \quad (7.6)$$

where I_L and V_C represent the steady-state quantities, and i_ℓ and v_c are the small-signal perturbations.

Substituting Eqs.(7.5) and (7.6) into (7.1) and (7.2) results in

$$\frac{di_L}{dt} = \frac{1}{L} [-f(I_L + i_\ell) - (V_C + v_c)] \quad (7.7)$$

161

$$\frac{dv_C}{dt} = \frac{1}{C} \; [\; -f(V_C + v_c) - (\; I_L + i_\ell \;)\;] \qquad (7.8)$$

Expanding Eqs.(7.7) and (7.8) in a Taylor series about the equilibrium points, the equations of the first order approximation are

$$f(I_L + i_\ell) = f(I_L) + r_S \, i_\ell \qquad (7.9)$$

where

$$r_S = \left. \frac{df(i_L)}{di_L} \right|_{I_L}$$

and similarly,

$$f(V_C + v_c) = f(V_C) + \frac{1}{r_L} \, v_c \qquad (7.10)$$

where

$$\frac{1}{r_L} = \left. \frac{df(v_C)}{dv_C} \right|_{V_C}$$

where r_S and r_L are the incremental resistances (tangential slope) of the solar array output curve and the load line, respectively, at the equilibrium points.

Employing Eqs.(7.3) through (7.10), Eqs.(7.7) and (7.8) can be simplified as

$$\frac{di_\ell}{dv_c} = \frac{(\;1/L\;)\;(\;-r_S \, i_\ell - v_c\;)}{(\;1/C\;)\;(\;i_\ell - (1/r_L)\,v_c\;)} \qquad (7.11)$$

162

Note that the value of r_S is the same as the output resistance at a point on the solar array I-V curve. The system eigenvalues are expressed as

$$\lambda_1, \lambda_2 = \frac{1}{2} \left[-\left(\frac{r_S}{L} + \frac{1}{r_L C}\right) + \left[\left(\frac{r_S}{L} + \frac{1}{r_L C}\right)^2 - \frac{4}{LC}\left(1 + \frac{r_S}{r_L}\right)\right]^{\frac{1}{2}} \right]$$

$$(7.12)$$

From Eq.(7.12), the stability of each equilibrium point can be determined for given parameter values. For the load line shown in Fig.7.1, the following results are observed.

In Region #1: $r_L > 0$

The equilibrium point, P_{e1} is stable and is either "node" (real) or "focus" (complex).

In Region #2: $r_L < 0$, $|r_S| < |r_L|$

λ_1 and λ_2 are both real but of opposite sign, and Point P_{e2} is a "saddle" and is unstable.

In Region #3: $r_L < 0$, $|r_S| < |r_L|$

The stability of Point P_{e3} depends on the parameter values.

Since the normal mode of operation should be in Region #3, the values of L and C in Fig.7.2 must be chosen to provide the stable equilibrium points in this region and to allow further analysis. However, it must be noted that the equi-

163

librium points in Region #1 are always stable and those in region #2 are always unstable (saddle points) regardless of the parameter values. The value of r_L in the constant power region is

$$r_L = \left.\frac{\partial v_C}{\partial i_r}\right|_{V_C,\ I_R} = \left.-\frac{P_C}{i_r^2}\right|_{i_r = I_R} \quad (7.13)$$

Approximate values of r_S and r_L can be found simply by drawing tangential slopes to the solar array I-V curve and load line, respectively, for each equilibrium point.

To construct a state-plane trajectory the isoclines for each equilibrium point are derived using Eq.(7.11).

$$\frac{di_\ell}{dv_C} = 0 \quad \rightarrow \quad i_\ell = -\frac{1}{r_S} v_C \quad (7.14)$$

$$\frac{di_\ell}{dv_C} \rightarrow \infty \quad \rightarrow \quad i_\ell = \frac{1}{r_L} v_C \quad (7.15)$$

The results in Eqs.(7.14) and (7.15) are the tangential slopes to the source and load curve at each equilibrium point, thus the trajectories cross the solar array curve horizontally and the load line vertically. Near the equilibrium points which have real eigenvalues, the trajectories follow the slope of the eigenvectors of the system, γ.

164

$$\gamma_1, \gamma_2 = \frac{L}{2} \left[-\left(\frac{r_S}{L} - \frac{1}{r_L C} \right) + \left[\left(\frac{r_S}{L} - \frac{1}{r_L C} \right)^2 - \frac{4}{LC} \right]^{\frac{1}{2}} \right] \quad (7.16)$$

Using the above results, the state plane trajectories can be sketched. Fig.7.3 illustrates the trajectories for the case where the equilibrium point P_{e3} is a stable node. As shown in the figure, the trajectories are separated by the separatrix that has the slope γ_2 at P_{e2}. The two starting points P_1 and P_2 in Fig 7.3 approach two entirely different steady states, even though the initial states differ by only a small amount.

For the solar array model used in this study the following cases are set up for the computer simulations. As mentioned above, if we assume that point P_{e3} in Region #3 is stable then there can be four possible cases:

i) P_{e1} - node, P_{e3} - node

ii) P_{e1} - node, P_{e3} - focus

iii) P_{e1} - focus, P_{e3} - node

iv) P_{e1} - focus, P_{e3} - focus

However, investigation of the cases i) and ii) are sufficient to understand the behaviors of the system. The results from simulating these cases are shown in Fig.7.4(a) and 7.4(b) given the following system operating conditions.
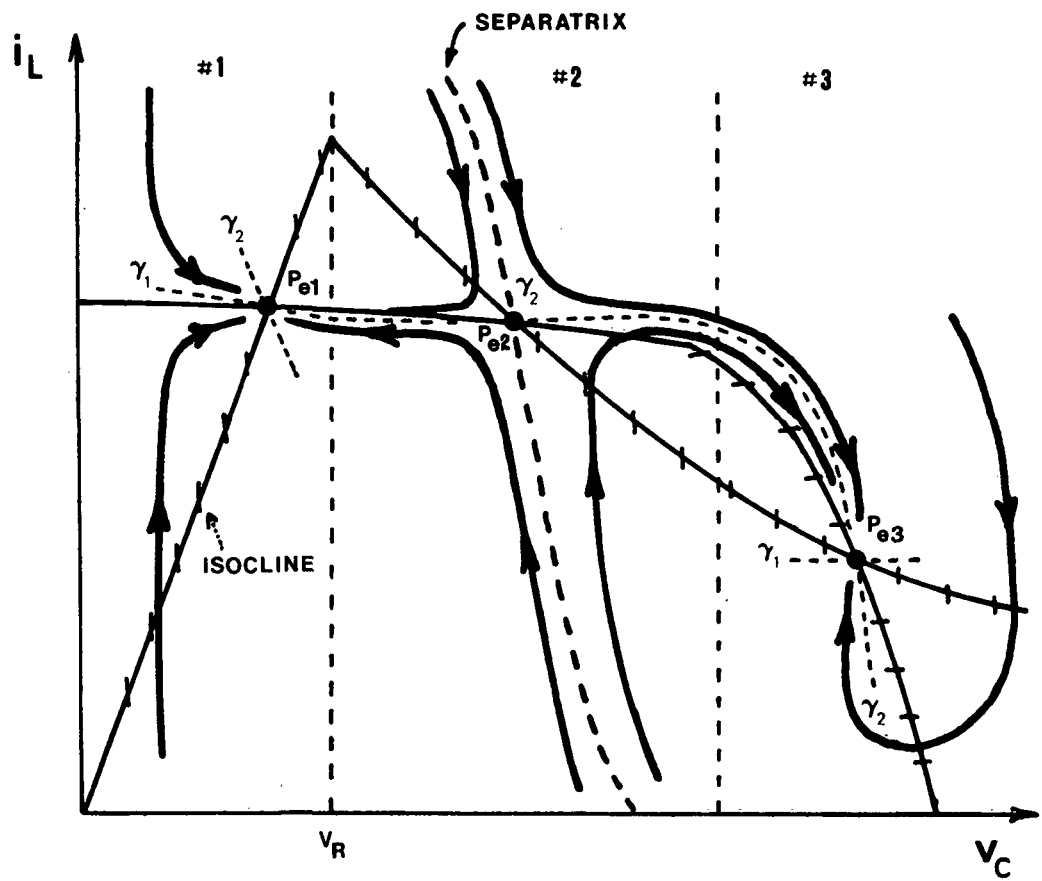
Figure 7.3 State-plane trajectories of the system in Fig. 7.2

The solar array short-circuit current, I_{ss}, is 45.41A, the open-circuit voltage, V_{oc}, is 32.0V, and the maximum power is 1050 watts. The constant-power load line is set to 850 watts, and the boundary of Region #1 and #2, V_R, is 15V. The values of r_S and r_L at the equilibrium points in each region are listed in the following table.

	P_{e1}	P_{e2}	P_{e3}
I_L	45.38	45.02	30.34
V_C	12.03	17.31	28.02
r_S	64.92	37.3	0.20
r_L	0.025	-0.56	-1.47

The cases i) (P_{e3} node) and ii) (P_{e3} focus) are shown in Fig.7.4a and 7.4b. The eigenvalues and the slope of the eigenvectors for the particular values of L and C are listed in the figure. In Fig.7.4, the separatrix is clearly illustrated. It is obtained by adjusting the initial condition that is located near the line estimated from information about γ_2 at P_{e2}. The trajectories from the initial points in the left-hand side of the separatrix (P_1 through P_6) converge to P_{e1}, and those in the right-hand side of the separatrix (P_7 through P_{12}) to P_{e3}.

Since in Region #1 the system bus voltage is not regulated, the desirable mode of operation should be in Region #3. This implies that there needs a limiting mechanism that
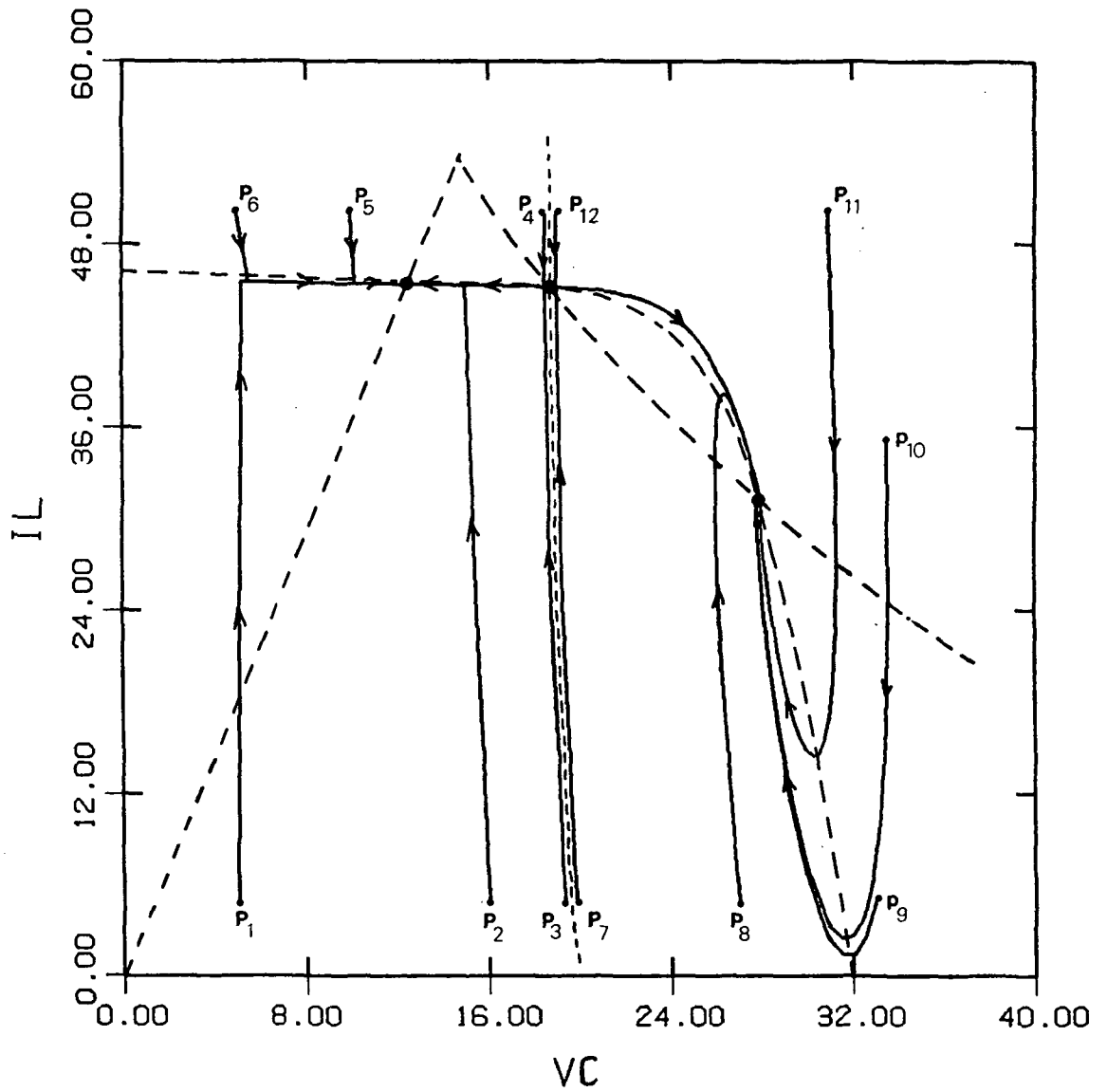
Figure 7.4(a) *Simulation of state-plane trajectories for the case where the equilibrium point P_{e3} is 'stable node'*

(L = 10 μH, C = 500 μF)
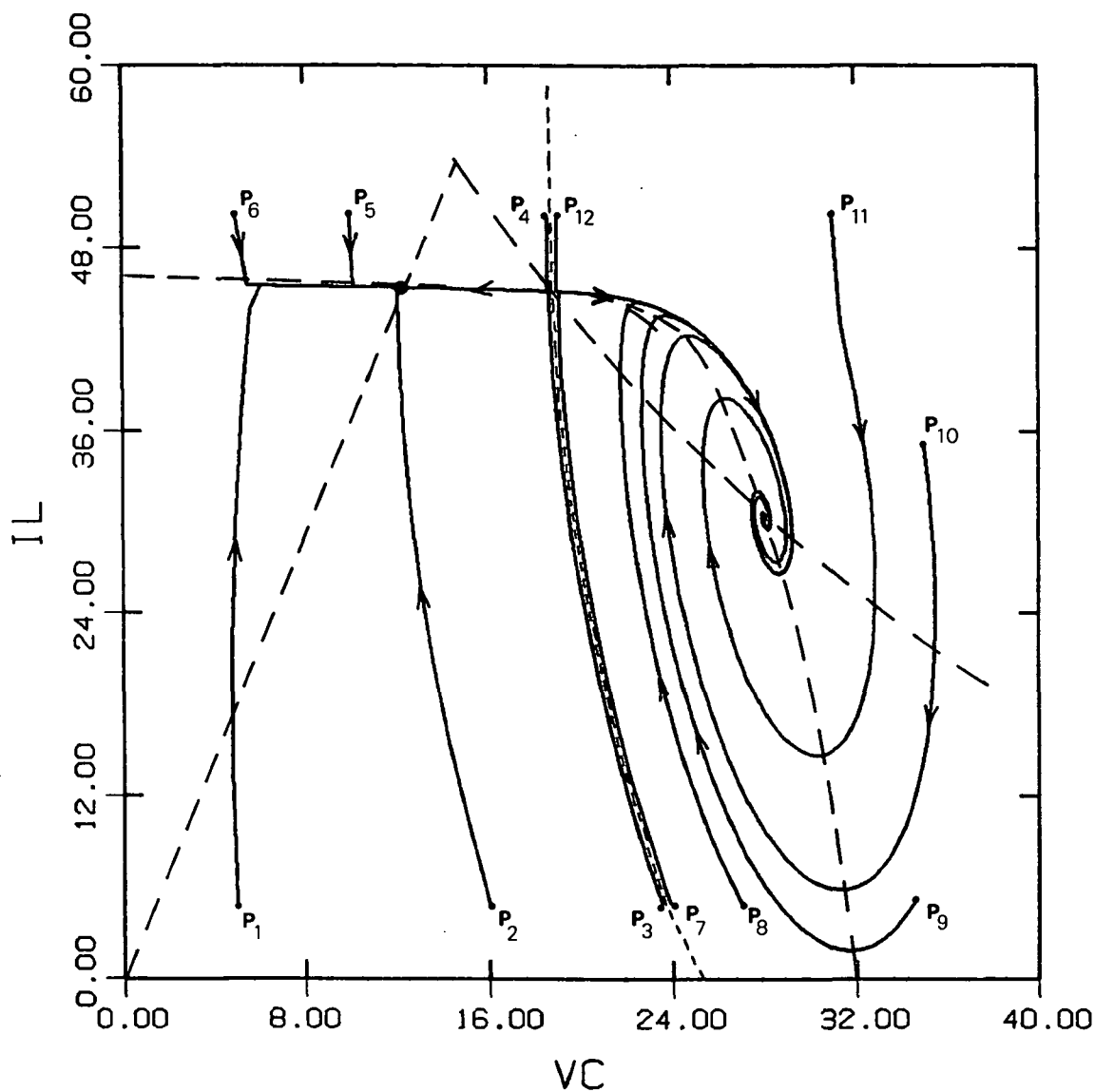
Figure 7.4(b)   *Simulation of state-plane trajectories for the*
case where the equilibrium point P_{e3} is 'stable focus'

(L = 30 μH,   C = 500 μF)

prevents the operating point from settling into Region #1 or a triggering method to move it to Region #3 even if the operating point starts in Region #1. The limiting mechanism will be described in the following section. A triggering method is illustrated as follows.

Suppose that the operating point is at rest in Region #1. One way to move this operating point into Region #3 is to decrease the load power below the solar array curve so that the only one desired equilibrium point exists. For the load line shown in Fig. 7.5, the equilibrium points associated with Region #1 and #2 have moved outside these regions, and therefore they no longer exist. However, the behavior of the state trajectories can be still seen by defining virtual equilibrium points, P_{e1}' and P_{e2}', for which the slopes of the eigenvectors are also sketched.

Fig.7.6 shows the simulation result using the previous system for the case i). In Fig.7.6(a), the trajectory starts from an arbitrary initial point, P_1 and moves to P_2 for a load power of 800 watts (Curve #1). As the load power continuously decreases, the operating point moves along the solar array curve until it reaches Curve #2. Further decrease in the load power beyond this point moves the operating point from P_3 to P_4, then to P_5 for Curve #3. Fig.7.6(b) shows the time history of v_c corresponding the trajectory from P_1 to P_5.
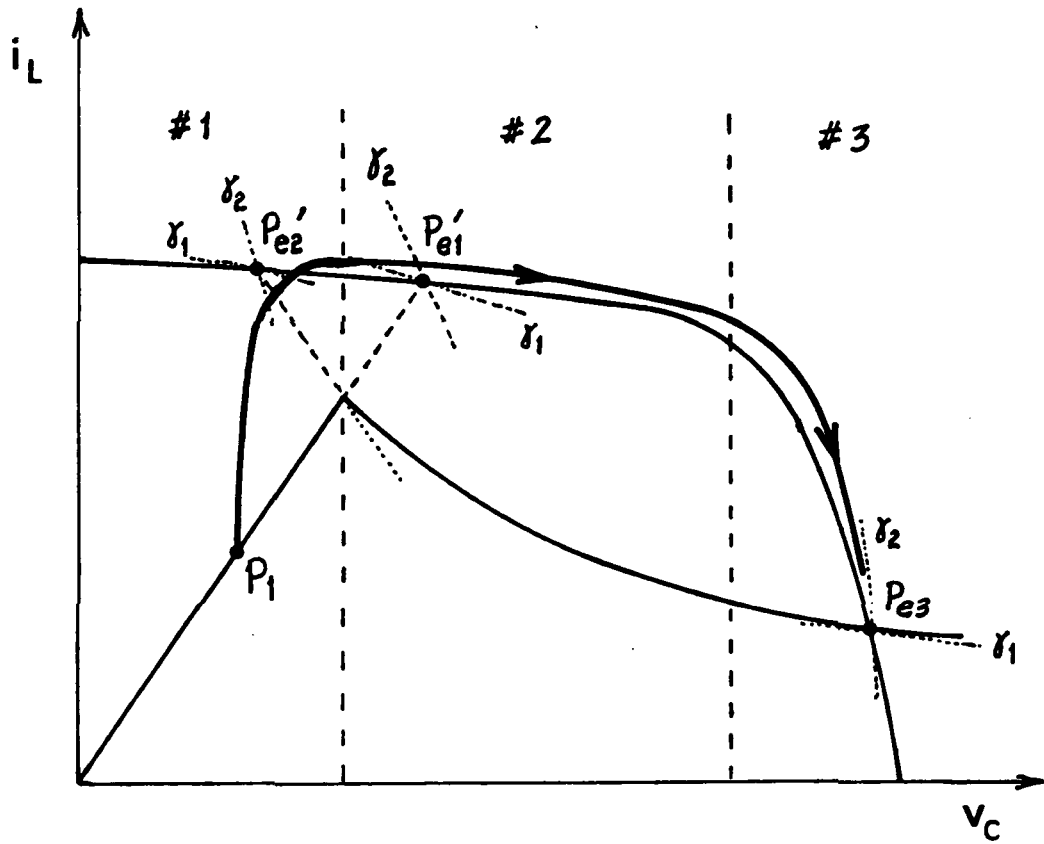
Figure 7.5 A trajectory from the initial operating point
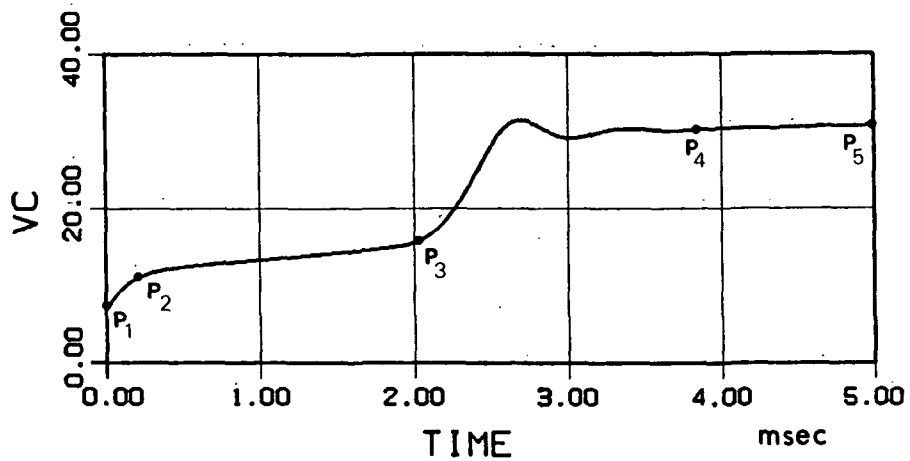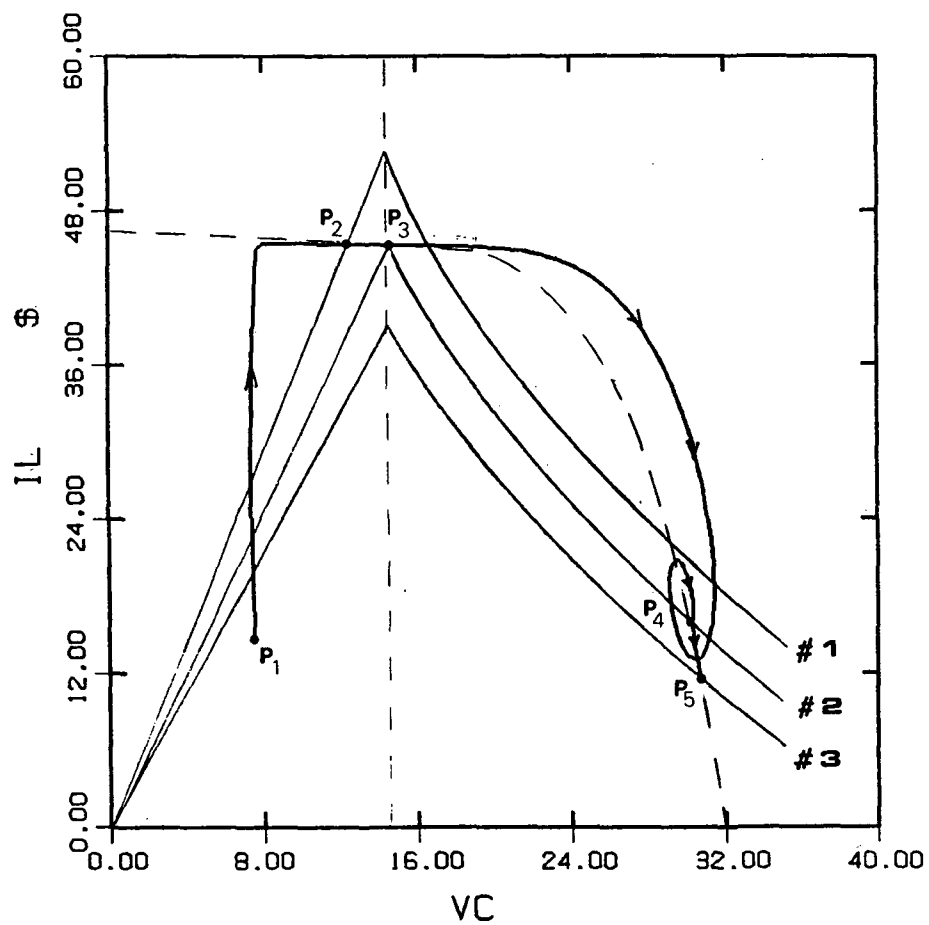in Region #1 to Region #2

Figure 7.6 Simulation of the triggering method from the
undesired stable region to the desired region
(a) state-plane trajectory
(b) time history of the bus voltage

172

The above stability analysis for the system in Fig.7.2 can be extended to the following cases.

System in the battery discharging mode: Figure 7.7 illustrates the system in the battery discharging mode of operation. The battery discharging current can be expressed as a function of the bus voltage with an output admittance, $1/r_B$. The state equations are then,

$$\frac{di_L}{dt} = \frac{1}{L} (-f(i_L) - v_C) \qquad (7.17)$$

$$\frac{dv_C}{dt} = \frac{1}{C} (i_L - \frac{1}{r_B} v_C - f(v_C)) \qquad (7.18)$$

Following the same procedures as in the previous derivations, the state equations near the equilibrium point are

$$\frac{di_\ell}{dv_c} = \frac{(1/L) \quad (-r_S i_\ell - v_c)}{(1/C) [i_\ell - [(1/r_L)+(1/r_B)] v_c]} \qquad (7.19)$$
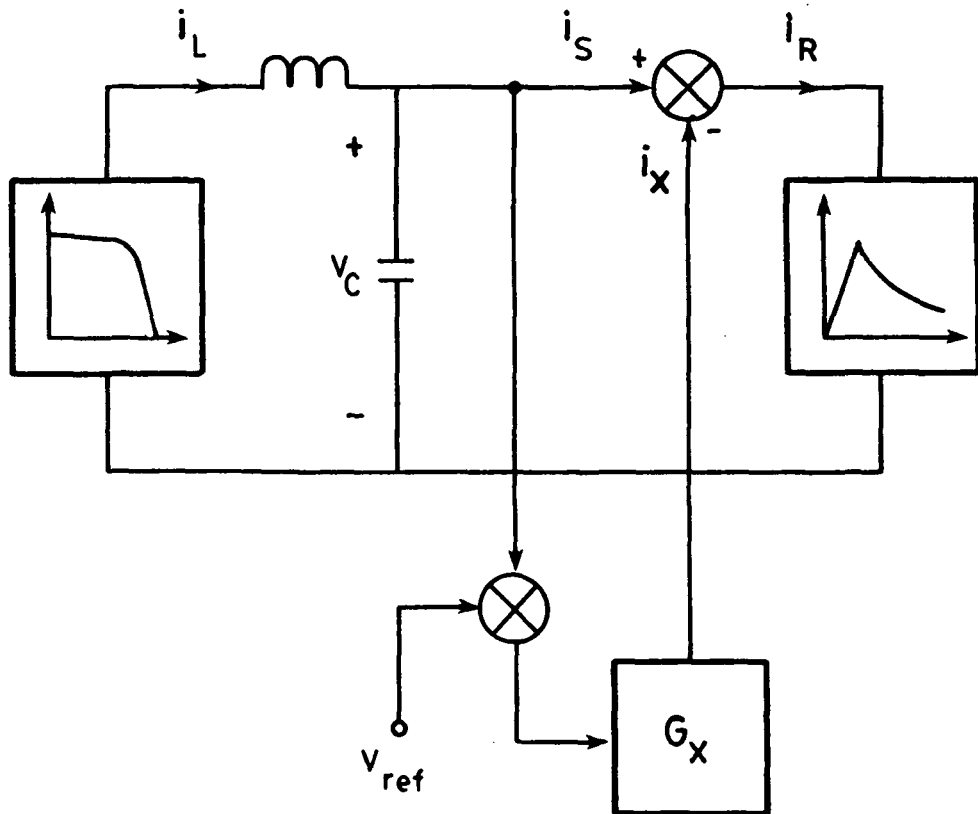
Figure 7.7 Simplified block diagram of the system in Fig.7.2
with the shunt regulator or the battery discharger

$$G_x = \begin{cases} Y_{sh} & : \quad \text{for shunt mode} \\ \\ 1/r_B & : \quad \text{for battery discharge mode} \end{cases}$$

Then the eigenvalues are obtained as

$$\lambda_1, \lambda_2 = \frac{1}{2}\left[-\left(\frac{r_S}{L} + \frac{1}{r_E C}\right) + \left[\left(\frac{r_S}{L} + \frac{1}{r_E C}\right)^2 - \frac{4}{LC}\left(1 + \frac{r_S}{r_E}\right)\right]^{\frac{1}{2}}\right] \quad (7.20)$$

where

$$r_E = r_L \parallel r_B$$

Comparing Eqs.(7.12) and (7.20), the additional term, $1/r_B$, stabilizes the system, which can be explained as the system is operating on the stiff voltage source line.

System in the shunt mode: Figure 7.7 also can be used to illustrate the system in the shunt mode of operation. In this mode of operation, Eqs.(7.17) and (7.18) are valid if the $1/r_B$ term is replaced by the shunt transadmittance, Y_{sh}. Figure 7.8 shows the state plane trajectories and the time history of the states, with and without the shunt regulator. This figure clearly shows the effect of the additional term, $1/r_B$ described above such that the system without the shunt regulator is quite oscillatory while that with the shunt regulator has faster responses and the system appears to have real valued eigenvalues.
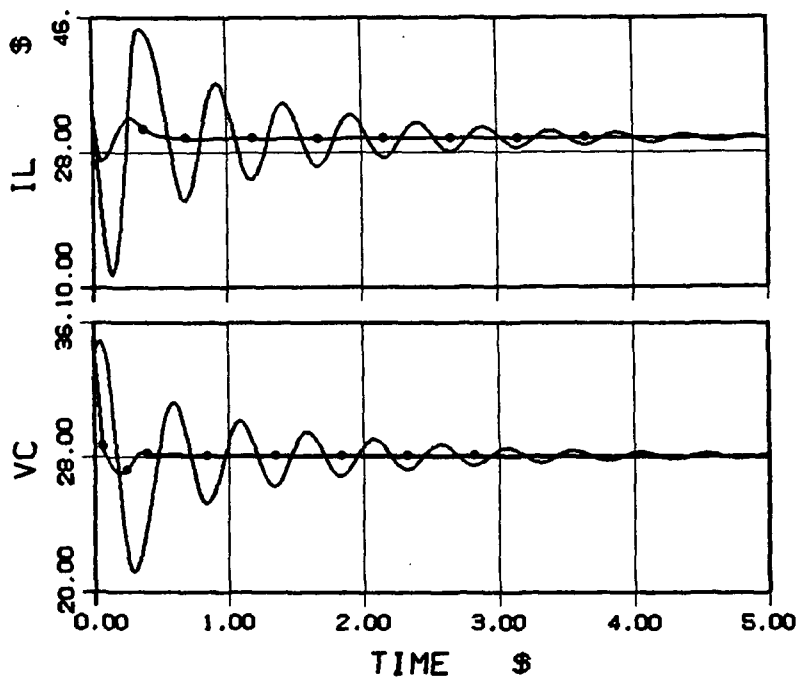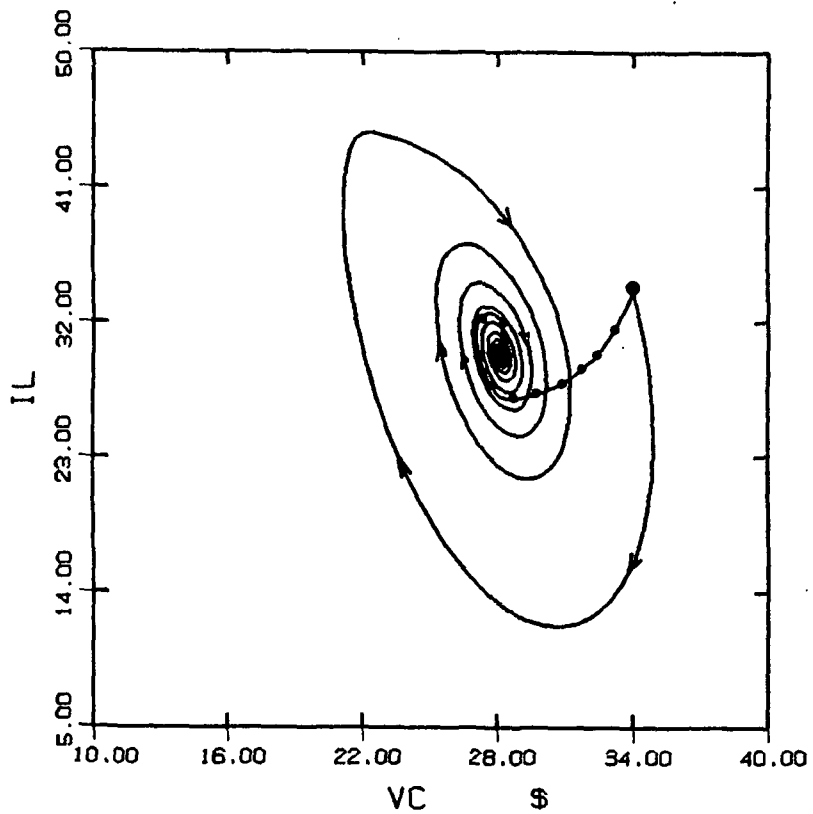
Figure 7.8 *Comparison in the system response with and without the shunt*

●─●─●─● : with shunt
───── : without shunt

176

7.3 ANALYSIS OF THE OPERATING POINT NEAR THE SOLAR ARRAY MAXIMUM-POWER POINT

To utilize the maximum available power from the solar array, several approaches were proposed in [7] and [10] to place the operating point as close to the solar array maximum-power point as possible. However, near the solar array maximum power point, the dynamic resistance of the solar array is very sensitive to changes in the operating condition and, consequently, may result in system open loop instability.

To derive the solar array maximum-power point, one can differentiate the constant-power load line, $P_a = VI$, and set it to zero.

$$\frac{\partial P_a}{\partial V} = V \frac{\partial I}{\partial V} + I = 0 \qquad (7.21)$$

$$\frac{V}{I} = - \frac{\partial V}{\partial I} \qquad (7.22)$$

Equation (7.22) states that at the maximum-power point, the constant-power load line, r_L, is equal to the dynamic output resistance of the solar array, r_o, as shown in Fig.7.9.
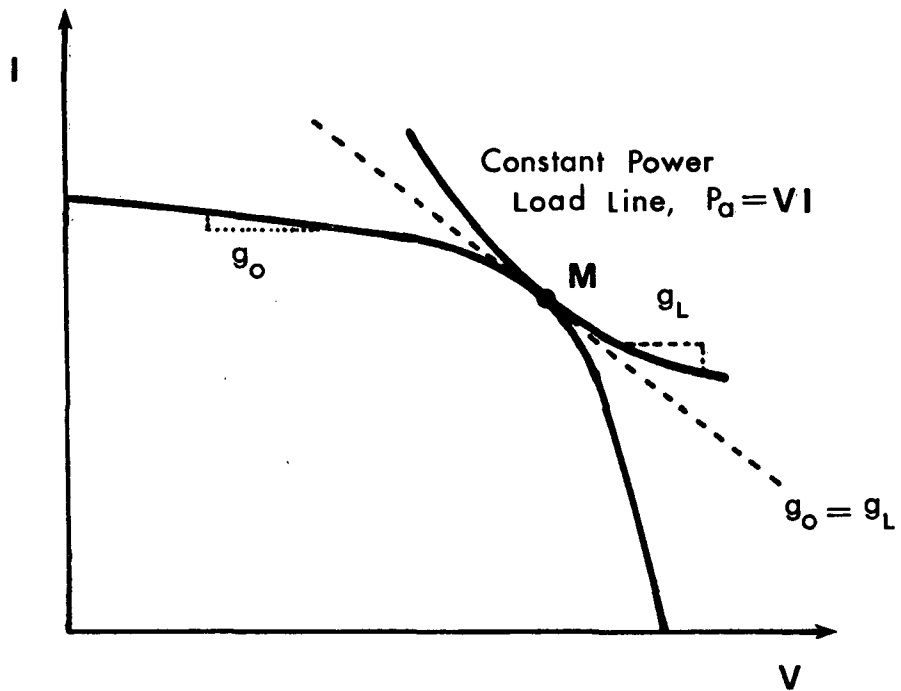
Figure 7.9 *Relationships of solar array characteristic and constant power load line at the maximum power point, M*

To analyze the behavior of an equilibrium point near the maximum power point, one can consider the solar array small-signal model.[9] One of the system eigenvalues at the equilibrium point is

$$\lambda = - \frac{1}{C_{eq} (1 + R_{eq} / r_L)}$$ (7.23)

where C_{eq} is the equivalent shunt capacitor in the solar array small-signal model.

From Eq.(7.23) , for $r_L < 0$, the system is:

stable   if $|r_o| < |r_L|$,   and

unstable   if $|r_o| > |r_L|$

In the stable region near the maximum-power point, M, the magnitudes of r_o and r_L are close together and the eigenvalue is close to the origin, which implies very poor transient response and stability margin. In this respect it is desirable to operate the system in a region where $|r_o| << |r_L|$. This can be seen from the step transient response simulation using the system model developed in Section 7.2 (Fig.7.2).

Figure 10(a) shows the response of the step change in the load power from 800 watts to 790 watts, and Fig.7.10(b) from 1040 watts to 1030 watts which is close to the maximum-power point (1050 watt). Therefore, to design a controller to utilize the maximum available power from the solar array, one must take into consideration of the stability of the operating point and the transient behavior of the system. One way to overcome this problem is to use the shunt regulator to dissipate some solar array power. In this mode of operation, the system can be stabilized as shown in Section 7.2.
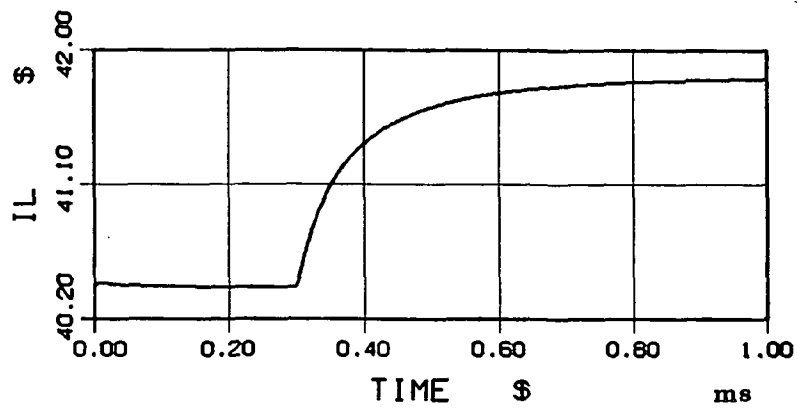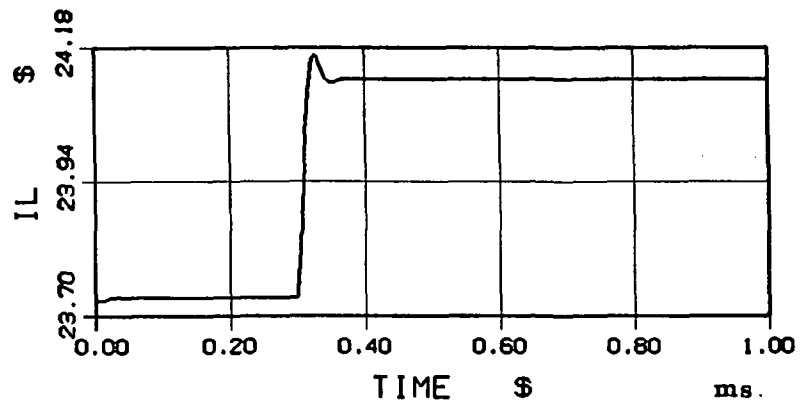
Figure 7.10   *Step load transient responses*

(*a*) *800 to 790 watt step*
(*b*) *1040 to 1030 watt step*

7.4 ANALYSIS AND SIMULATION OF THE SYSTEM OPERATING MODES

A direct energy transfer(DET) system whereby the primary power source, a solar array, is coupled through a main distribution bus directly to the spacecraft electrical loads. The various power-conditioning components, as shown in Fig.7.11, are activated only as needed, thus requiring the system to process only the amount of power needed to maintain the bus at the specified voltage level. A system mode of operation is determined by the power system control unit. The Central Control Unit (CCU) continuously monitors the bus voltage and commands the system to operate in the battery-discharging mode when v_{bus} is less than V_{rb}, the battery discharger regulation voltage, or in the shunt-active mode when v_{bus} is greater than V_{rs}, the shunt regulation voltage. When v_{bus} is between V_{rb} and V_{rs}, there exists a "dead band" at which the load power is equal to solar array output power. When the shunt is activated, any variation of the bus voltage generates a proportional shunt current, i_{sh}. The shunt current together with the load current sinks the solar array current and regulates the bus voltage. When the system operates in the battery-discharge mode, the bus voltage is regulated by the battery discharger. The solar array current is set by the bus voltage on its output I-V curve and the battery-discharging current is the difference between the solar array current and the load current.
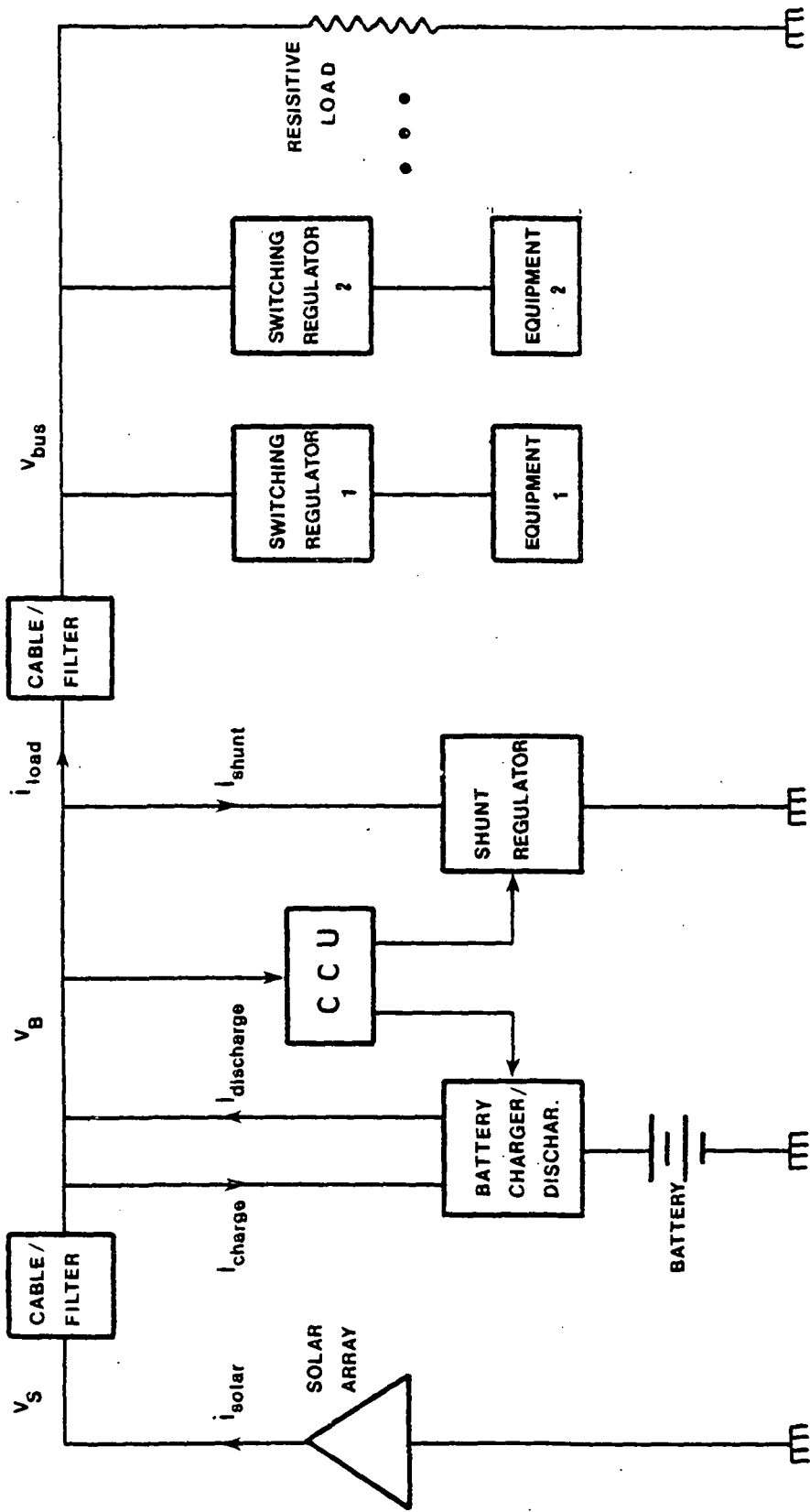
Figure7.11 Direct Energy Transfer (DET) spacecraft power system

In this work, modeling of the battery and the battery-charging electronic are omitted, thus, the battery is treated as an ideal voltage source. The entire system model includes solar array, shunt regulator, battery discharger and constant-power load. In order to simulate the system mode of operation including transition mode between shunt regulator and battery-discharging modes, a simplified DET system is configured using following component modules.

- [AR] --- solar array

- [FS] --- shunt regulator

- [BP] --- battery discharger power stage

- [PZ] --- two-pole two-zero compensator

- [WM] --- PWM(constant frequency control)

- [PT] --- constant power load

Figure 7.12 [SIM.MOD] displays user input model description data. Figure 7.13 [SIM.MGL] shows EASY5 generated DET system configuration. Figure 7.14 [SIM.MGL] is EASY5 generated required input data list, and user furnished input parameter values and simulation commands are shown in Fig.7.15 [SIM.ANC].

```
*********************************************
**** DET(NASA) SYSTEM LARGE SIGNAL MODEL ****
** REVISED 3/4/86
*********************************************
MACRO FILE NAME=MACROS
LIST MACRO COMPONENTS=AR,FS,PT,BP,PZ,WM
MODEL DESCRIPTION
LOCATION=4,AR,INPUTS=MC(S,2=IX)
LOCATION=25,FS,INPUTS=AR(VB=VB)
LOCATION=1,PT,INPUTS=AR(VB=VL)
LOCATION=43,BP,INPUTS=AR(VB=V2),WM(IQ=IQ)
LOCATION=16,PZ,INPUTS=AR(VB=VD)
LOCATION=46,WM,INPUTS=PZ(VE=VE)
LOCATION=22,MC,INPUTS=FS(IH=S,1),BP(ILL=S,3),PT(IL=S,4)
END OF MODEL
PRINT
```

Figure 7.12   User Input Model Description   [SIM.MOD]

185

Figure 7.13   EASY5 generated system configuration
[SIM.MGL]

INPUT DATA REQUIREMENTS LIST

PARAMETERS REQUIRED

COMPONENT	PARAMETER NAME (AND DIMENSION DATA FOR VECTOR AND MATRIX PARAMETERS)			
AR	LL AR	LLSAR	NP AR	NS AR
	FV AR	R AR	L AR	C AR
	FC AR	TA AR		
FS	VR FS	R1 FS	R2 FS	R3 FS
	VSAFS	ILMFS	GM FS	VTHFS
PT	PC PT	SW PT	PWOPT	TC PT
	VR PT	PW1PT	PW2PT	
BP	V2LRP	EPSBP	GAMBP	V1 BP
	L BP	RL BP		
PZ	WM PZ	WP PZ	WZ1PZ	WZ2PZ
	K PZ	ER PZ		
WM	TI WM	VP WM	VQ WM	ER WM
	VI WM	VCXWM	VCNWM	DMNWM
	CICWM	SCMWM	ILXWM	DMXWM
MC	C1 MC	C2 MC	C3 MC	C4 MC

STATES (INITIAL CONDITIONS AND ERROR CONTROLS REQUIRED)

COMPONENT	STATE NAME (AND DIMENSION DATA FOR VECTOR AND MATRIX STATES)	
AR	IL AR	VB AR
BP	IL BP	
PZ	X1 PZ	X2 PZ

Figure 7.14   EASY5 generated Input data requirement List   [SIM.MGL]

187

```
TITLE=NASA(LARGE SIGNAL)
PARAMETER VALUES
R   AR = .001,  C   AR = 1000E-6, L   AR = 1E-6, LL AR = 1.
LLSAR = 0.,     TA AR = 301., FC AR = 8E-5,   FV AR = -2E-3
NP AR = 324,    NS AR = 58
************************

INITIAL CONDITIONS
VB AR = 28.141
IL AR = 29.694
********
***********

**FULL SHUNT
PARAMETER VALUES
VR FS = 28.14,  VSAFS = 15
R1 FS = 12400,  R2 FS =2.2E6,  R3 FS = 1.78419
GM FS =4,       VTHFS = 3,     ILMFS = 45
********
***
PARAMETER VALUES
C1 MC=1, C2 MC=-1, C3 MC=1, C4 MC=1
************
*******
PC PT=1
VR PT=15
PWOPT=700, SW PT=50000
PW1PT=700, PW2PT=1000
TC PT=1
INITIAL CONDITIONS
IL BP=0
PARAMETER VALUES
L   BP=100E-6
RL BP=1E-3
V1 BP=20
V2LBP=28
GAMBP=.75
EPSBP=1E-3
K   PZ=.2153625, ER PZ=6
*WM PZ=23.3E3
WM PZ=43E3
WZ1PZ=1256, WZ2PZ=6.28E3
WP PZ=50E3
TI WM=20E-6, VP WM=3, VQ WM=.5
ER WM=6, CICWM=0, SCMWM=0
VCXWM=10., VCNWM=0
DMXWM=1, DMNWM=0
ILXWM=20
PRINTER PLOTS
ONLINE PLOTS
INT MODE=4
DISPLAY1
VB AR
DISPLAY2(OVERPLOT)
IL AR, IH FS, IL PT, ILLBP
DISPLAY3(OVERPLOT)
VR WM, VC WM
TMAX=1.2E-3, TINC=1E-6
PRATE=100, OUTRATE=10
SIMULATE
XIC-X
PARAMETER VALUES
*TC PT=.2E-3
LLSAR=-250
TMAX=1.99E-3, TINC=2E-7
SIMULATE
```

Figure 7.15   User Input Analysis Program   [SIM.ANC]

The system operating condition is subject to change due to a constantly varying load- power consumption and the solar array power generations. The DET system shown in Fig.7.11 is simulated to observe how the system operating point moves from one mode to another. Figure 7.16 illustrates the case in which the solar array I-V characteristic varies according to the illumination level. In this example, the illumination level is set to be linearly time varying from Curve #1 (shunt active mode) to Curve #4 (battery discharging mode) as illustrated in Fig.7.16.

From Fig.7.16 and the simulation result in Fig.7.17, the system mode of operation is described as follows: Starting from Curve #1 and the corresponding operating point A, the operating point travels along the shunt regulation line, V_{rs} until the solar array power decreases to Curve #2. In this mode, the shunt regulator is activated. It absorbs the excessive current generated by the solar array through the shunt elements (i_{sh}). Between Curve #2 and #3 the dead band mode exists where both the shunt regulator and battery discharger are deactivated. Thus, the operating point travels along the load line from point B to C. Further decrease in the illumination level activates the battery discharger. The operating point then follows the battery-discharging regulation line, V_{rb}. In this mode, the load power is supplied by the solar array and the battery.
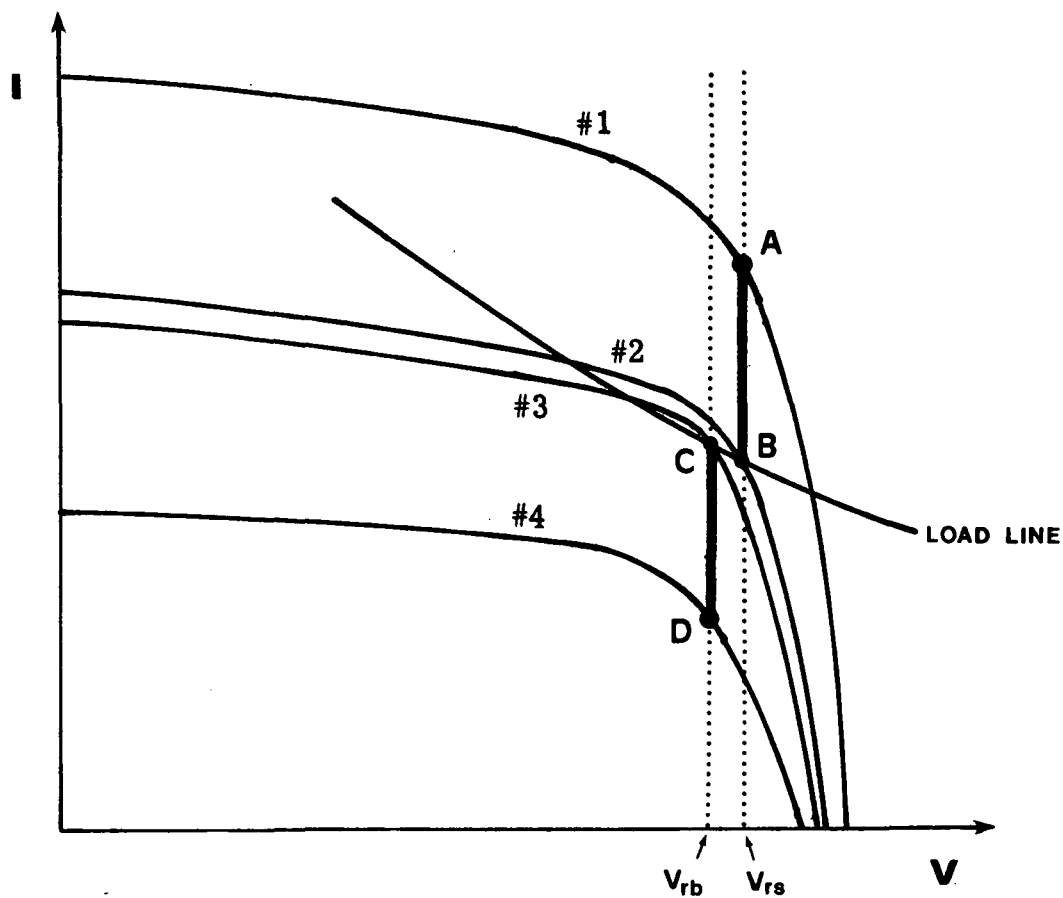
Figure 7.16 *DET system mode of operation for the solar array illumination level changes*

Figure 7.18 illustrates the case where the load power is linearly varying while the solar array I-V curve is fixed. From the Fig.7.18 and the simulation results in Fig.7.19, the system mode of operation is described as follows: With the solar array curve fixed and the load line below Curve #2, the operating point is set at Point A. As the load power increases beyond Curve #2, the shunt regulator is deactivated, and the operating point travels on the solar array curve until Point B. Further increase in the load power beyond Curve #3 activates the battery discharger, and the operating point moves along the battery discharger regulation line to Point C.

Figure 7.20 shows simulation results when load is changed abruptly at 0.2ms from curve #1 to curve #4 in Fig.7.18. As the solar array can not afford the demand of load power, the shunt regulator is deactivated promptly and battery takes over the shortage.
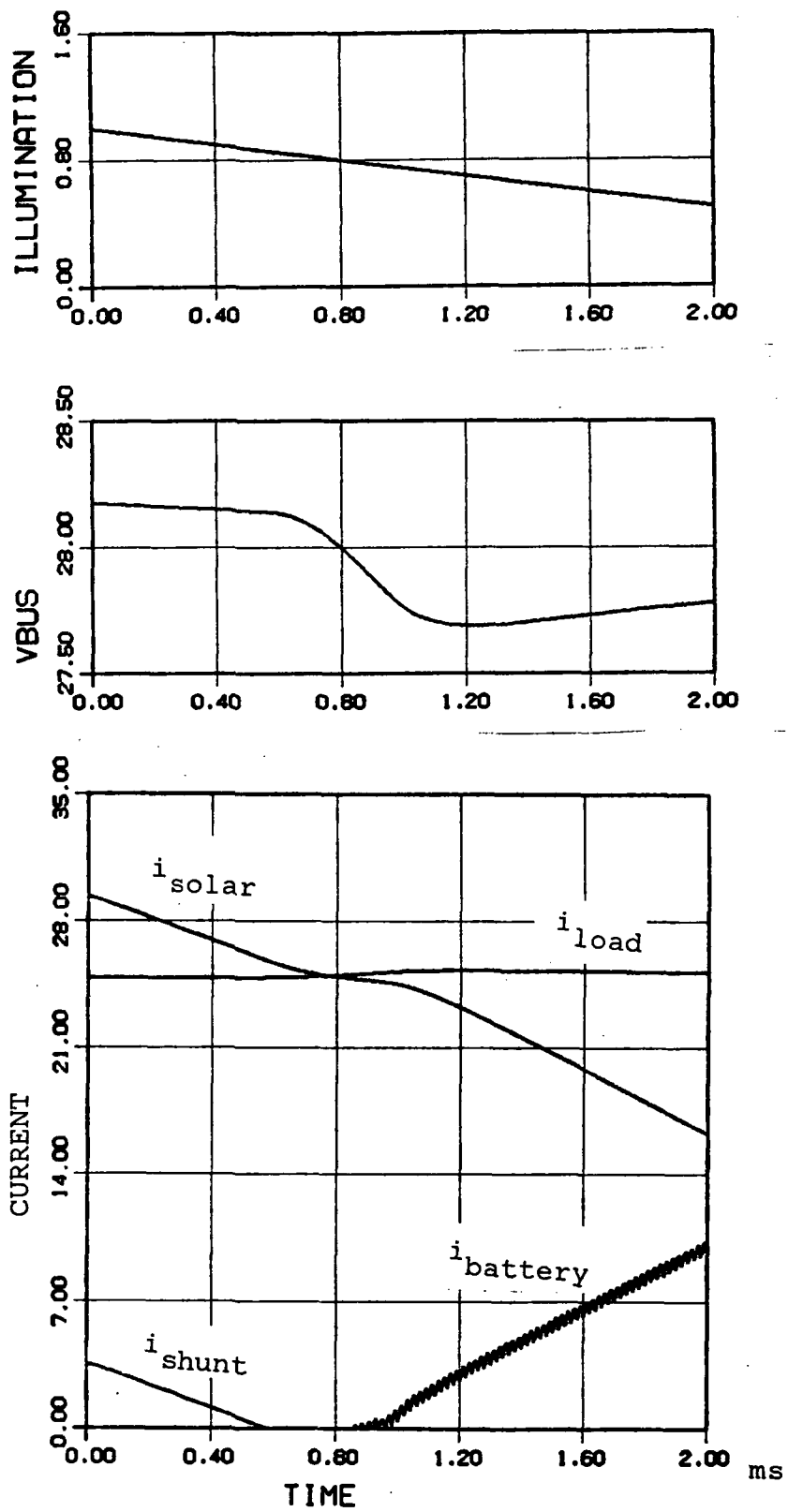
Figure 7.17   Simulation of the DET system for the solar array

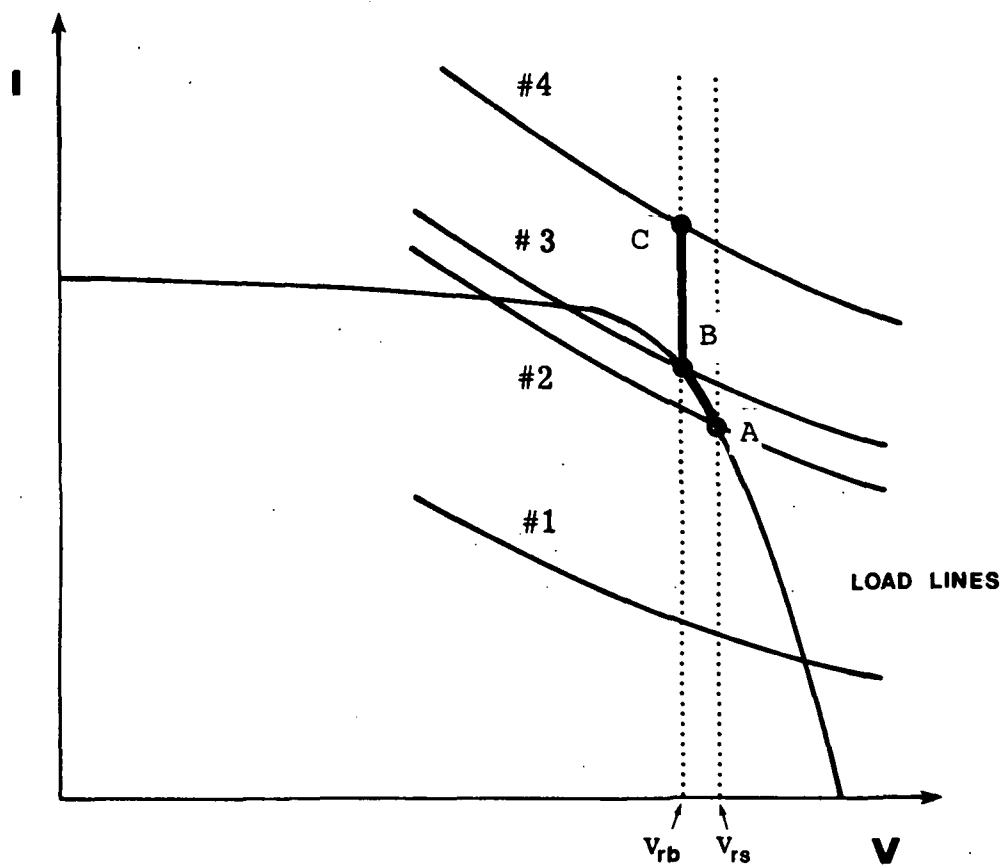illumination changes in Fig.7.16

192

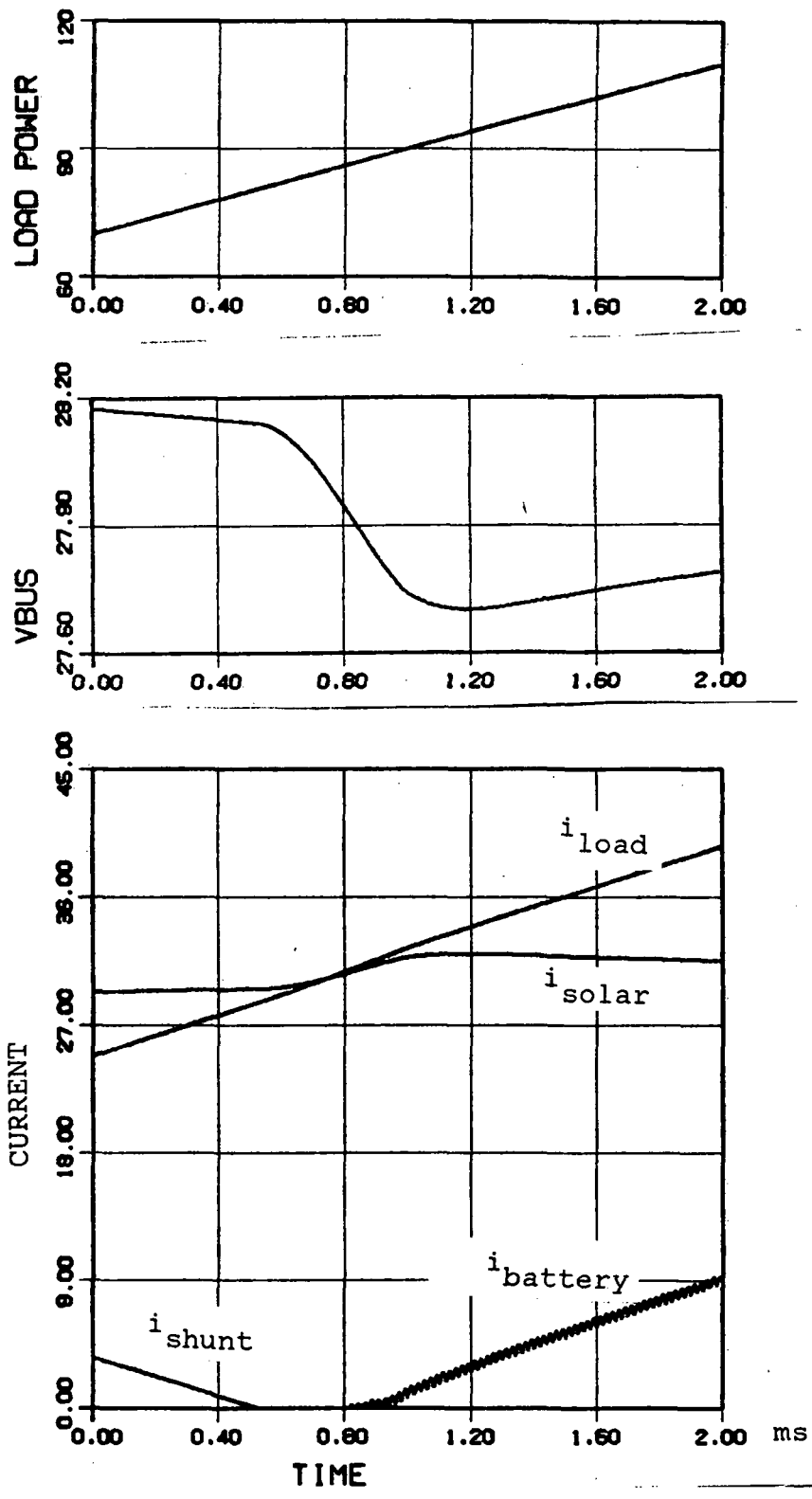Figure 7.18 DET system mode of operation for the load power changes

C-3

Figure 7.19   Simulation of the DET system for the
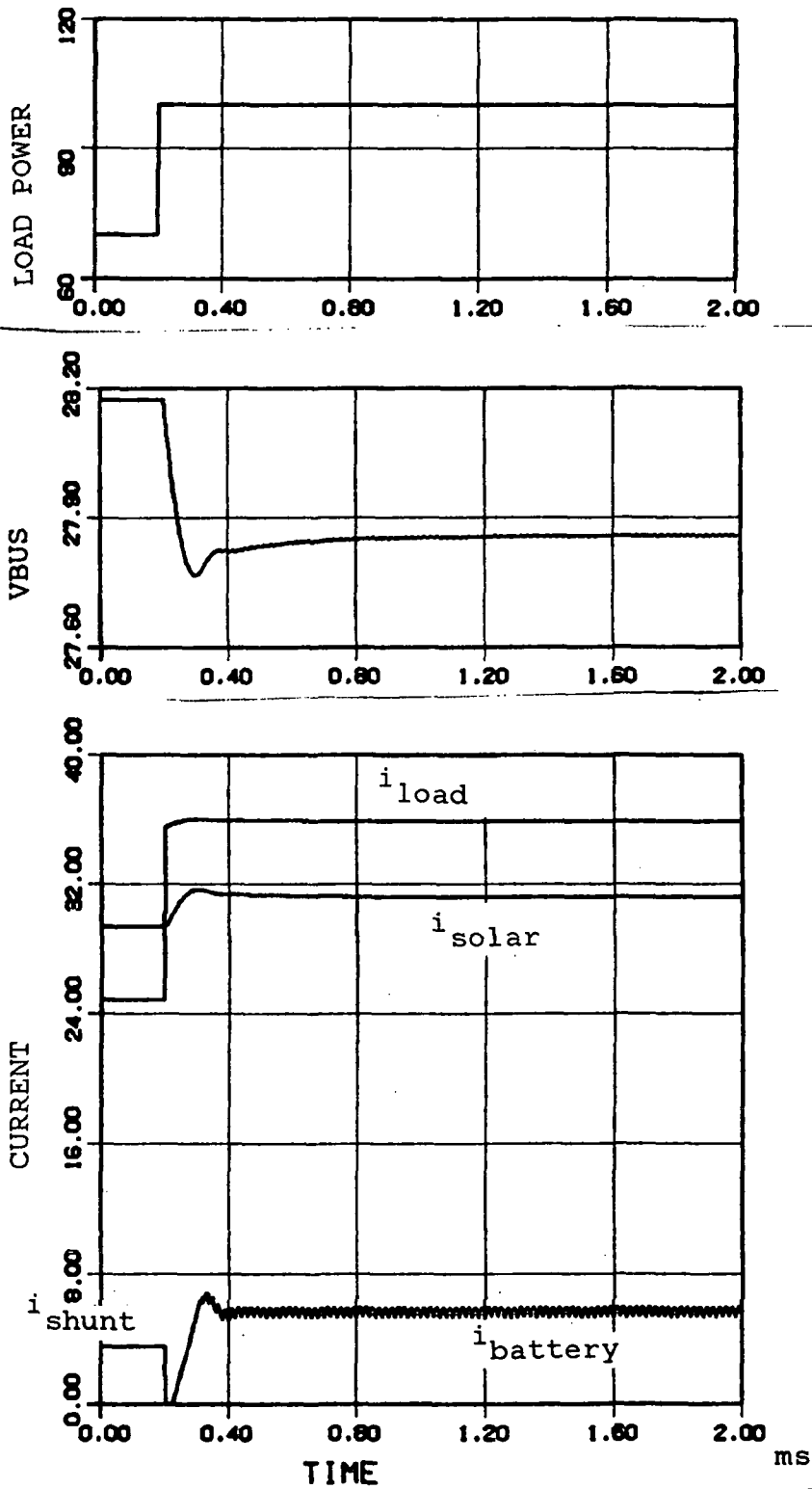linear load changes in Fig.7.18

194

Figure 7.20   Simulation of the DET system for the
step load changes in Fig.7.18

195

7.5 SIMULATIONS OF SOLAR-ARRAY SWITCHING SYSTEM
AND PARTIAL-SHUNT SYSTEM

A solar array switching system with a buck converter is simulated in the shunt mode where the solar array switching actually occurs.

The solar array switching system [NASA2.MOD](Fig.7.21) is configured as shown in Fig.7.22. The solar array switching unit [AS] is connected with a shunt regulator [FS] and an input filter [FI] for the buck converter. The buck converter control loop consists of a compensator model [ZP] and a PWM model [WM]. Finally, a load model [LO] is connected to the buck converter power stage model [BC].

The simulation results (Fig.7.23) begin with a steady state in the shunt mode. Since the shunt current is less than 5A, the solar array switching does not occur during the first .2 msec. At 2 msec, the load is step changed so that the load current drops sharply. Since the load-power demand is reduced the shunt current increases accordingly. As the shunt current reaches the preset value of 5A, the solar array switching occurs according to the logic shown in Fig.4. in section 4.2. The responses of bus voltage and buck converter output voltage are also given in Fig.7.23.

The input requirements data list and the analysis program [NASA2.ANC] used for this simulation are given in Figs.7.24-25.

```
MACRO FILE NAME = MACROS

***********************************************************
*  SOLAR ARRAY SWITCHING UNIT SYSTEM WITH A BUCK   *  *
*  CONVERTER LOAD)                                 *  *
***  REVISED ON 3/12/95                            *  *
***********************************************************

LIST MACRO COMPONENTS = AS,FS,FI,BC,LO,ZP,WM
MODEL DESCRIPTION
LOCATION= 1,AS,   INPUTS=FS(IH=IH), MC(S,2=IX)
LOCATION=23,FS,   INPUTS=AS(VB=VB)
LOCATION= 4,FI,   INPUTS=AS(VB=V1),  BC(I1=I2)
LOCATION= 6,BC,   INPUTS=FI(V2=V1),  LO(IL=I2),  WM(IQ=IQ)
LOCATION=10,LO,   INPUTS=BC(V2=V1)
LOCATION=29,ZP,   INPUTS=BC(V2=VO)
LOCATION=37,WM,   INPUTS=ZP(VE=VE)
LOCATION=41,MC,   INPUTS=FS(IH=S,1),FI(I1=S,3)
END OF MODEL.
PRINT
```
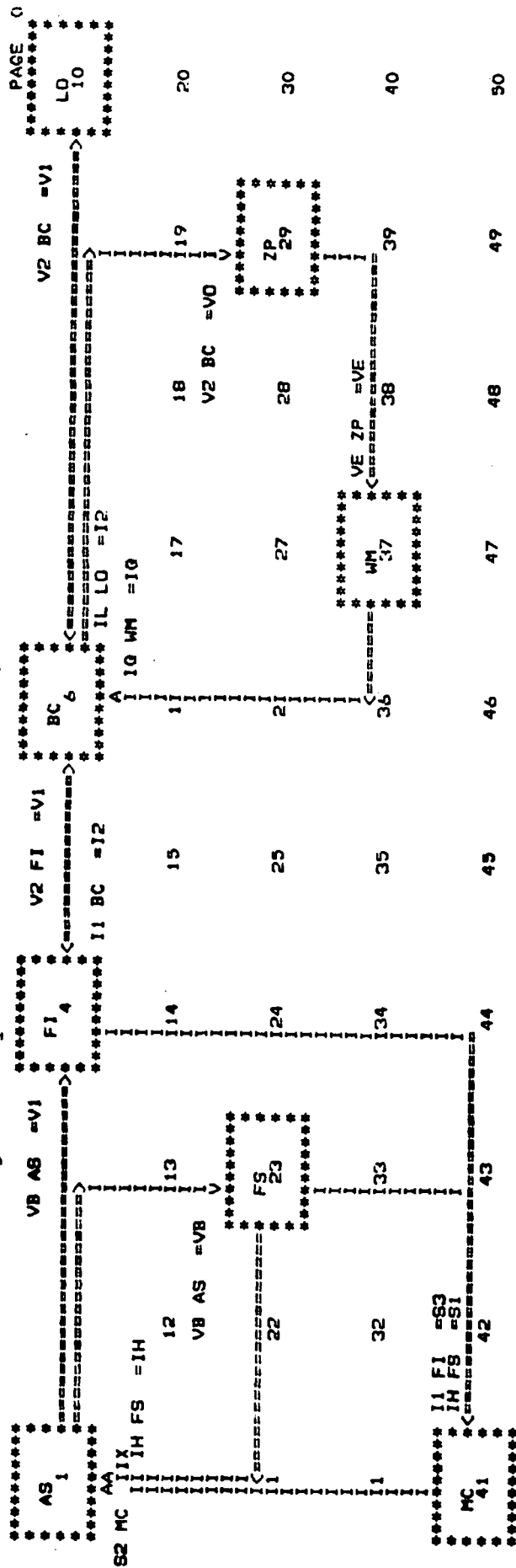
Fig.7.21 System Model Generation [NASA2.MOD]
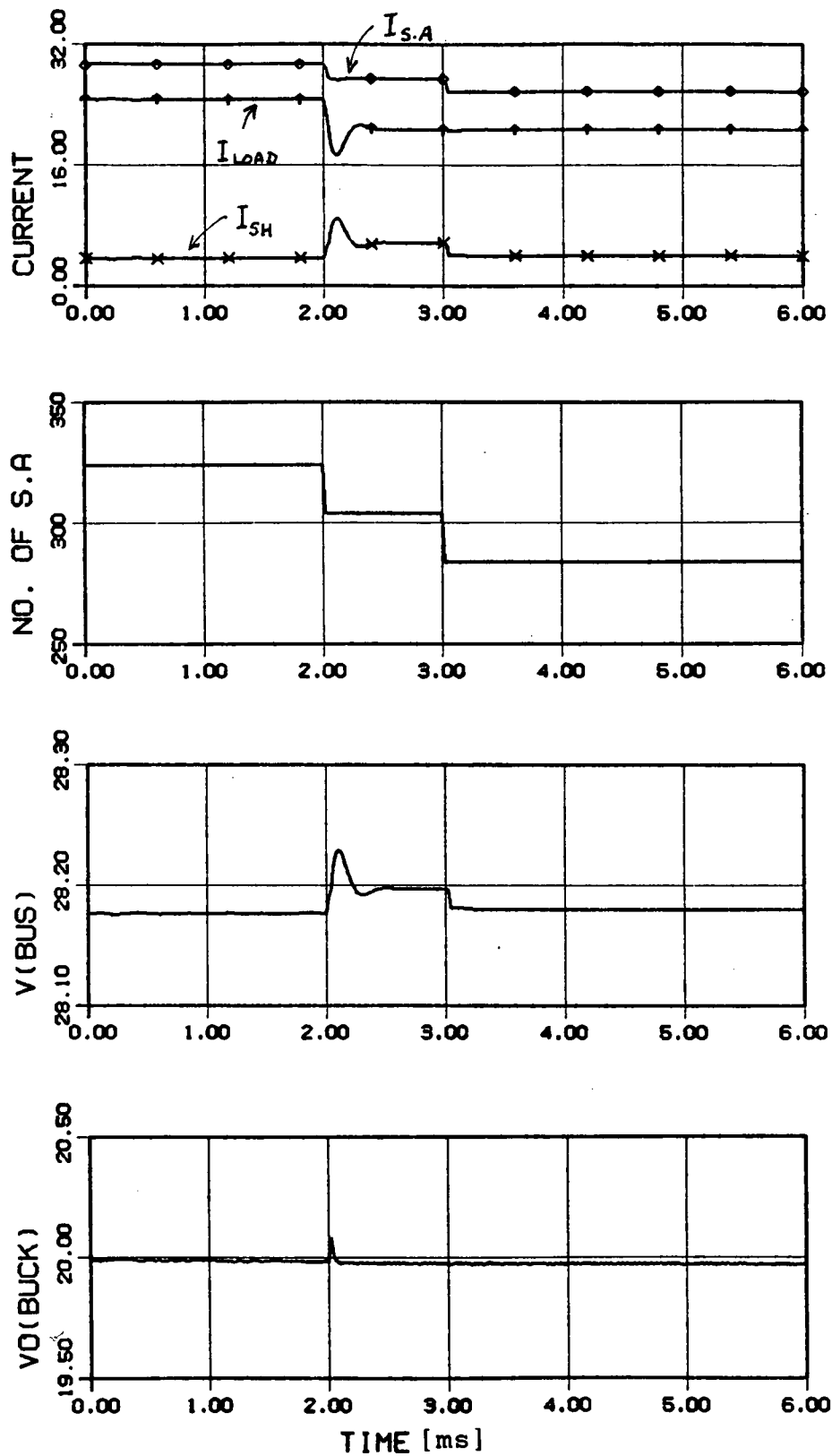

Fig.7.22 Schematic Diagram of [NASA2.MOD]

197

Fig.7.23 Simulation Results of SASU System with Buck Converter

INPUT DATA REQUIREMENTS LIST

PARAMETERS REQUIRED

PARAMETER NAME (AND DIMENSION DATA FOR VECTOR AND MATRIX PARAMETERS)

COMPONENT						
AS	NP AS L AS	DL AS C AS	NN?AS RI AS	NS AS	R AS	C1 AS
FS	VR FS VSAFS	R1 FS ILMFS	R2 FS	R3 FS	GN FS	VTHFS
FI	R FI	L FI	C FI			
BC	RL BC	RC BC	L BC	C BC		
LO	RA LO	TC LO	RB LO	L LO	C LO	
ZP	WM ZP	WP ZP	WZ12P	WZ22P	X ZP	ER ZP
WM	TI WM VI WM	VP WM	VO WM	ER WM	CICWM	SCMWM
MC	S4 MC	C1 MC	C2 MC	C3 MC	C4 MC	

STATES   (INITIAL CONDITIONS AND ERROR CONTROLS REQUIRED)

STATE NAME (AND DIMENSION DATA FOR VECTOR AND MATRIX STATES)

COMPONENT			
AS	VC1AS	IL AS	VB AS
FI	I1 FI	V2 FI	
BC	IL BC	VC BC	
LO	IL LO	VC LO	
ZP	X1 ZP	X2 ZP	VE ZP

Fig.7.24 Input Data Requirements List

199

```
TITLE=NASA(LARGE SIGNAL)
*****************************************************
*TITLE = SOLAR ARRAY SWITCHING SYSTEM WITH          *
*           SHUNT REGULATOR AND A BUCK CONVERTER LOAD *
*****************************************************
PARAMETER VALUES
R  AS = .001,  C  AS = 5E-5,     L  AS = 1E-6
C1 AS = 1.E-3,  R1 AS = 1.0
NP AS = 324,   NS AS = 58,   NNPAS =20,  DL AS = .001
****************************
INITIAL CONDITIONS
VB AS = 28.155,  IL AS = 29.479,  VC1AS = 28.194
*********
PARAMETER VALUES
VR FS = 28.14,  VSAFS = 15.
R1 FS = 12400,  R2 FS = 2.2E6,  R3 FS = 1.78419
GM FS = 4,       VTHFS = 3,       ILMFS = 45
*********
C1 MC=1,C2 MC=1,C3 MC=1,C4 MC=0
*
INITIAL CONDITIONS
I1 FI = 27.985,  V2 FI = 28.
PARAMETER VALUES
R  FI=0.05,   L  FI=3E-6,   C  FI=1000E-6

**BC (POWER STAGE)
INITIAL CONDITIONS
IL BC=9.47,VC BC=20
PARAMETER VALUES
L  BC=1E-4,C  BC=4E-4
RL BC=5E-2,RC BC=1E-1

**VTG LOOP COMPENSATER
K  ZP=.3,  ER ZP=6
WM ZP=4E3
WZ1ZP=5E4,WZ2ZP=1.25E2
WP ZP=1E6

** PWM
TI WM=20E-6,VP WM=6,VQ WM=.5
ER WM=6,CICWM=0,SCMWM=0

** LOAD
RA LO=0.65,RB LO=.6,TC LO=100E-3
L  LO=1E-6,C  LO=1E-6
INITIAL CONDITIONS
X1 ZP=34400,X2 ZP=.73,VE ZP=.3
IL LO=10,VC LO=20

PRINTER PLOTS
ONLINE PLOTS
INT MODE=4
TMAX=3E-3,  TINC=2E-7
PRATE= 100,  OUTRATE=100
SIMULATE

XIC-X
PARAMETER VALUES
RA LO = 0.65,  RB LO = .76,  TC LO = 2E-3
DISPLAY1
V2 BC
INT MODE=4
DISPLAY5
VB AS
DISPLAY2 (OVERPLOT)
IH FS,IO AS,I1 FI
DISPLAY3,NPPAS
TMAX=6E-3,TINC=2E-7
PRATE=50,OUTRATE=100
SIMULATE
```

Fig.7.25 User's Parameter Values and Analysis Commands [NASA2.ANC]

For the partial shunt system simulation, a similar system [PSS6.MOD] (Fig.7.26) replaced the SASU model [AS] with the partial shunt model [AP] in the previous system configuration is developed as shown in Fig.7.27.

The simulation results (Fig.7.28) begins with a steady state in the shunt mode so that the currents and voltages are constant for the first 2 msec. Since the load is step changed at 2 msec, the load current drops sharply. An increase of shunt current results in a decrease of the output voltage across the lower portion of the solar array. The voltage across the upper solar array increases due to a decrease in the load current. As a result, the bus voltage is regulated within the specified range. The output voltage of the buck-converter reaches the steady- state value after a short transient. The input requirements list and the analysis program [PSS6.ANC] used for this simulation are given in Figs.7.29-30.

```
MACRO FILE NAME = MACROS

***************************************************
* PARTIAL SHUNT SYSTEM WITH BUCK CONVERTER LOAD   *
***************************************************
* REVISED ON 3/3/1966

LIST MACRO COMPONENTS = AP,FS,FI,BC,LO,ZP,WM
MODEL DESCRIPTION
LOCATION= 1,AP,  INPUTS = FS(IH=IH),  FI(I1=IL)
LOCATION=23,FS,  INPUTS = AP(VB=VR)
LOCATION= 4,FI,  INPUTS = AP(VB=V1),  BC(I1=I2)
LOCATION= 6,BC,  INPUTS = FI(V2=V1),  LO(IL=I2),  WM(IQ=IQ)
LOCATION=10,LO,  INPUTS = BC(V2=V1)
LOCATION=29,ZP,  INPUTS = BC(V2=VO)
LOCATION=47,WM,  INPUTS = ZP(VE=VE)
END OF MODEL
PRINT
```
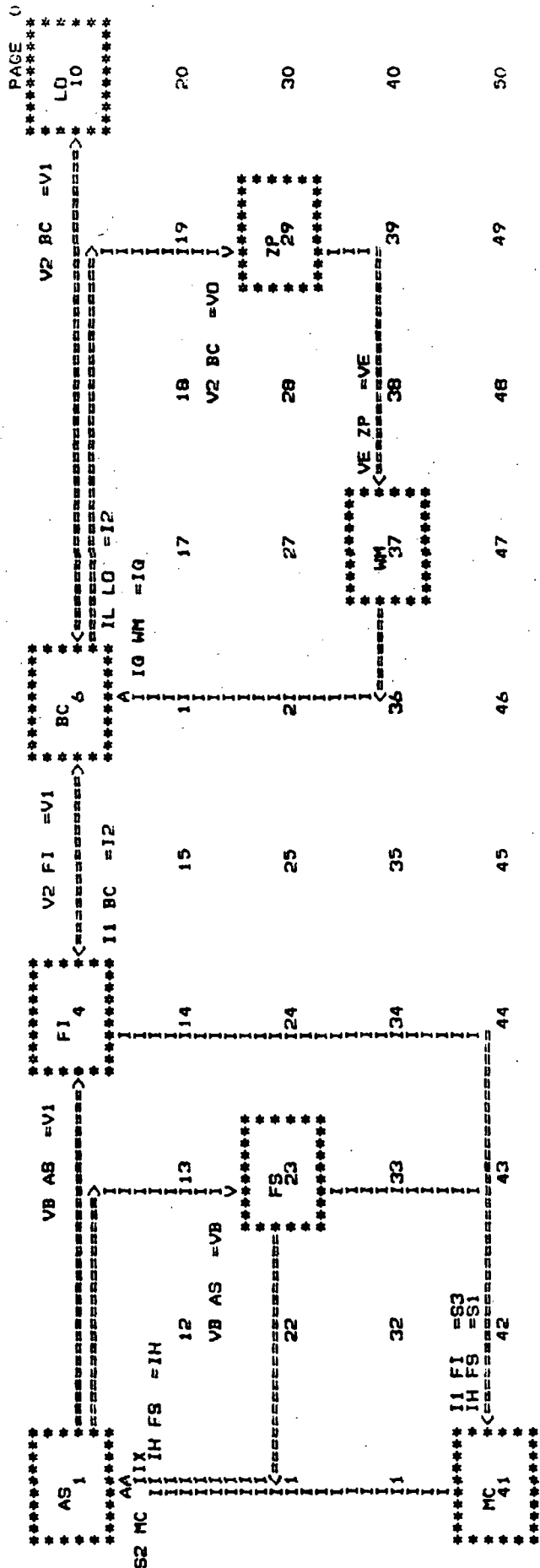
Fig.7.26 System Model Generation [PSS6.MOD]
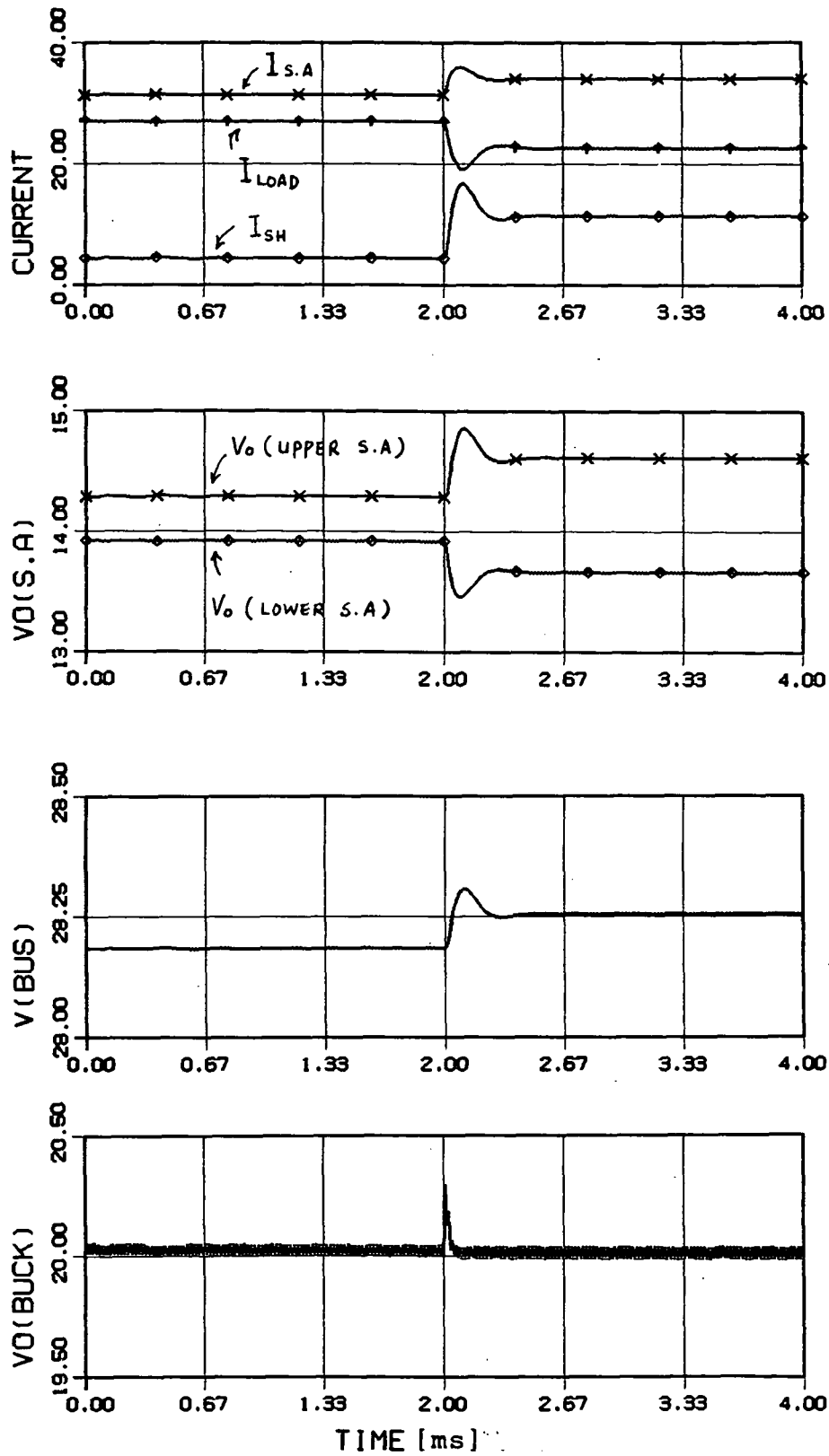

Fig.7.27 Schematic Diagram of [PSS6.MOD]

202

Fig.7.28 Simulation Results of Partial Shunt System
with Buck Converter

203

INPUT DATA REQUIREMENTS LIST

PARAMETERS REQUIRED

PARAMETER NAME (AND DIMENSION DATA FOR VECTOR AND MATRIX PARAMETERS)

COMPONENT						
AP	LL AP / VILAP	NP AP / V2HAP	NS1AP / V2LAP	NS2AP / R AP	ILMAP / C AP	V1HAP / L AP
FS	VR FS / VSAFS	R1 FS / ILMFS	R2 FS	R3 FS	GM FS	VTHFS
FI	R FI	L FI	C FI			
BC	RL BC	RC BC	L BC	C BC		
LO	RA LO	TC LO	RB LO	L LO	C LO	
ZP	WM ZP	WP ZP	WZ1ZP	WZ2ZP	K ZP	ER ZP
WM	TI WM / VI WM	VP WM	VG WM	ER WM	CICWM	SCMWM

STATES (INITIAL CONDITIONS AND ERROR CONTROLS REQUIRED)

STATE NAME (AND DIMENSION DATA FOR VECTOR AND MATRIX STATES)

COMPONENT			
AP	VR AP	IL1AP	
FI	I1 FI	V2 FI	
BC	IL BC	VC BC	
LO	IL LO	VC LO	
ZP	X1 ZP	X2 ZP	VE ZP

Fig.7.29 Input Data Requirements List

204

```
TITLE=NASA(LARGE SIGNAL)

******************************************************
*TITLE = PARTIAL SHUNT SYSTEM WITH BUCK CONVERTER *
*           LOAD                                   *
******************************************************
PARAMETER VALUES
R   AP = .001,  C   AP = 500E-6,  L   AP = 1E-6,  NP AP = 324
NS1AP = 29,    NS2AP = 29,    LL AP =1.,    ILMAP = 45
V1HAP = 15.976,  V1LAP = 12.57,  V2HAP = 15.976,  V2LAP = 12.57
***************************
INITIAL CONDITIONS
VC AP = 28.161
IL1AP = 28.409
********
PARAMETER VALUES
VR FS = 28.14,   VSAFS = 15.
R1 FS = 12400,   R2 FS = 2.2E6,  R3 FS = 1.78419
GM FS = 4.    ,  VTHFS = 3. ,    ILMFS = 45.
*
INITIAL CONDITIONS
I1 FI = 27.985,  V2 FI = 28.
PARAMETER VALUES
R   FI=0.05,   L   FI=3E-6,   C   FI=1000E-6

**BC (POWER STAGE)
INITIAL CONDITIONS
IL BC=10, VC BC=20
PARAMETER VALUES
L   BC=1E-4, C   BC=400E-6
RL BC=5E-2, RC BC=1E-1

** COMPENSATOR
K   ZP = 0.3,  ER ZP =6
WM  ZP =4E3
WZ1ZP =5E4,  WZ2ZP = 1.25E2
WP  ZP =1E6

** PWM
TI WM=20E-6, VP WM=6, VQ WM=.5
ER WM=6, CICWM=0, SCMWM=0

** LOAD
RA LO = 0.6,  RB LO=2.8, TC LO=100E-3
L   LO =1E-6, C   LO=1E-6
INITIAL CONDITIONS
IL LO=10, VC LO=20

INT MODE=4
PRINTER PLOTS
ONLINE PLOTS
****************************
TMAX=3E-3, TINC=2E-7
PRATE=10, OUTRATE=100
SIMULATE

XIC-X
PARAMETER VALUES
RA LO = 0.6,  RB LO = 0.7,  TC LO = 2E-3
INT MODE=4
DISPLAY1(OVERPLOT)
VB AP
DISPLAY2 (OVERPLOT)
I2 AP,  IH FS,  I1 FI
DISPLAY3 (OVERPLOT)
VO1AP,  VO2AP
DISPLAY4
V2 BC
TMAX=4E-3, TINC=2E-7
PRATE=100,  OUTRATE=50
SIMULATE
```

Fig.7.30 User's Parameter Values and Analysis Commands [PSS6.ANC]

7.6 CONCLUSIONS

In this chapter, various solar array system modes of operation in the large-signal sense are analyzed using the state-plane method. The analysis shows that any equilibrium point in Region #2 of Fig.7.1 is unstable with real eigenvalues. The state-plane trajectories are separated by a separatrix that passes through Region #2. The state-trajectories converge to either one of the two stable equilibrium points located in Region #1 or #3. Thus the behavior of the system is quite different on either sides of the separatrix. Since only the equilibrium point in Region #3 is the desirable operating point, a control method to move the operating point from Region #1 to Region #3 is discussed. The analysis also suggests a means that leads the system to the desired mode of operation under start-up.

The behavior of the operating point near the solar array maximum-power point is analyzed. As far as stability and transient response are concerned, the equilibrium points near the maximum-power point, in general, are less commendable than in the region where the magnitude of the solar array output resistance is small, or in the range of a stiffer voltage source.

The solar array system modes of operation including the shunt regulator, battery and switching regulator load are described. The entire DET system is simulated for a contin-

uously varying illumination level and the behavior of the system in various modes of operation are analyzed.

REFERENCES

1. J. Cassineli, et al., "Analytical Modeling of Spacecraft Power System," Final Report to NASA GSFC, 1982, TRW, Redondo Beach, CA

2. Boeing Computer Services, "EASY5 Dynamics Analysis System User's Guide," 1983

3. B. C. CHO, F. C. LEE, "Feaibility Study of Analytical Modeling Spacecraft Power System," Final Report to Naval Research Lab., 1983, VPI&SU

4. J. M. Voss, J. G. Gray, "A Regulated Solar Array Model - A Tool For Power System Analysis," IEEE PCSC 1970 pp.12-17

5. A. Capel, et al., "Power System Simulation of Low Orbit Spacecraft: The EBLOS Computer Program," IEEE PESC 1982, pp.272-285

6. Robert L. Bailey, "Solar-Electrics Research and Development," Ann Arbor Science, 1980, pp.112

7. D. K. Decker, J. Cassinelli, "High Power Solar Array Switching Regulation," Sixteenth IECEC Record, Atlanta, 1981

8. Paul S. Nekrasov, "Partial Shunt Regulation," AAS 68-067, 14th Annual Meeting AAS, May 1968, Dedham, Mass

9. B. C. Cho, "Modeling and Analysis of Spacecraft Power Systems," Ph.D. Dissertation, 1985, VPI & SU

10. E. N. Costogue, S. Lindena, "Comparison of Candidate Solar Array Maximu Power Utilization Approaches," IECEC 1976, pp.1449-1456

11. F. C. Lee, "User's Design Handbook for a Standardized Control Module for DC to DC Converters," Final Report to NASA CR., 1980, VPI&SU